INTRACELLULAR TRAFFICKING OF RICIN A CHAIN IN RELATION TO ITS CYTOTOXICITY AND DEPURINATION ACTIVITY IN *SACCHAROMYCES CEREVISIAE*

By

QING YAN

A Dissertation submitted to the

Graduate School-New Brunswick

Rutgers, The State University of New Jersey

In partial fulfillment of the requirements

for the degree of

Doctor of Philosophy

Graduate Program in Plant Biology

written under the direction of

Nilgun E. Tumer

and approved by

_____

_____

_____

_____

_____

New Brunswick, New Jersey

[Oct, 2013]

ABSTRACT OF THE DISSERTATION

Intracellular trafficking of ricin A chain in relation to its cytotoxicity and depurination activity in *Saccharomyces cerevisiae*

by QING YAN

Dissertation Director:

Nilgun E. Tumer

Ricin is a heterodimeric protein composed of ricin A chain (RTA) and ricin B chain (RTB). The extreme toxicity of ricin is mainly attributed to the enzymatically active RTA, which specifically removes an adenine residue from the universally conserved α-sarcin/ricin loop (SRL) in the 28S rRNA and inhibits protein synthesis. For RTA to exert its depurination activity, it has to undergo retrograde transport pathway to enter the cytosol. Therefore, the intracellular trafficking of RTA is an important aspect of ricin mediated cell death. The goal of the present study is to understand the structural features of RTA which contribute to its intracellular transport and the host factors involved in its trafficking in *Saccharomyces cerevisiae*. To visualize RTA, the enhanced green fluorescent protein (EGFP) is fused to mature RTA (matRTA-EGFP) containing 267-amino acid residues and precursor RTA (preRTA-EGFP) containing a 35-amino acid N-terminal extension followed by mature RTA. When preRTA-EGFP is expressed in the endoplasmic reticulum (ER) lumen of *Saccharomyces cerevisiae*, it follows two parallel pathways: 1) the well characterized ER-to-cytosol dislocation through

the ER-associated degradation (ERAD) pathway, 2) vacuole transport after initial localization to the ER. In chapter two, I studied the roles of the important structural domains and sequence motifs of RTA in its trafficking and toxicity by mutational analysis. I showed that the 26-amino acid signal peptide within the N-terminal extension of preRTA is responsible for the ER targeting and the following nine-amino acid propeptide is important for glycosylation and efficient vacuole transport. The *N*-glycosylation of RTA promotes efficient ER export to the cytosol and vacuole, and contributes to the toxicity of RTA. The C-terminal hydrophobic domain of RTA is critical for transport out of the ER. In chapter three, I further investigated how the ER-to-vacuole transport and ER-to-cytosol dislocation pathways of preRTA affect its depurination and toxicity by using wild type preRTA and nontoxic preRTA mutants. The altered sequence motifs in preRTA lead to different translocation pathways. This provides the advantage of studying the contribution of their trafficking pathways to the toxicity of RTA. I present evidence that vacuole transport is an alternative degradation pathway of preRTA and contributes to the depurination reduction. The dislocated wild type preRTA and preRTA mutants have differential requirements for the cytosolic ERAD component peptide:*N*-glycanase (PNGase; yeast Png1), which is involved in the degradation of its substrates. In chapter four, the roles of yeast cellular components in the trafficking of RTA were studied to unravel the host genes in the ricin trafficking pathways. A genome wide screen of yeast nonessential gene knockout collection against RTA led to the discovery of genes in the Hrd1p complex and AP-2 complex, whose deletions conferred resistance to preRTA but

not to matRTA. The components of the Hrd1p complex are responsible for the dislocation of preRTA. The Apl3p subunit of AP-2 complex is involved in the vacuole transport of preRTA. The study has provided important insights into the mechanism of intracellular trafficking of RTA and its role in toxicity.

ACKNOWLEDGEMENT

First and foremost, I sincerely appreciate my advisor, Dr. Nilgun E. Tumer. During the past six years, she led me through many difficulties of my research. She put her patience in leading me to make progress from the beginning. Her dedication to science and to the lab set a good example for me. I would like to thank Dr. Xiaoping Li. She has given me tremendous advice on my research. She has been a good teacher and a friend whom I always turned to when I met difficulties. I am very grateful for the input of my entire committee. Drs. Barth Grant, Thomas Leustek, Juan Dong and Michael Lawton have always provided valuable suggestions for my research and I appreciated every conversation we have had. I am lucky that I have joined this lab. Drs. John McLaughlin, Michael Pierce, Kerrie May and Jennifer Nielsen Kahn have given me a lot of advice and always patiently taught me whenever I met problems in my research. Dr. John McLaughlin also performed the preliminary screen to identify the yeast resistant mutants used in Chapter four. Dr. Jiachi Chiou, Anwar Bin Umer, Debaleena Basu and Yijun Zhou have been good friends to me and gave me a lot of pleasure to work in this lab. Last but not least, I am blessed that I am deeply loved by my parents. They have been good examples to me since I was young. Their curiosity to knowledge, dedication to work, persistence toward goals and optimistic in life are the things I always respect. They also did their best to support me during my doctoral study. There were many difficulties, but nothing more joyful than conquering them. I am glad that I can do it by all of your help.

TABLE OF CONTENTS

LIST OF TABLES

LIST OF FIGURES

CHAPTER 1: Introduction

TOXICITY OF RICIN

Ricin is a naturally occurring toxin produced by the castor bean plant *Ricinus communis*. Ricin is highly potent. It is believed that the toxicity of ricin is attributed to the depurination of the adenine residue in the large 28S rRNA and subsequent inhibition of protein synthesis. The intoxication occurs when ricin is injected, ingested or inhaled. As little as 500 μg of ricin can kill an adult. The severity of intoxication increases with the amount of the toxin incorporated into the cells. The symptoms arise after 3 to 20 h after injection or ingestion, leading to dysfunction of liver and kidneys. Fatal cases show hemorrhagic necrosis in intestines and heart and edema in lungs. Because of its high potency and wide accessibility, ricin has been used as a bioterrorist weapon and remains a serious threat worldwide. Recently, ricin has been found in several threat letters to the White House in 2013.

STRUCTURE AND FUNCTION OF RICIN

Ricin is a heterodimeric protein, consisting of ricin A chain (RTA) and ricin B chain (RTB). RTA and RTB are joined by a single disulfide bond (1), as shown in Figure 1.1.

RTA is an *N*-glycosidase composed of 267 amino acids. The precursor form of RTA has a 35-amino acid N-terminal extension. In yeast, the first 26-residue signal peptide directs RTA into the endoplasmic reticulum (ER) and is cleaved

there (2). The following nine-residue propeptide is responsible for the extent of glycosylation and efficient vacuole transport (2). The C-terminus of RTA has a hydrophobic stretch which is important for the interaction with the membrane lipid bilayer, thus facilitating the export from the ER (2-4). RTA has two consensus glycosylation sites which are Asn10-Phe11-Thr12 and Asn236-Gly237-Ser238. We have recently reported that glycosylation does not affect the enzymatic activity of RTA, but facilitates its entry into the cytosol (2).

The crystal structure of RTA resolved at 2.8 Å revealed that RTA contains 7 α-helices (5). The α-helix E forms the backbone of RTA and contains the active site cleft. Site-directed mutagenesis and systematic deletion of amino acids suggested that most of the amino acids that result in inactive RTA variants are clustered at the bottom of the putative active site cleft (6-8). However, systematic deletion of amino acids also showed that some amino acids, although located distance away from the active site cleft, were critical for the activity of RTA. The contribution of these amino acids to the activity of RTA was explained by an indirect effect caused by α-helix D. The disruption of the amphiphilicity of α-helix D led to the inactivation of RTA, because the hydrophobic and hydrophilic properties of helix D shielded helix E from the solvent (9). To correlate the structural features of RTA to its toxicity, mutational analyses have been widely conducted. It was shown that Glu-177 and Arg-180 within the active site cleft are important for the rate-limiting step of the depurination reaction. The mutations of these residues result in a reduction in k_{cat} but not k_m. However, the residues Tyr80 and Tyr123 are involved in substrate binding (10, 11).

RTB is a lectin which binds to the glycoproteins and glycolipids on the cell surface and promotes the endocytosis of the holotoxin. X-ray crystallography revealed that RTB has two globular domains. Each domain has identical folding topology (5) and contains three smaller subdomains (12). RTB is an *N*-glycosylated *N*-galactose specific lectin. RTB has at least three lectin binding sites located at subdomain 1 alpha, 1 beta and 2 gamma (13). The lectin binding sites contribute to the cell surface galactose binding ability (14).

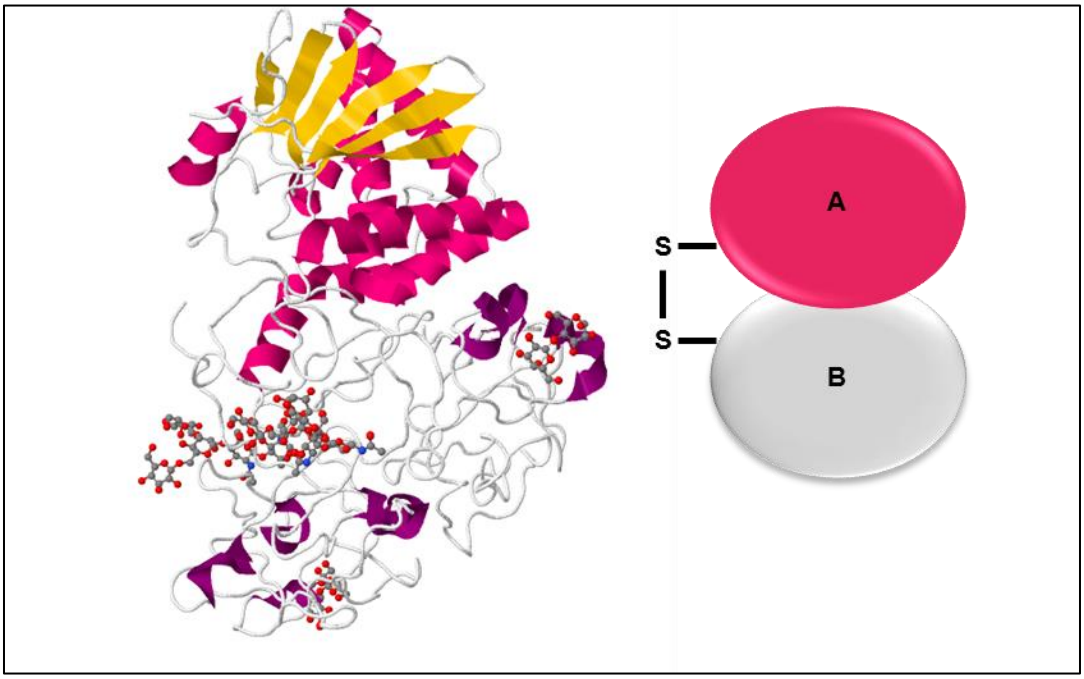

Figure 1.1 Structural and schematic representations of ricin. RTA and RTB are covalently linked by a single disulfide bond. Alpha-helices of RTA are represented by red barrels and β-strands of RTA are represented by yellow arrows. RTB contains two globular domains, which are shown in grey (Image from the RCSB PDB (www.pdb.org) of PDB ID 2AAI (15)).

MODE OF ACTION

Ricin belongs to a family of proteins that are capable of inactivating the eukaryotic ribosomes, termed ribosome inactivating proteins (RIPs). They widely exist in plants, bacteria and fungi. As shown in Figure 1.2, the type 1 RIPs are proteins that consist of a single chain, including pokeweed antivirus protein (PAP), saporin, trichosanthin, *etc*. They have *N*-glycosidase activity. The type 2 RIPs are heterodimeric proteins composed of both A chain and B chain. In this group, ricin, abrin, and agglutinin are well known. The A chains are functionally equivalent to the type 1 RIPs. The B chains of the type 2 RIPs bind to the galactose receptor on the cell surface and facilitate the endocytosis of the A chains, which eventually enter the cytoplasm to inactivate ribosomes. The type 1 RIPs are less potent since they lack the cell binding B chains.

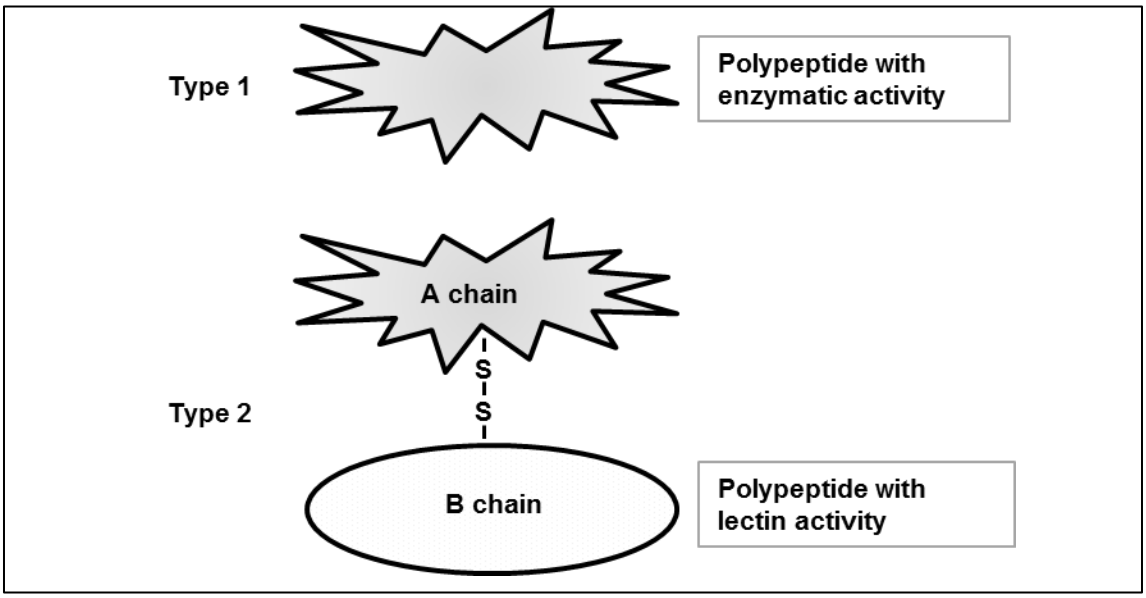

Figure 1.2 Schematic representation of the structure of type 1 and 2 ribosome-inactivating proteins (RIPs). The type 1 RIP consists only of the

enzymatic polypeptide. The type 2 RIP consists of a binding polypeptide B chain linked to the enzymatically active A chain by a disulfide bond.

Yaeta Endo and Kunnio Tsurugi had earliest series of publications on the mechanism of action of the lectin RTA. RTA has *N*-glycosidase activity. The enzymatically active RTA hydrolytically cleaves the *N*-glycosidic bond of the A_{4324} residue of the 28S rRNA (16-18). The A_{4324} residue belongs to a specific tetranucleotide loop GAGA that is specifically recognized by RTA on the rRNA (19). This tetranucleotide loop is contained in the conserve sequence (5'-AGUACGAGAGGAAC-3'), termed α-sarcin/ricin loop (SRL), of the eukaryotic ribosomes (16). The SRL is also the target for a ribotoxin, α-sarcin. Unlike ricin, the reaction catalyzed by α-sarcin leads to the cleavage of the phosphodiester bond of the 28S rRNA (Figure 1.3). RTA directly acts on the RNA, since RTA is able to depurinate naked 28S rRNA. However, naked 28S rRNA is less sensitive to RTA, suggesting that the integrity of the secondary structure of rRNA is important (17). RTA employs its surface charge to target the ribosomes (20). Electrostatics interaction of RTA with ribosomes fits in a two-step binding model. This model suggests that RTA is initially concentrated on the ribosomes in a slow and nonspecific manner. This interaction promotes the subsequent fast and specific interaction of RTA with the ribosome stalk (21), which is required for ribosome binding and toxicity of RTA (22). The irreversible depurination by RTA damages the SRL, which inhibits the GTP-dependent binding of EF2 and inactivates protein synthesis at the translocation step (23).

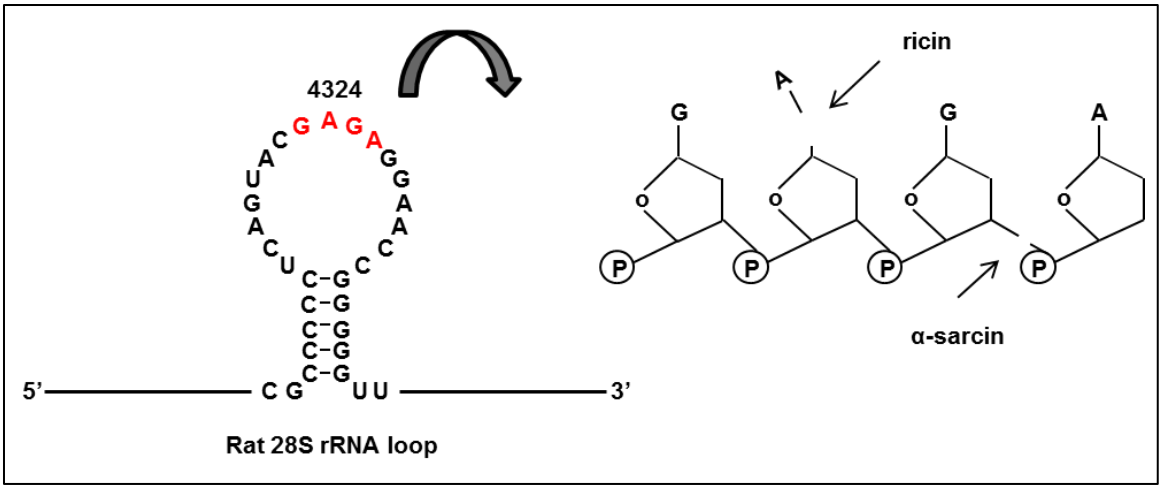

Figure 1.3 Schematic representation of the biochemical action of ribosome-inactivating proteins (RIPs) such as ricin. The RIPs remove an adenine residue within the α-sarcin/ricin loop on the large 28S ribosomal subunit, whereas ribotoxins such as α-sarcin hydrolyzes the phosphodiester bond. They both lead to the inactivation of the ribosomes and cause protein synthesis inhibition.

INTRACELLULAR TRAFFICKING OF RICIN

In mammalian cells, when ricin is added extracellularly, it has to undergo the retrograde transport pathway to reach its substrate ribosomes in the cytosol (Figure 1.4). The retrograde transport pathway of ricin initiates with endocytosis facilitated by RTB. It is then delivered to the early endosomes. From there, a small amount of ricin is transported to the *trans*-Golgi network (TGN). Subsequently, it goes to the ER where RTA is reductively separated from RTB by the protein disulfide isomerase (PDI) and becomes activated. RTA gains entry into the cytosol through the retrotranslocon residing in the ER membrane.

Kirsten Sandvig and coworkers pioneered the research of ricin intracellular trafficking in mammalian cells. Although clathrin is a key component in the endocytosis and several reports clearly suggested clathrin-dependent endocytosis of ricin, the clathrin-independent endocytic uptake also exists for

ricin internalization (24). Acidification of cytosol of several cell lines strongly reduced the clathrin-dependent endocytosis of other proteins due to the reduced pinch off of the coated vesicles, whereas the endocytosis and the toxicity of ricin was not affected under this condition, indicating an alternative endocytic pathway existed for ricin (25). More recent studies provided accumulated evidence for clathrin-independent endocytosis of ricin. By overexpression of the mutant dynamin, which can inhibit clathrin-dependent endocytosis, the authors found that the endocytosis of ricin was not affected (26, 27).

Only a small amount of ricin can be transported from the endosomes to the Golgi apparatus. A large portion of internalized ricin is either recycled back to the cell surface or sent to the lysosomes and degraded (28). Because of this reason, to distinguish the population that goes through retrograde transport pathway with the one that does not, ricin is modified to contain a tyrosine sulfation site, which can be sulfated in the Golgi apparatus and used to quantify entry into the Golgi. Several studies showed that ricin delivery from the endosomes to the TGN depends on a number of factors. Earlier research proved that the endosomes to Golgi transport of ricin is independent of clathrin, GTPase Rab9 and Rab11 (29). Further investigation found that small GTPase Rab6A and Rab6A' are both involved in the transport from the endosomes to the Golgi apparatus. The loss of function of Rab6A can be compensated by up-regulation of Rab6A' (30). Another GTPase, dynamin, although is not involved in the endocytosis as mentioned above, is instead required for the transport of endocytosed ricin to the Golgi apparatus, since overexpression of mutant dynamin strongly inhibits the sulfation

of ricin (26). Calcium has been implicated to have an important role in several steps of the intracellular transport. With thapsigargin and A23187 treatment to the cell, the cytosolic calcium level was elevated. The increased level of calcium stimulated the transport of ricin to the Golgi apparatus by about 20 times, demonstrating that endosome to Golgi transport of ricin is regulated by calcium (31). Lipid phosphorylation is also an important regulation of intracellular transport. Phosphatidylinositol (PI) 3-kinase hVps34, which is the human homologue of yeast Vps34, is critical for endosome to Golgi transport. Several methods to reduce the activity of hVps34, including chemical inhibition, expressing dominant negative mutant of hVps34 and expressing small interfering RNA targeted to the messenger RNA of hVps34, convergently inhibited the transport of ricin from the endosome to the Golgi apparatus. In line with this, ricin transport from the endosomes also depends on the sorting nexin (SNX) 2 and SNX 4, which are effectors in the hVps34-dependent pathway (32). Recently, another protein belonging to the sorting nexin protein family, SNX8, the yeast homologue of Mvp1p, has been demonstrated to reduce the endosome to TGN transport of ricin slightly by knockdown, but have an opposite effect on Shiga toxin (33). Endosome to Golgi transport of ricin is also affected by the membrane cholesterol level. Both increased and reduced cholesterol levels inhibit intracellular trafficking to the Golgi as indicated by quantification of ricin sulfation (34). Cholesterol only affects the Golgi transport of ricin bound to glycoproteins, but not to glycolipids (35). Recent research identified small molecules such as

Retro-2, which were able to inhibit the endosome to Golgi transport, thus protecting mice from lethal nasal exposure to ricin (36).

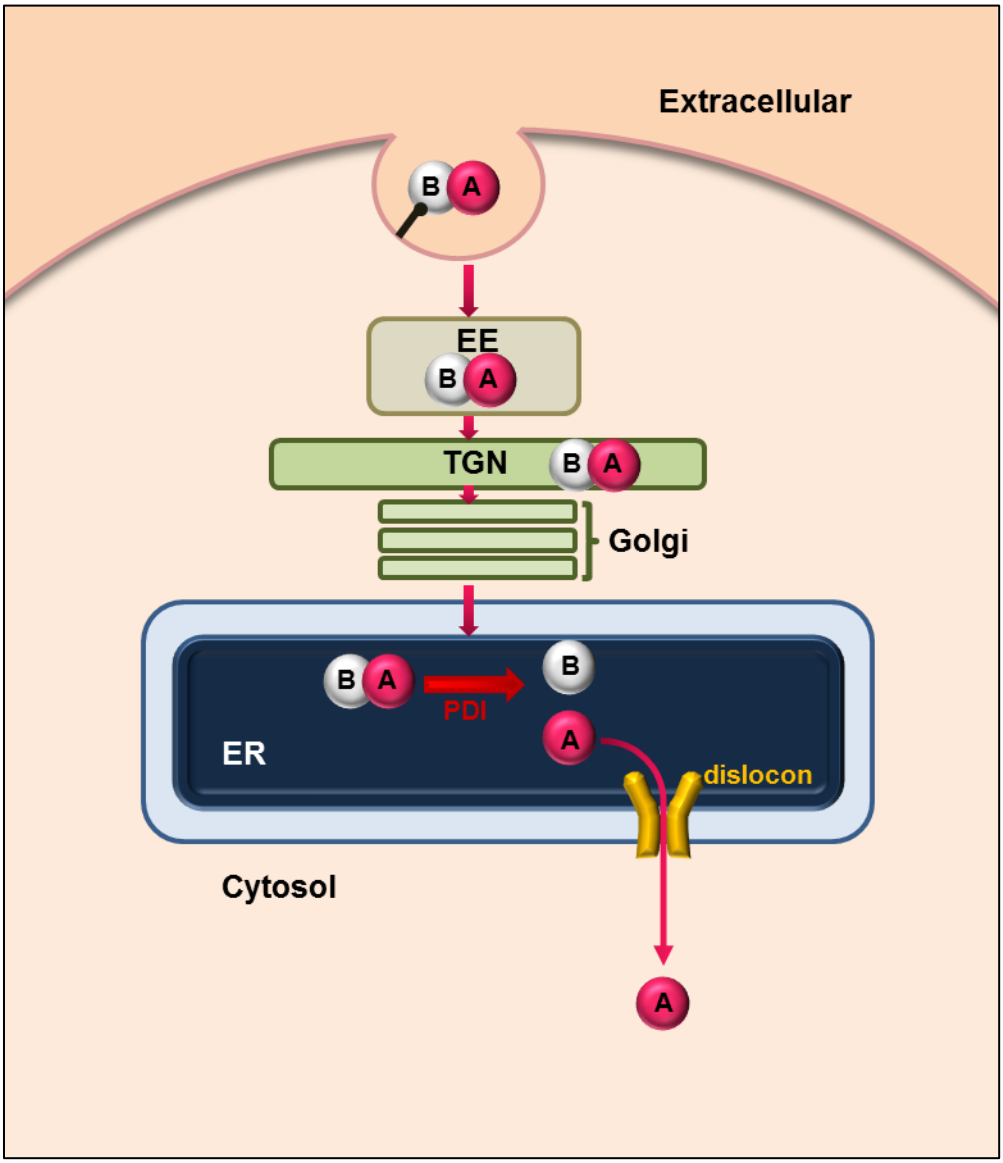

Figure 1.4 The intracellular trafficking pathway of ricin in mammalian cells. RTB binds to the galactose receptors on cell surface and promotes the endocytosis. After entering the cell by endocytosis, ricin undergoes vesicle-mediated retrograde transport through the early endosomes (EE), the *trans*-Golgi network (TGN) and to the ER. In the ER, RTA is separated from RTB by the protein disulfide isomerase (PDI) and becomes activated. RTA interacts with luminal chaperones in the ERAD-L pathway and is then delivered to the

retrotranslocon through which it is dislocated to the cytosol. In the cytosol, RTA refolds with the help of cytosolic chaperones.

Some bacterial toxins such as cholera toxin have a polypeptide sequence - Lys-Asp-Glu-Leu (KDEL), which serves as an ER retrieval sequence leading the Golgi-to-ER transport of the toxin. Addition of an ER retrieval sequence KDEL increases the toxicity of RTA to both Vero and Hela cells, but does not increase the enzymatic activity. This experiment suggests that ER retrieval sequence promotes the retrotranslocation of RTA to the ER and subsequently to the cytosol (37). However, RTA does not have such a sequence or its homologue (38). Shiga toxin, also lacking a KDEL sequence, uses the Rab6A-dependent retrograde transport to enter the ER. However, ricin retrotransport to the ER is Rab6A and COPI independent (39). The structural features that contribute to the Golgi to ER transport of ricin remain elusive. It was demonstrated that in addition to facilitating the endocytosis of RTA, the galactose binding activity of RTB plays a role in the Golgi to ER transport of ricin. The mutations in both galactose binding domains of RTB significantly reduced the toxicity of ricin, which was not attributed to the reduced endocytosis (40). The result implied that ricin has to bind to a galactosylated component that undergoes retrograde transport itself. In light of this assumption, *in vivo* or *in vitro* experiments further found that ricin interacts with rat liver calrecticulin which has a C-terminal KDEL motif and is galactosylated. It may have implication on how ricin reaches the ER from the Golgi (41). Lipids not only participate in the endosome to TGN transport of ricin, it is recently shown that they are also involved in the TGN to ER transport. A

cytoplasmic phospholipase A_2 (PLA_2) was demonstrated to play a role in the TGN to ER transport of ricin. Inhibition of PLA_2 activity protected the cells against ricin challenge (42). Although the mechanisms of TGN to ER transport have been demonstrated, it should be noted that ricin can bypass the Golgi apparatus and still intoxicate Chinese hamster ovary (CHO) cells (43).

In the ER, RTA is activated after it is separated from RTB. The disulfide bond between RTA and RTB is critical for the transport of the enzymatically active RTA to the cytosol (44). It was reported that only free RTA is capable of dislocating to the cytosol (45, 46). The reductive separation of RTA from RTB is catalyzed by the protein disulfide-isomerase (PDI) in the ER (47), leading to the activation of ricin (48). Another protein, thioredoxin reductase, is also involved in this process by activating the PDI (48). In addition to PDI, the ER membrane localized thioredoxin-like transmembrane (TMX) protein can also reductively activate ricin and thereby facilitating the dislocation of RTA and increasing its toxicity to the cell (49). In order to dislocate to the cytosol, partial unfolding of RTA is required, since it was found that introduction of an intrachain disulfide bond decreased the cytotoxicity of RTA (50). When RTA dislocates through the ER membrane, its hydrophobic C-terminus interacts with the membrane bilayer and facilitates this process (51).

ER-ASSOCIATED DEGRADATION (ERAD) PATHWAY

The final step in the retrograde transport, dislocation from the ER, is crucial for ricin to reach its substrate ribosomes. The newly synthesized proteins in the

ER are subjected to the scrutiny of the ER quality control (ERQC) system. The ERQC within the secretory pathway involves ER retention, ERAD and retrieval from downstream organelles. RTA is regarded as a misfolded protein and is thought to use the ERAD pathway to enter the cytosol (52). The ERAD pathway has been studied with a number of canonical substrates such as CPY* and PrA* in yeast, and CFTR mutant and type I membrane proteins including class I major histocompatibility complex (MHC) heavy chain in mammalian cells. Although RTA and these proteins use the seemingly identical pathway, the cellular components in the pathway that are involved in each protein's dislocation are likely to be diverse. The knowledge of how RTA traverses the ERAD pathway will provide broader understanding of the intoxication mechanisms of RTA.

In yeast, the dislocation of RTA requires the prior trafficking to the Golgi and retrieval back to the ER (53). Mutant strains containing a temperature sensitive lesion in Sec12p or Sec23p, which affects COPII mediated vesicle transport in ER-to-Golgi, stabilized RTA in pulse-chase analysis at restrictive temperature. In line with this, Erp2p of the p24 mediator of the ER-to-Golgi trafficking conferred growth advantage when deleted (53). After ER retrieval, two ERAD components, Htm1 (the yeast homolog of mammalian EDEM) and Yos9 (the yeast homolog of mammalian OS-9), are both required for RTA dislocation and their functions are *N*-glycan dependent (54). Consistent with this, in mammalian cells, EDEM, which is an ER degradation enhancing α-mannosidase-like protein, is also required for the toxicity of RTA (4). The C-terminal hydrophobic domain of RTA is critical for the EDEM recognition, since a single mutation on this domain would reduce the

interaction between EDEM and RTA (55). In the next step, RTA dislocates via the protein conducting channel. It was initially believed that in yeast, the Sec61 translocon was the channel to transport RTA out of the ER, which also imports newly synthesized proteins to the ER (56). The Sec61 translocon has been shown to co-immunoprecipitate with RTA (56) and when this translocon was compromised, RTA was stabilized in yeast (57). However, in contrast, a recent study suggested that RTA required Der1, but not Sec61 for degradation (54). It is worth noting that the conflicting results were derived from using different RTA mutants. Der1 is a component of the Hrd1 ubiquitin ligase complex. In yeast, several studies demonstrated that RTA dislocates via Hrd1 ubiquitin ligase complex (53, 58). RTA is not ubiquitinated, since ricin has low lysine content which is the site for ubiquitination (59). Once in the cytosol, the folded RTA mutant and misfolded RTA mutant have different requirements for the cytosolic ERAD components in yeast. The folded RTA mutant RTA_{E177D} dislocates independent of Cdc48 complex, but with the engagement of the 19S proteasome cap protein Rpt4p; whereas, the misfolded RTA mutant RTA_{Δ} is recruited by Cdc48p, deglycosylated by peptide:*N*-glycanase (PNGase; yeast Png1), which is in complex with proteasome via Rad23, and is finally degraded by the proteasome requiring Rpt2p ATPase activity (53) (Figure 1.5).

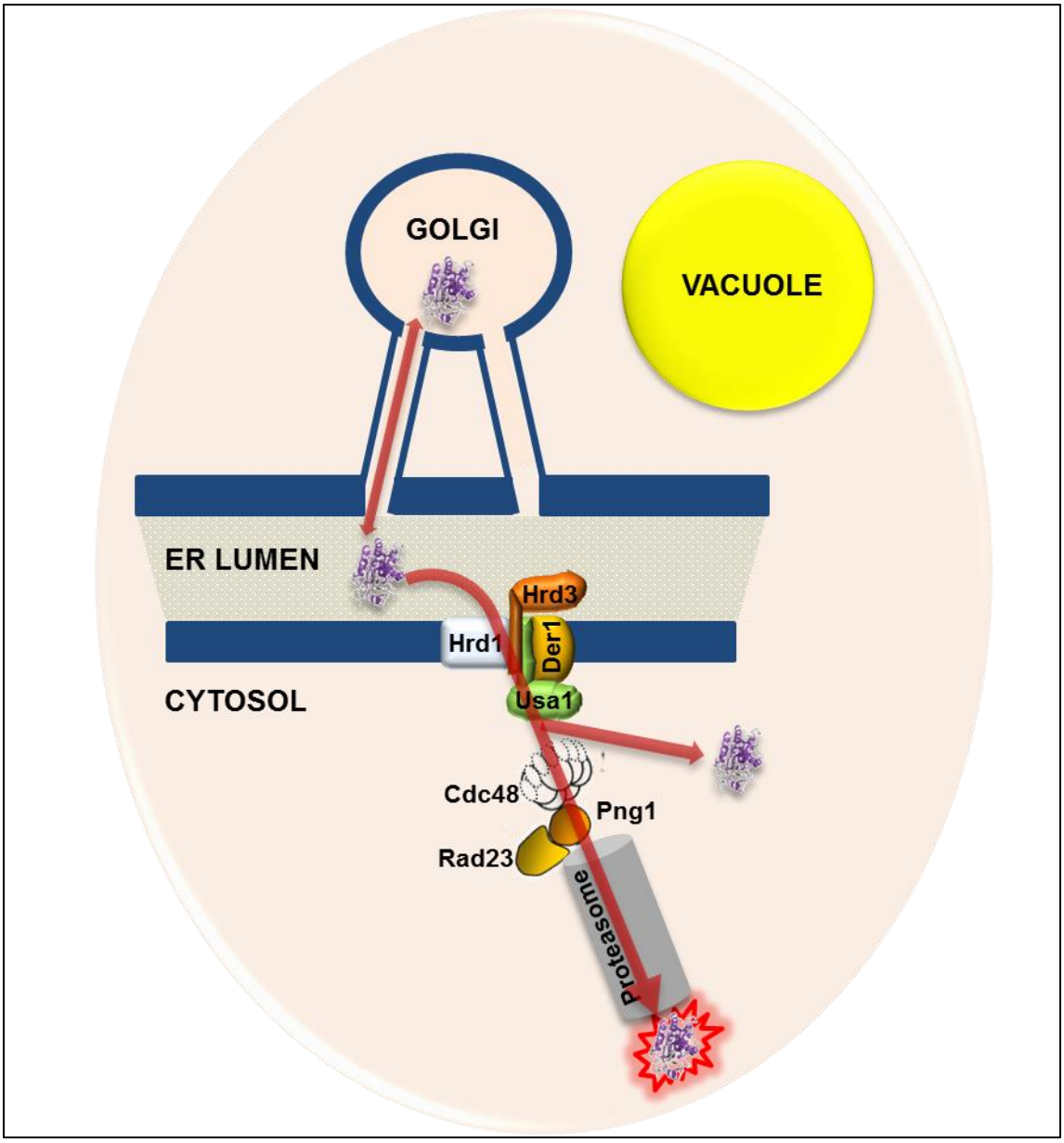

Figure 1.5 The ERAD pathway for RTA in yeast. The dislocation of RTA requires prior bidirectional ER-Golgi transport. RTA uses the Hrd1 ubiquitin ligase complex as the retrotranslocon for dislocation. The Hrd1 ubiquitin complex consists of Hrd1, Hrd3, Der1 and Usa1. After RTA enters into the cytosol, a misfolded RTA_{Δ} is deglycosylated by the cytosolic peptide:*N*-glycanase (Png1), which is linked to the Rad23 for efficient degradation in the proteasome. The folding conserved RTA_{E177D} can evade the proteasomal degradation.

SUMMARY OF WORK TO BE PRESENTED

The present research is focused on answering the questions of what trafficking pathway is exploited by RTA in yeast; how the structural features of RTA is related to its trafficking and toxicity; What function of *N*-glycosylation of RTA is in signaling the ERAD in the ER luminal side and the cytosolic side; What and how the cellular components are involved in the RTA toxicity. To directly visualize the intracellular trafficking of RTA in yeast, the enhanced green fluorescent protein (EGFP) was tagged to the precursor and mature forms of RTA and its mutants (Figure 1.6). The toxicity of RTA was assessed by the viability assay as an end point measurement of the activity of RTA (Figure 1.7). The depurination assay was conducted at several time points as readouts to indicate the kinetic of depurination reaction of RTA (Figure 1.8). In chapter two, mutational analysis was conducted to reveal the function of the 26-amino acid signal peptide and nine-amino acid propeptide within the N-terminal extension of RTA. Since the *N*-glycosylation is considered as an important recognition signal for the ERAD substrate, the role of *N*-glycosylation in the intracellular trafficking and toxicity of RTA will be presented. In chapter three, to extend the understanding of the intracellular trafficking of RTA, a series of nontoxic RTA mutants identified from random mutagenesis were used. I investigated the effects of altered sequence motifs on the trafficking and toxicity of RTA. The requirement for the ERAD component Png1 of RTA mutants was tested. Finally, in chapter four, the cellular components that potentially contribute to the toxicity of RTA were pooled out from a genome-wide screen against RTA. I investigated the

trafficking, toxicity and depurination of RTA in the deletion strains to determine the role of each component in the RTA intoxication.

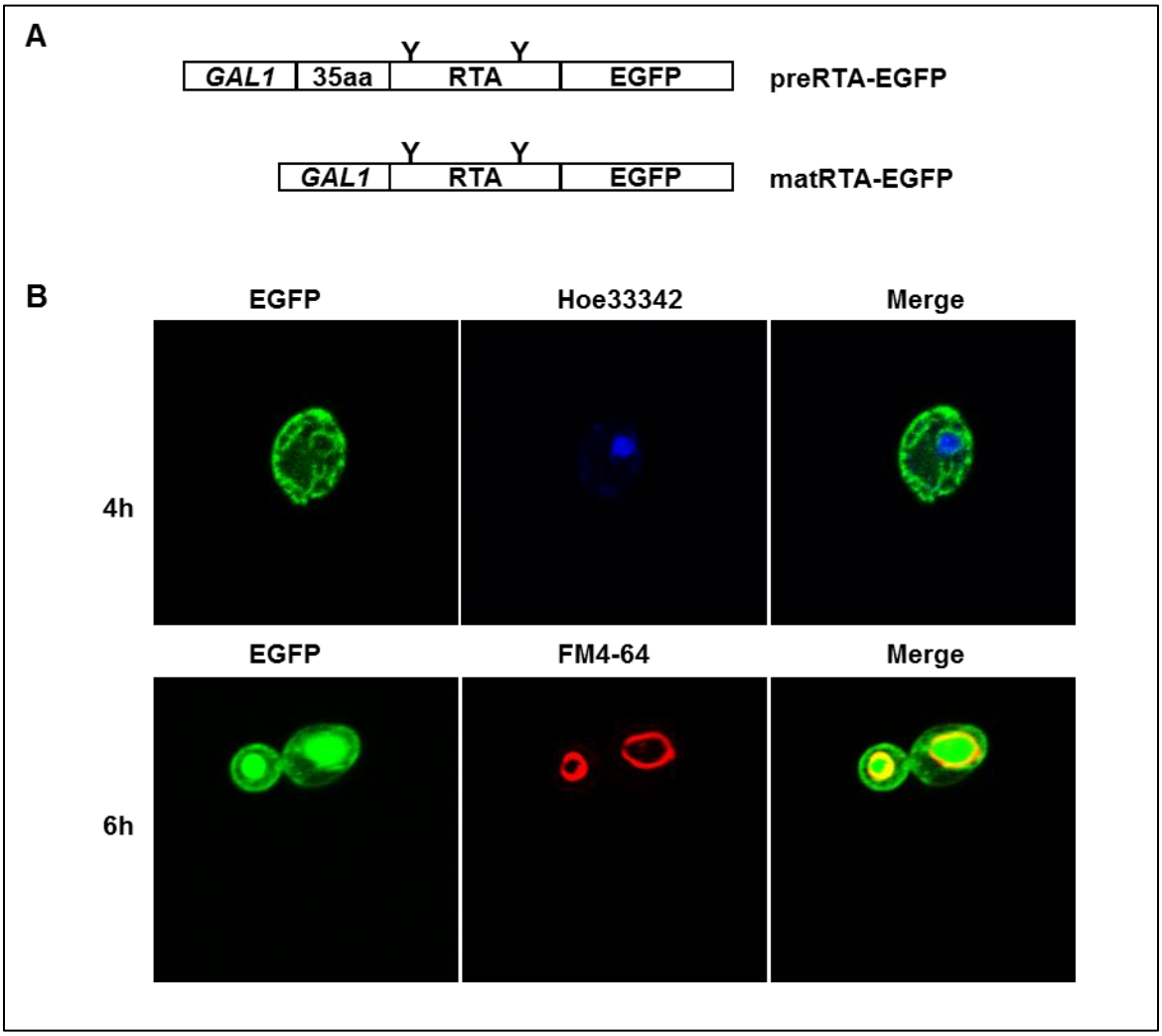

Figure 1.6 The RTA-EGFP fusions. (A) Schematic of precursor and mature RTA with EGFP tag fusions. PreRTA with 35-residue N-terminal extension (including 26-amino acid residue signal peptide and nine-amino acid propeptide) or mature RTA with only 267-residue RTA are fused with the EGFP at the C-termini. The expression is under the control of the inducible *GAL1* promoter. (B) The localization of EGFP tagged preRTA in live *Saccharomyces cerevisiae*. Wild type yeast cells carrying preRTA-EGFP were grown in SD medium with glucose and induced with galactose for the time point indicated in the figure. Yeast cells were treated with Hoechst 33342 to stain the nucleus or with FM4-64 to stain the vacuole. The intracellular localization of preRTA-EGFP was performed with Zeiss

LSM 710 Confocal Microsope. Merged images show localization of preRTA-EGFP relative to the nucleus or the vacuole.

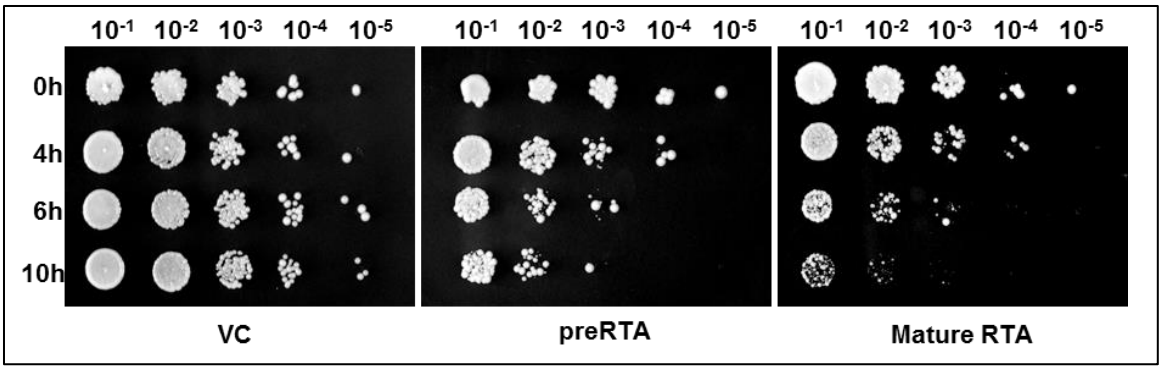

Figure 1.7 Viability of yeast cells expressing vector control (VC), preRTA and mature RTA. Yeast cells were first grown in SD-Leu supplemented with 2% glucose and then transferred to SD-Leu supplemented with 2% galactose. At the indicated hours of post induction, a series of ten-fold dilutions were plated on media containing 2% glucose and grown at 30 ^{o}C for approximately 48 h. The yeast cells expressing preRTA and mature RTA had growth defects compared with the cells expressing vector control (VC).

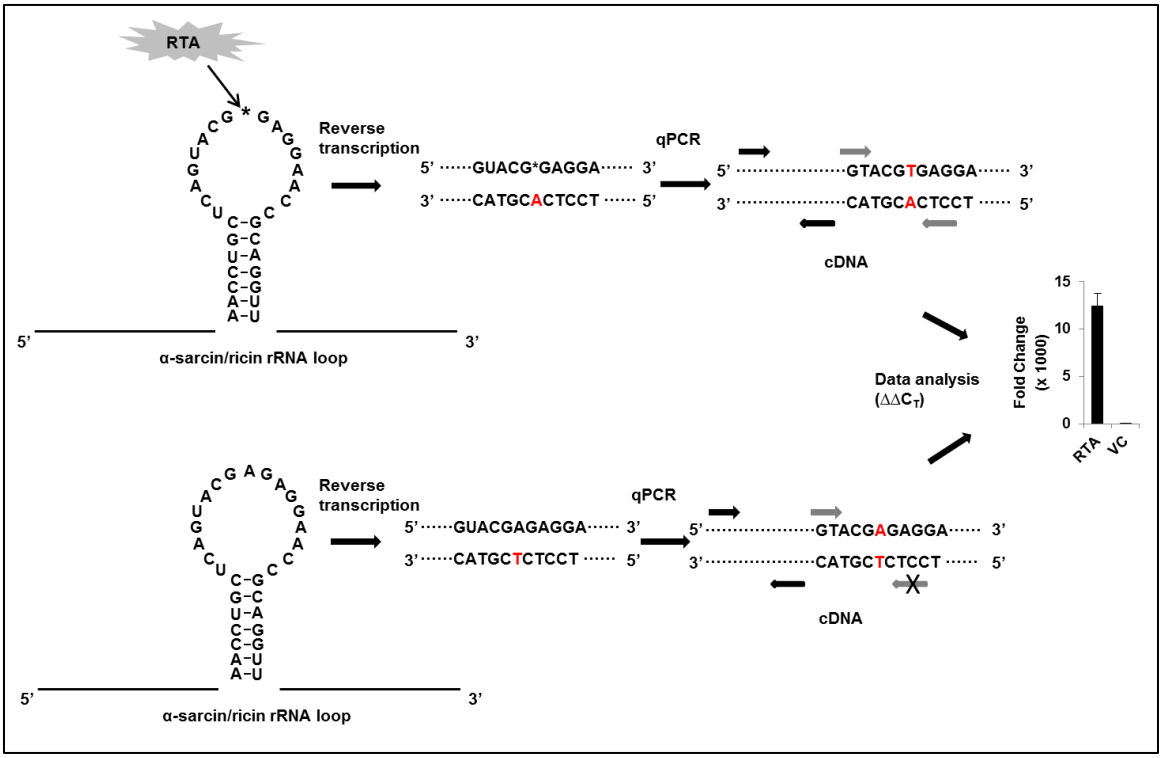

Figure 1.8 Schematic representation of the depurination analysis by qRT-PCR. RTA depurination leaves an abasic site on the yeast 25S rRNA. The reverse transcriptase incorporates an adenosine (A) opposite to the lesion, leading to an A to T transversion on the synthesized cDNA strand. The reference primer set amplifies the cDNA away from the altered site, quantifies the total 25S rRNA. The target primer set specifically anneals to the altered site, quantifies the depurinated rRNA. The data are then analyzed with the $\Delta\Delta C_T$ Method.

CHAPTER 2: *N*-glycosylation does not affect the catalytic activity of ricin A chain but stimulates cytotoxicity by promoting its transport out of the endoplasmic reticulum

SUMMARY

Ricin A chain (RTA) depurinates the α-sarcin/ricin loop after it undergoes retrograde trafficking to the cytosol. The structural features of RTA involved in intracellular transport are not known. To explore this, we fused EGFP to precursor (preRTA-EGFP), containing a 35-residue leader, and mature RTA (matRTA-EGFP). Both were enzymatically active and toxic in *S. cerevisiae*. PreRTA-EGFP was localized in the endoplasmic reticulum (ER) initially and was subsequently transported to the vacuole, while mature RTA remained in the cytosol, indicating that ER localization is a prerequisite for vacuole transport. When the two glycosylation sites in RTA were mutated, mature form was fully active and toxic, suggesting that the mutations do not affect catalytic activity. However, nonglycosylated preRTA-EGFP had reduced toxicity, depurination and delayed vacuole transport, indicating that *N*-glycosylation affects transport of RTA out of the ER. Point mutations in the C-terminal hydrophobic region restricted RTA to the ER and eliminated toxicity and depurination, indicating that this sequence is critical for ER exit. These results demonstrate that *N*-glycosylation and the C-terminal hydrophobic region stimulate the toxicity of RTA by promoting ER export. The timing of depurination coincided with the timing of

vacuole transport, suggesting that RTA may enter the cytosol during vacuole transport.

INTRODUCTION

Ricin, extracted from the castor bean (*Ricinus communis*), is a type 2 ribosome-inactivating protein (RIP) or an AB toxin, consisting of a catalytic A chain (RTA) linked to a cell binding B chain (RTB). RTA is an *N*-glycosidase, which specifically depurinates an adenine residue from the universally conserved α-sarcin/ricin loop (SRL) in the 28S rRNA, inhibiting protein synthesis (17). RTB is a lectin which specifically binds to cell surface glycolipids or glycoproteins with β-1,4-linked galactose residues and facilitates endocytosis of RTA (60). Ricin is one of the most toxic substances known and can cause severe morbidity and mortality. There are no specific protective measures or therapeutics effective against ricin intoxication and there is an urgent unmet need for therapy. In the castor bean, ricin is synthesized as a preproprotein with a 35-residue N-terminal leader, followed by the 267-residue mature RTA, which is connected to the 262-residue RTB by a 12-residue internal linker. Preproricin is translocated to the endoplasmic reticulum (ER) via the first 26-residue signal peptide in plants (61). After cleavage of the signal sequence in the ER, proricin is *N*-glycosylated, a disulfide bond is formed between RTA and RTB and within RTB (1). Proricin is then transported via the Golgi complex to the vacuole where the N-terminal nine-residue propeptide and the linker between RTA and RTB are processed to form

mature ricin, which accumulates in protein storage vacuoles in the castor bean endosperm (62).

In mammalian cells, ricin is internalized either by clathrin-dependent or clathrin-independent mechanisms (60). After endocytosis, ricin is initially delivered to early endosomes. From there, it is either recycled back to the cell surface or delivered via late endosomes to lysosomes and is eventually degraded. Only a small portion of ricin follows the retrograde pathway from endosomes to the trans-Golgi network (TGN) (63). RTA is active only after it is separated from RTB in the ER by reduction of the disulfide bond (44). Reductive separation of RTA and RTB in the ER exposes a hydrophobic region at the C-terminus, which is proposed to mediate the association of RTA with the ER membrane (47, 48). RTA enters the cytosol by a process termed dislocation or retrotranslocation (56, 64). Dislocation is the most critical step in RTA trafficking, since RTA exerts its toxic effect on ribosomes after it enters the cytosol. RTA is thought to utilize the specific components of the ER associated degradation (ERAD) pathway for dislocation and has unique characteristics compared with other ERAD substrates (65). Since very few RTA molecules reach the Golgi and the ER in mammalian cells, RTA variants containing sulfation and glycosylation sites have been used to study retrograde transport (66). These studies identified components of the ERAD pathway, such as the ER degradation enhancing α–mannosidase I-like protein (EDEM), which participates in dislocation of RTA (4). Yeast has been used to probe the mechanism of dislocation of RTA by targeting enzymatically attenuated RTA variants to the ER lumen (67). A folding

competent RTA variant required the Hrd1p (HMG-CoA reductase degradation-1 protein) for dislocation in yeast (67). Trafficking to the Golgi from the ER was also required for dislocation of the RTA variants in yeast (67). SEL1L, a regulator of the HRD complex, promoted dislocation of an enzymatically attenuated RTA variant to the cytosol in mammalian cells (68). Png1p, Htm1p and Yos9p were implicated in the degradation of a glycosylated structurally defective RTA variant, but were not required for efficient degradation of the nonglycosylated form (69). Some of these studies were carried out with enzymatically attenuated RTA variants, which may differ from wild type RTA in their requirements for dislocation, while others with structurally defective forms, which were unable to fold into an active conformation and appeared to act as *bonafide* ERAD substrates.

Structural features of wild type RTA involved in dislocation remain to be determined. Ricin contains four glycosylation sites, two on RTA and two on RTB. *N*-glycosylation occurs on asparagines 10 and 236 in the consensus Asn-X-Ser/Thr motifs in RTA (70) in the ER (66). The role of *N*-glycosylation in intracellular transport, *in vivo* depurination and cytotoxicity of RTA has not been examined. Recombinant nonglycosylated RTA is as active in inhibiting protein synthesis as plant derived glycosylated RTA *in vitro* (8), suggesting that glycosylation does not affect the catalytic activity of RTA. However, deglycosylated RTA is approximately one thousand fold less toxic than glycosylated RTA in mice and has been evaluated as a vaccine (71). Toxicity of ricin isoforms correlates with their glycosylation levels in immunotoxins targeted

against cancer cells (72). Moreover, addition of a C-terminal glycosylation signal increases the toxicity of the recombinant RTA compared to the nonglycosylated form (66). These studies suggest a potential role for glycosylation in the toxicity of RTA. However, glycosylation was reported not to affect trafficking, since both glycosylated and nonglycosylated ricin precursor ultimately accumulated in the protein bodies in the castor bean (62).

In the present study, we examine the trafficking of wild type RTA in yeast using the EGFP tagged precursor, which contains the native N-terminal leader. We investigate the role of glycosylation in intracellular transport, depurination activity and cytotoxicity of wild type RTA. Our results show that RTA is transported to the ER initially and then to the vacuole. Mutation of the *N*-glycosylation sites does not affect the catalytic activity of RTA, but reduces toxicity and delays depurination and vacuole transport. These results demonstrate for the first time that *N*-glycosylation contributes to the toxicity of RTA by promoting more efficient transport out of the ER. Mutation of the C-terminal hydrophobic stretch prevents vacuole transport, depurination and cytotoxicity, indicating that this sequence is critical for ER exit.

RESULTS

The precursor form of RTA is transported from the ER to the vacuole in yeast

To examine the trafficking of RTA *in vivo* in yeast, we fused the enhanced green fluorescent protein (EGFP) to the C-terminal end of the precursor (preRTA-EGFP) or the mature form of RTA (matRTA-EGFP) (Figure 2.1A). The

preRTA-EGFP contained the native 35-residue N-terminal leader followed by the mature RTA, while matRTA-EGFP did not contain the leader. To determine if the C-terminal EGFP fusions affected the toxicity of RTA, we examined the viability of yeast expressing preRTA or mature RTA with or without EGFP at 10 hours post induction (hpi) (Figure 2.1B). EGFP tagging reduced the toxicity of preRTA. However, preRTA-EGFP was still 12 times more toxic than the vector control (VC) (Figure 2.1B). EGFP tagging did not affect the toxicity of mature RTA. Both matRTA and matRTA-EGFP were about two orders of magnitude more toxic than VC. PreRTA and preRTA-EGFP were slightly less toxic than matRTA and matRTA-EGFP, respectively (Figure 2.1B). PreRTA and matRTA with the C-terminal EGFP tag had similar depurination activity as preRTA and matRTA without the EGFP tag by dual primer extension analysis (73) at 10 hpi (Figure 2.1C). Furthermore, recombinant matRTA-EGFP had similar activity (IC_{50} 31.3 pM) as the recombinant matRTA without the EGFP tag (IC_{50} 28.4 pM) by *in vitro* translation in the rabbit reticulocyte lysate (Figure 2.1D). Thus, the presence of the EGFP tag does not affect the depurination activity of RTA or its ability to inhibit translation, while causing some reduction in the toxicity of preRTA.

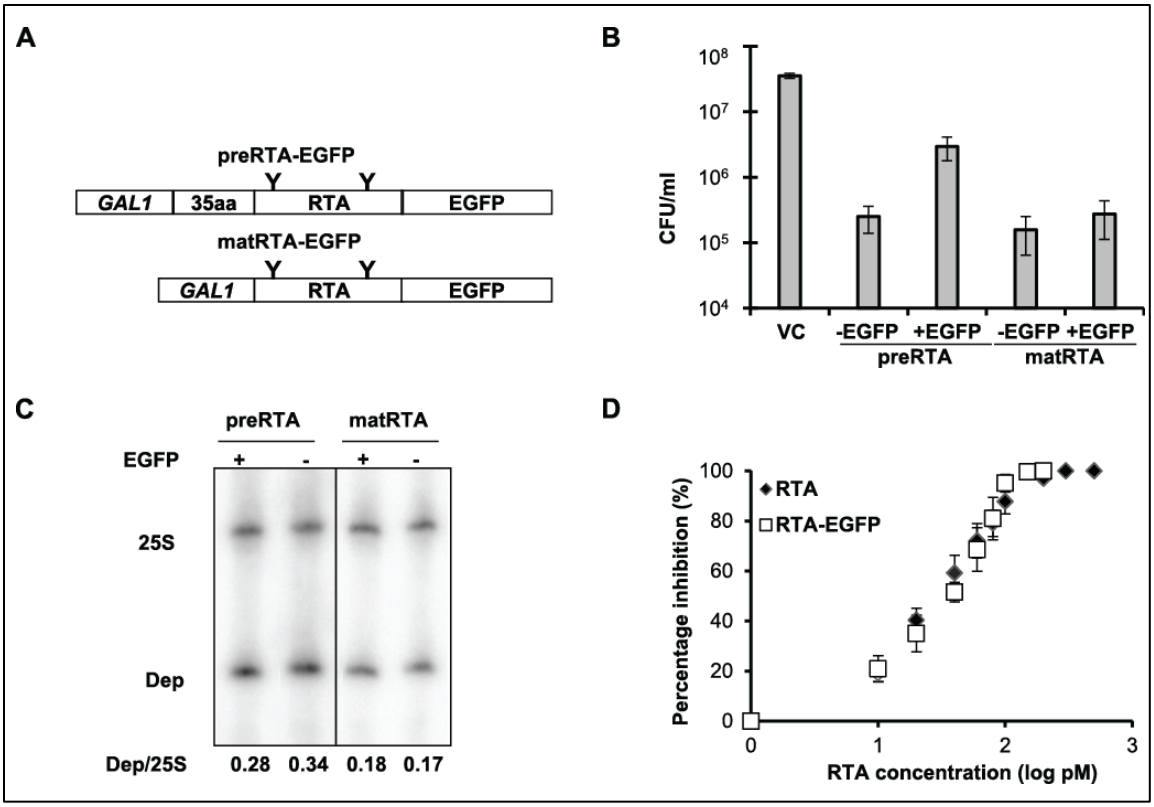

Figure 2.1 Cytotoxicity and enzymatic activity of RTA-EGFP fusions. (A) Schematic representation of the C-terminal EGFP fusions with the precursor (preRTA-EGFP) and mature form of RTA (matRTA-EGFP). PreRTA contains the 35-residue leader and the 267-residue mature RTA, while mature RTA contains only the 267-residue RTA downstream of the *GAL1* promoter. "Y" indicates the glycosylation sites. (B) Viability of yeast harboring the empty vector (VC), preRTA, preRTA-EGFP, mature RTA and mature RTA-EGFP. The CFU/ml was calculated based on the analysis of eleven different transformants at 10 hpi. (C) Ribosome depurination in yeast expressing the precursor and mature form of RTA with and without the EGFP tag. Total RNA isolated after 10 h of growth on galactose was analyzed by dual primer extension analysis using two different end-labeled primers, the depurination primer (Dep), which was used to measure the extent of depurination, and the 25S rRNA primer (25S), which was used to measure the total amount of 25S rRNA (73). The depurination was quantified by calculating the ratio between the intensity of depurination product (Dep) relative to the intensity of the 25S rRNA (25S) and is shown below each lane. (D) Translation inhibition by recombinant RTA-EGFP and recombinant RTA without EGFP. Purified RTA-EGFP and RTA were added to the Flexi Rabbit Reticulocyte Lysate System at 0, 10, 20, 40, 60, 80, 100, 200, 500, 1000 pM. The reaction was incubated at 30 °C for 30 min and the luciferase activity was measured. Data are the mean ± SE of at least 3 individual experiments.

We examined the localization of preRTA-EGFP at various times after induction by epifluorescence microscopy. PreRTA-EGFP showed perinuclear localization at 2 hpi indicative of ER localization (Figure 2.2A). To determine if it co-localized with the ER, preRTA-EGFP and matRTA-EGFP were transformed into yeast harboring the ER marker, RFP-tagged Alg9 (Alg9-RFP) (74). Epifluorescence microscopy indicated that preRTA-EGFP co-localized with the ER marker, while matRTA-EGFP did not (Figure 2.3). The perinuclear pattern was confirmed by indirect immunofluorescence with yeast harboring preRTA without the EGFP tag (Figure 2.4). At 4 hpi, preRTA-EGFP co-localized with the vacuole in 40% of the cells (*n*=57) as indicated by co-localization with the red-fluorescent probe FM4-64, which stains the vacuole membranes (75) (Figure 2.2A). At 6 hpi, 88% (*n*=54) and at 24 hpi 100% (*n*=33) of preRTA-EGFP co-localized with the vacuole. In contrast, matRTA-EGFP remained in the cytosol at all time points (Figure 2.2B). Immunoblot analysis indicated that preRTA-EGFP migrated slower than matRTA-EGFP, suggesting that it was glycosylated (Figure 2.2C). In order to distinguish the glycosylated form from the nonglycosylated form, yeast membrane fraction was treated with Endoglycosidase H (Endo H), which cleaves the *N*-linked mannose-rich oligosaccharides (76). The slower migrating form changed in mobility after Endo H treatment (Figure 2.2C), indicating that it represented the *N*-glycosylated form of preRTA-EGFP. In contrast, matRTA-EGFP only had a single form, which did not change in mobility after EndoH treatment, indicating that it was not glycosylated (Figure 2.2C). These results confirmed that preRTA-EGFP was translocated into the ER and was glycosylated,

while matRTA-EGFP remained in the cytosol and was not glycosylated. To confirm that vacuole localization was not an artifact of the EGFP tag, we isolated the vacuole fraction from cells expressing preRTA without EGFP and preRTA-EGFP at 14 hpi. Immunoblot analysis showed that both preRTA and preRTA-EGFP were present in the vacuole, as well as in the membrane and cytosol (Figure 2.2D). The vacuole fraction had some ER membrane contamination based on the signal from Dpm1p, the ER membrane marker. However, the amount of Dpm1p in the vacuole fraction was only 18% of that in the membrane fraction, while RTA expression level was similar in the two fractions (Figure 2.2D), suggesting that the presence of RTA in the vacuole fraction was not due to the ER contamination. The preRTA appeared as several forms in the vacuole fraction, which may be due to processing in the vacuole. The vacuole marker, Vph1p, encoding the Vacuolar H^+-ATPase was 100-kDa in the membrane fraction, but 75-kDa in the vacuole fraction (Figure 2.2D), possibly due to proteolysis during vacuole isolation (77). These results demonstrate that the 35-residue N-terminal leader contains information for targeting RTA to the ER and from the ER to the vacuole in yeast and provide evidence that ER localization is a prerequisite for vacuolar transport.

Ribosome depurination is a sensitive indicator of RTA transport to the cytosol. We examined the level of depurination over time using qRT-PCR (Figure 2.2E) (78). In this assay, two pairs of primers are used to amplify the target amplicon (depurinated SRL) and the reference amplicon (25S rRNA) and the data are analyzed by the comparative ΔC_T method ($\Delta\Delta C_T$) (78). Depurination

level of preRTA-EGFP was negligible at 0 hpi, but matRTA-EGFP had detectable depurination activity, which was 15-fold higher than preRTA-EGFP. However, at 2 hpi preRTA-EGFP had similar depurination level as matRTA-EGFP, suggesting that preRTA-EGFP dislocated to the cytosol at 2 hpi. The depurination level for both proteins reached a peak level at 4 hpi. At 6 and 8 hpi, the depurination level of preRTA-EGFP was higher than that of matRTA-EGFP. These results indicate that the depurination by preRTA-EGFP was delayed compared to matRTA-EGFP, possibly because preRTA-EGFP was transported to the ER. The delayed depurination of preRTA-EGFP was consistent with its lower cytotoxicity compared to matRTA-EGFP (Figure 2.1B).

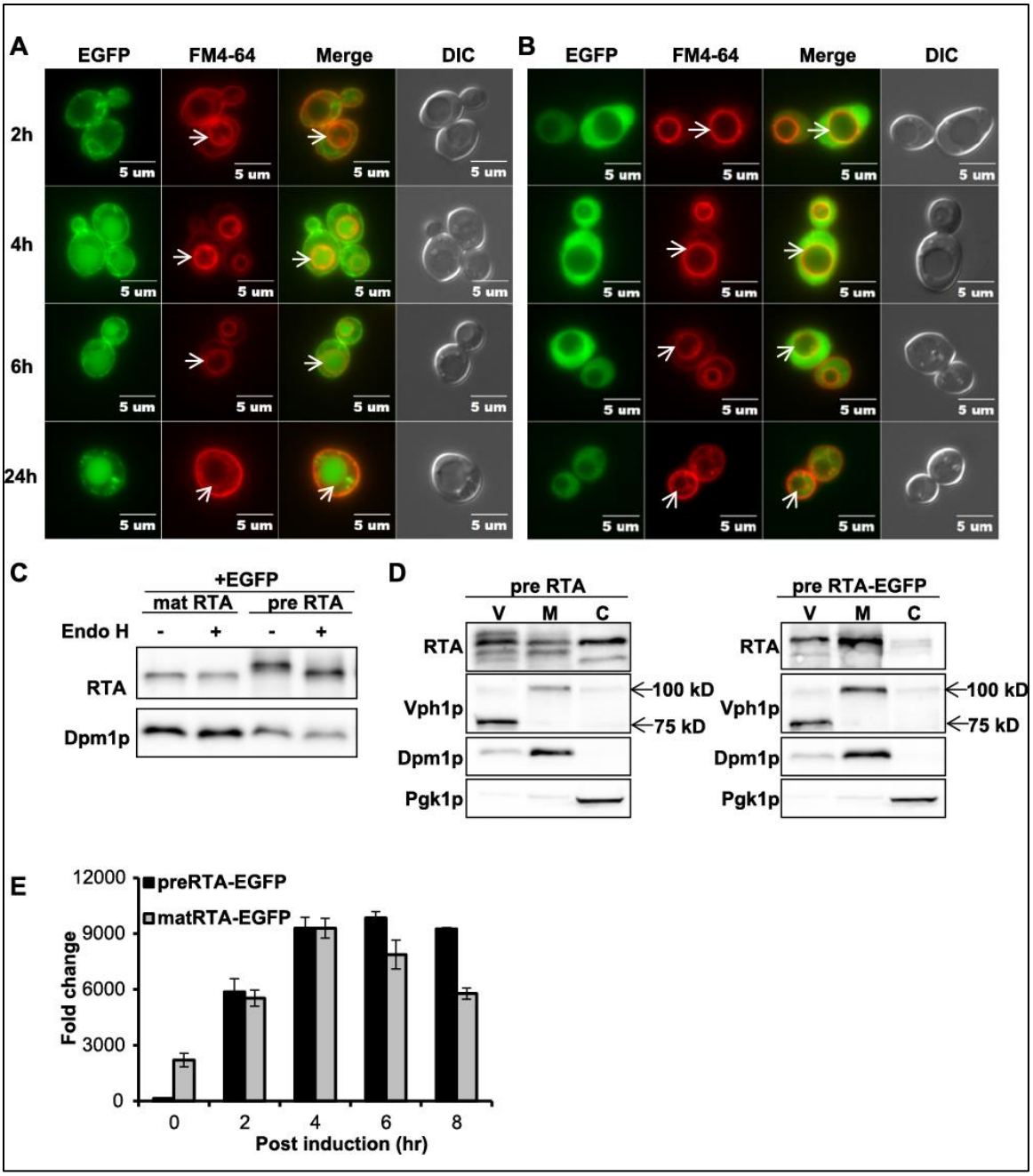

Figure 2.2 Intracellular transport, protein expression and depurination activity of preRTA-EGFP and mature RTA-EGFP. (A) Localization of preRTA-EGFP and (B) mature RTA-EGFP. Yeast cells were grown in SD medium with glucose and induced with galactose. The images were taken at 2, 4, 6 and 24 hpi with an Olympus BX41 fluorescence microscope. Yeast cells were treated with FM4-64 to stain the vacuole. Merged images show localization of each protein relative to the vacuole. The arrows indicate the vacuoles. (C) Immunoblot analysis of mature RTA-EGFP and preRTA-EGFP. Membrane fraction isolated at 6 hpi was treated with (+) or without (-) Endo H to cleave the glycans. The proteins (5 µg) were separated on a 10% SDS-polyacrylamide gel and probed with monoclonal anti-RTA (1:5000). The blot was reprobed with the ER

membrane marker Dpm1p as a loading control. (D) Immunoblot analysis of preRTA and preRTA-EGFP in vacuole (V), membrane (M) and cytosol (C) fractions. The proteins (5 µg) were separated on a 10% SDS-polyacrylamide gel and probed with monoclonal anti-RTA (1:5000). The blot was reprobed with vacuole membrane marker Vph1p, ER membrane marker, Dpm1p and cytosol marker, Pgk1p. (E) Ribosome depurination by preRTA-EGFP and matRTA-EGFP *in vivo* by qRT-PCR. Yeast ribosomes were extracted at 0, 2, 4, 6 and 8 hpi. Two pairs of primers were designed to amplify the target amplicon (depurinated SRL) and the reference amplicon (25S rRNA) (78). The data was analyzed by the comparative ΔC_T method ($\Delta\Delta C_T$). The y-axis indicates the fold change in depurination in yeast harboring the preRTA-EGFP and matRTA-EGFP over yeast harboring the empty vector. Data are mean ± SD from triplicates.

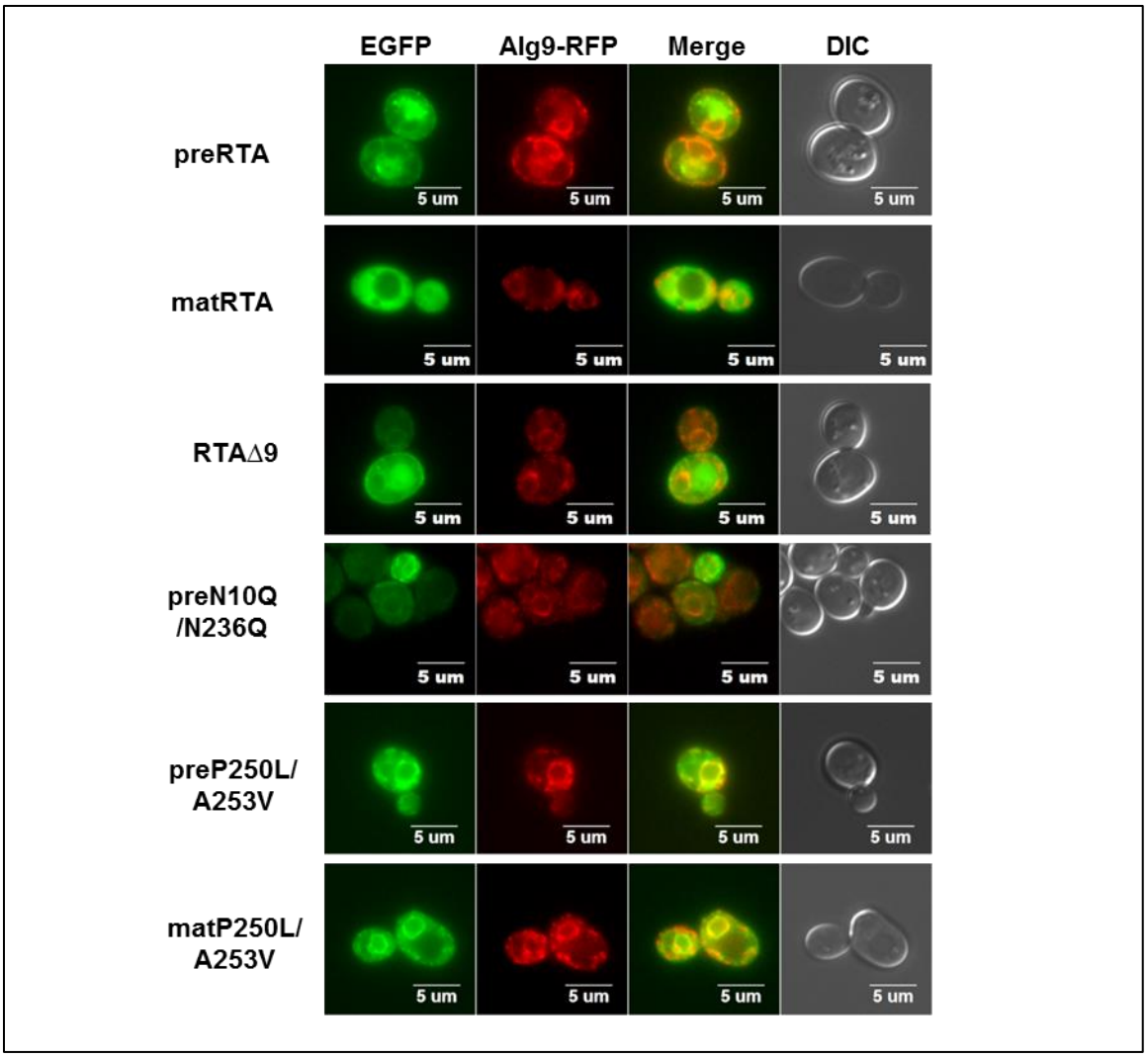

Figure 2.3 Co-localization of EGFP tagged wild type and mutant forms of RTA with the ER marker Alg9-RFP. The images were taken at 6 hpi with Olympus BX41 fluorescence microscope.

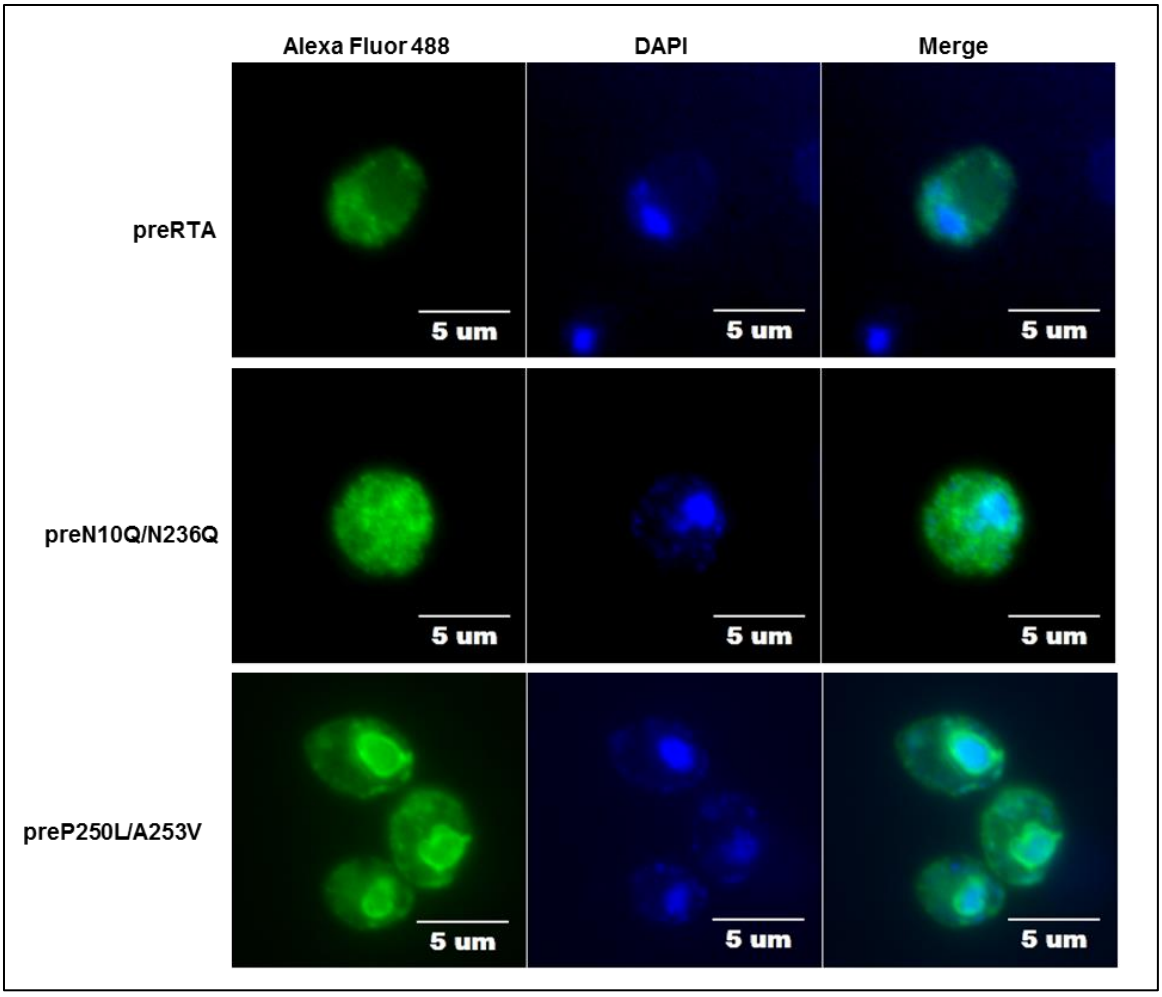

Figure 2.4 Indirect immunofluorescence of wild type and mutant forms of RTA. Yeast cells harboring preRTA, preN10Q/N236Q and preP250L/A253V were collected at 6 hpi and fixed with paraformaldehyde and spheroplasted with lyticase. The cells were attached to a poly-L-lysine coated Teflon slide and were incubated with primary monoclonal antibody against RTA and Alexa Fluor 488 conjugated anti-mouse secondary antibody. The nuclei were stained with DAPI. Merge shows perinuclear localization of the protein. The images were taken with Olympus BX41 epifluorescence microscope.

In tobacco, the first 26 amino acids of the 35-residue leader of RTA act as the signal peptide (61), while the following nine residues affect co-translational import and the extent of glycosylation (79). To determine if the N-terminal 26 and nine amino acids function similarly in yeast, we deleted the first 26 residues (RTAΔ26-EGFP) and the subsequent nine residues (RTAΔ9-EGFP) separately

and constructed C-terminal EGFP fusions with each protein (Figure 2.5A). Epifluorescence microscopy showed that RTAΔ26-EGFP remained in the cytosol at all time points after induction (Figure 2.5B) as matRTA-EGFP (Figure 2.2B), indicating that the first 26 residues are required for ER targeting in yeast as in plants.

RTAΔ26-EGFP migrated as a single band on SDS-PAGE, which did not change in mobility after Endo H treatment (Figure 2.5C), indicating that it was not glycosylated. RTAΔ26-EGFP reduced viability about 50-fold compared to the vector control at 10 hpi, and was almost as toxic as matRTA-EGFP (Figure 2.5D). Comparison of the level of depurination in yeast expressing RTAΔ26-EGFP with matRTA-EGFP (Figure 2.5F) showed that RTAΔ26-EGFP caused lower level of depurination than matRTA-EGFP at 4 hpi, but similar level of depurination at later time points. These results suggested that the presence of the nine-residue propeptide in RTAΔ26-EGFP did not have a major effect on the depurination activity and toxicity.

RTAΔ9-EGFP co-localized with the ER at 2 and 4 hpi (Figure 2.5E), which was confirmed by transforming RTAΔ9-EGFP into yeast harboring an ER marker (Figure 2.3). RTAΔ9-EGFP accumulated in the vacuole in 42% of the cells (*n*=78) at 6 hpi (Figure 2.5E), indicating that its vacuole transport was delayed. These results demonstrated that the nine-residue propeptide affected the transport of RTA to the vacuole. Immunoblot analysis (Figure 2.5C) showed that RTAΔ9-EGFP migrated as a single band and did not change in mobility after Endo H treatment, indicating that it was not glycosylated. RTAΔ9-EGFP migrated slower

than RTAΔ26-EGFP on SDS-PAGE (Figure 2.5C), suggesting incomplete cleavage of the signal peptide. Viability analysis showed that the cytotoxicity of RTAΔ9-EGFP was similar to preRTA-EGFP (Figure 2.5D). RTAΔ9-EGFP and preRTA-EGFP were more viable than RTAΔ26-EGFP and matRTA-EGFP at 10 hpi, suggesting that trafficking of RTAΔ9-EGFP and preRTA-EGFP to the ER delays depurination and reduces toxicity.

RTAΔ9-EGFP depurinated 1.7–fold less than preRTA-EGFP at 2 hpi, but reached a similar level at 4 hpi (Figure 2.5G). Subcellular fractionation at 6 hpi indicated that RTAΔ26-EGFP was present in the cytosol and membrane fraction and did not change in mobility after Endo H treatment (Figure 2.6A). In contrast, almost all of RTAΔ9-EGFP was associated with the membrane fraction and did not change in mobility after Endo H treatment (Figure 2.6A). These results demonstrate that the first 26 residues of the N-terminal leader mediate ER import, while the remaining nine residues influence ER import, glycosylation and vacuole transport of RTA.

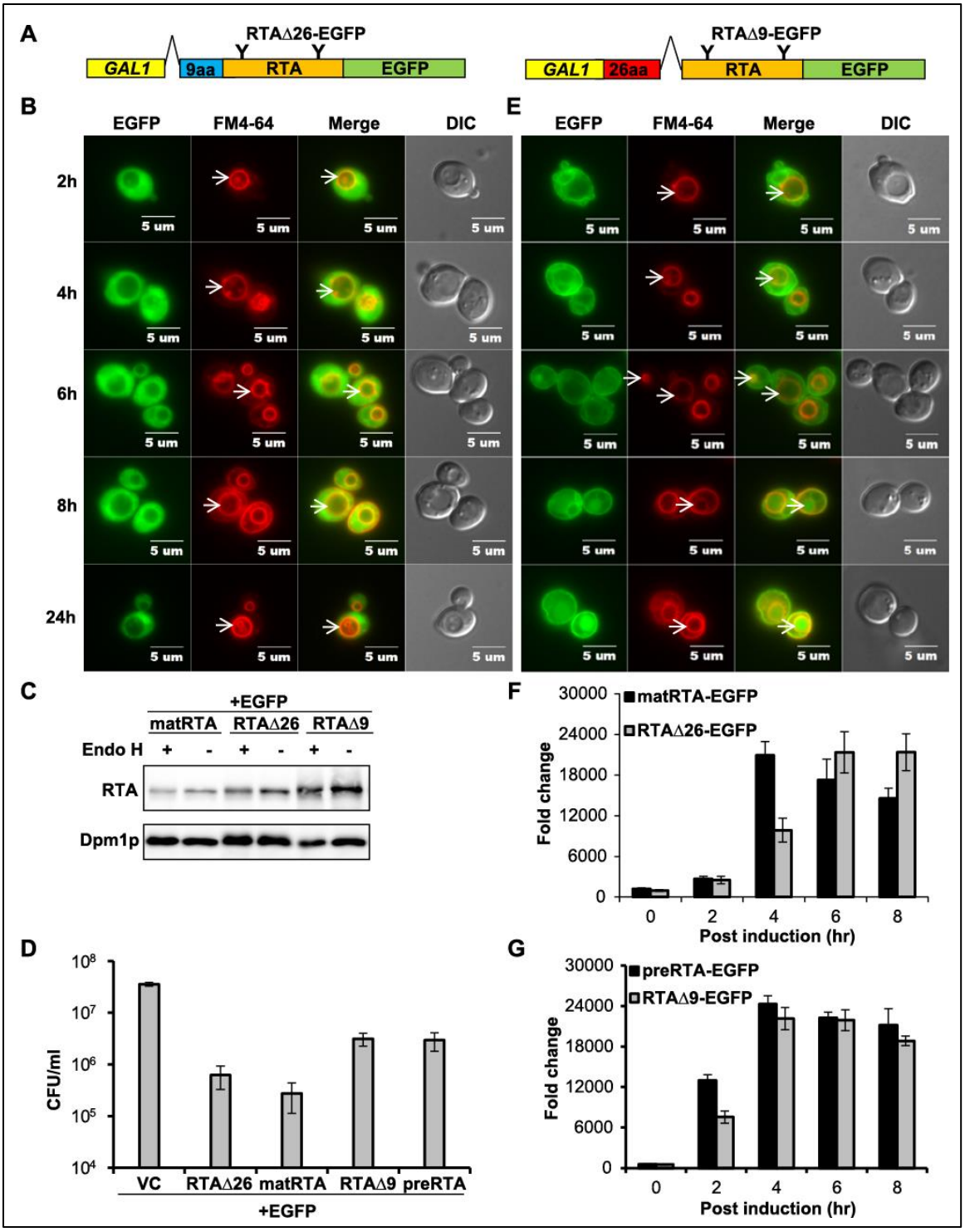

Figure 2.5 Intracellular transport, protein expression, cytotoxicity and depurination activity of RTAΔ26-EGFP and RTAΔ9-EGFP. (A) Schematic representation of RTAΔ26-EGFP and RTAΔ9-EGFP. RTAΔ26-EGFP contains a deletion of the 26-residue signal peptide, but contains the 9-residue propeptide upstream of the mature RTA. RTAΔ9-EGFP contains the 26-residue signal peptide, but does not contain the 9-residue propeptide upstream of the mature

RTA. (B) Intracellular transport of RTAΔ26-EGFP. Yeast cells expressing RTAΔ26-EGFP were grown in SD medium with glucose and induced with galactose. The images were taken at 2, 4, 6, 8 and 24 hpi with an Olympus BX41 fluorescence microscope. Cells were treated with FM4-64 to stain the vacuole. Merged images show localization of each protein relative to the vacuole. The arrows indicate the vacuoles. (C) Immunoblot analysis of membrane fraction isolated from cells expressing each protein at 6 hpi after treatment with (+) or without (-) Endo H to cleave the glycans. The proteins (5 µg) were separated on a 10% SDS-polyacrylamide gel and probed with monoclonal anti-RTA (1:5000). The blot was reprobed with the ER membrane marker Dpm1p as a loading control. (D) Viability of yeast expressing each protein and the vector control (VC). (E) Intracellular transport of RTAΔ9-EGFP was analyzed as in B. (F) Ribosome depurination by RTAΔ26-EGFP and matRTA-EGFP by qRT-PCR. (G) Ribosome depurination by RTAΔ9-EGFP and preRTA-EGFP by qRT-PCR. Data are mean ± SD from triplicates.

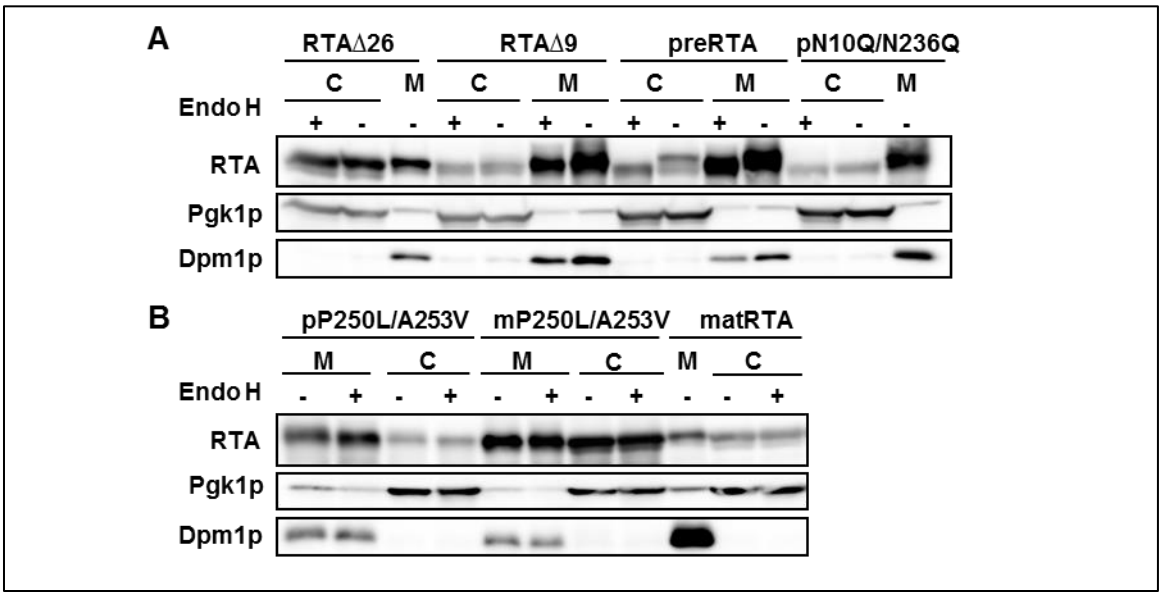

Figure 2.6 Subcellular fractionation of yeast expressing EGFP tagged wild type or mutant forms of RTA. Yeast cells were induced for 6 h, lysed and fractionated into membrane (M) and cytosol (C) fractions. The membrane and cytosol fractions were treated with (+) or without (-) Endo H to distinguish glycosylated proteins. The proteins were separated on a 10% SDS-polyacrylamide gel. Blots were initially probed with monoclonal anti-RTA and then reprobed with anti-Pgk1p and anti-Dpm1p.

Glycosylation of preRTA in the ER affects trafficking beyond the ER

The correlation observed between the absence of glycosylation and delayed vacuole transport of RTAΔ9-EGFP suggested that glycosylation might be important for transport of RTA out of the ER. To address this, we mutated the two glycosylation sites in RTA by substituting Asn10 and Asn236 with Gln (N10Q/N236Q). The C-terminal EGFP fusions were constructed with the precursor (preN10Q/N236Q-EGFP) and the mature (matN10Q/N236Q-EGFP) form (Figure 2.7A). As shown in Figure 2.7B, preN10Q/N236Q-EGFP was localized in the ER at 2 hpi and was detected in the vacuole in 45% of the cells (*n*=51) at 6 hpi, two hours later than wild type preRTA-EGFP (Figure 2.2A). Discrete foci were observed in cells expressing preN10Q/N236Q-EGFP (Figure 2.7B), possibly due to aggregation of the nonglycosylated preN10Q/N236Q-EGFP in the ER. The matN10Q/N236Q-EGFP remained in the cytosol at all time points (Figure 2.7C). Immunoblot analysis (Figure 2.7D) showed that preN10Q/N236Q-EGFP did not change in mobility after Endo H treatment, demonstrating the lack of glycosylation. The matN10Q/N236Q-EGFP comigrated with wild type matRTA-EGFP and did not change in mobility after EndoH treatment, consistent with cytosolic localization.

The viability analysis (Figure 2.7E) indicated that matN10Q/N236Q-EGFP had similar viability as wild type matRTA-EGFP. In contrast, preN10Q/N236Q-EGFP was more viable than wild type preRTA-EGFP. A similar increase in viability was observed when viability of untagged preN10Q/N236Q was compared to untagged wild type preRTA (Figure 2.8). These results confirmed

that the increase in viability of the preN10Q/N236Q-EGFP relative to wild type preRTA-EGFP was not due to the EGFP tag. Since transport of preN10Q/N236Q-EGFP to the vacuole was delayed in the absence of glycans, we further determined if the depurination activity was also affected. The depurination level of matN10Q/N236Q-EGFP and matRTA-EGFP was similar (Figure 2.7F). In contrast, depurination level of preN10Q/N236Q-EGFP was considerably lower than wild type preRTA-EGFP at all time points (Figure 2.7G). Depurination by preN10Q/N236Q-EGFP could not be detected until 4 hpi and the level was about one fourth of that observed with wild type preRTA-EGFP (Figure 2.7G). To confirm that this was not due to the EGFP tag, we examined depurination by the glycosylation mutants without the EGFP tag. Untagged matN10Q/N236Q depurinated at a similar level as untagged wild type mature RTA (Figure 2.9A), whereas depurination by untagged preN10Q/N235Q was inhibited and reached only about half the depurination level of the untagged wild type preRTA at 4 hpi (Figure 2.9B). These results demonstrate that the mutation of the glycosylation sites does not reduce the catalytic activity of RTA. However, lack of glycosylation reduces cytotoxicity by impairing depurination.

Subcellular fractionation indicated that only the glycosylated form of wild type preRTA-EGFP was observed in the ER, since it migrated faster after the Endo H treatment (Figure 2.6). The glycosylated form and a less abundant, faster migrating form were detected in the cytosol. Since RTA may be deglycosylated during dislocation (68), the less abundant form may represent the deglycosylated RTA. In contrast, preN10Q/N236Q-EGFP was primarily

associated with the membrane fraction (Figure 2.6A). A very low level of this mutant was detected in the cytosol and it migrated faster than the membrane associated fraction, suggesting that the nine-residue propeptide was processed. Since this processing step occurs in the vacuole (62), the faster migrating form might be released from the vacuole during the fractionation. The immunoblot analysis suggested that reduced depurination of preN10Q/N236Q-EGFP was not due to lower level of expression, since expression level of preRTA-EGFP and preN10Q/N236Q-EGFP was similar in the ER membrane (Figure 2.7D). These results indicate that glycosylation promotes transport of RTA out of the ER.

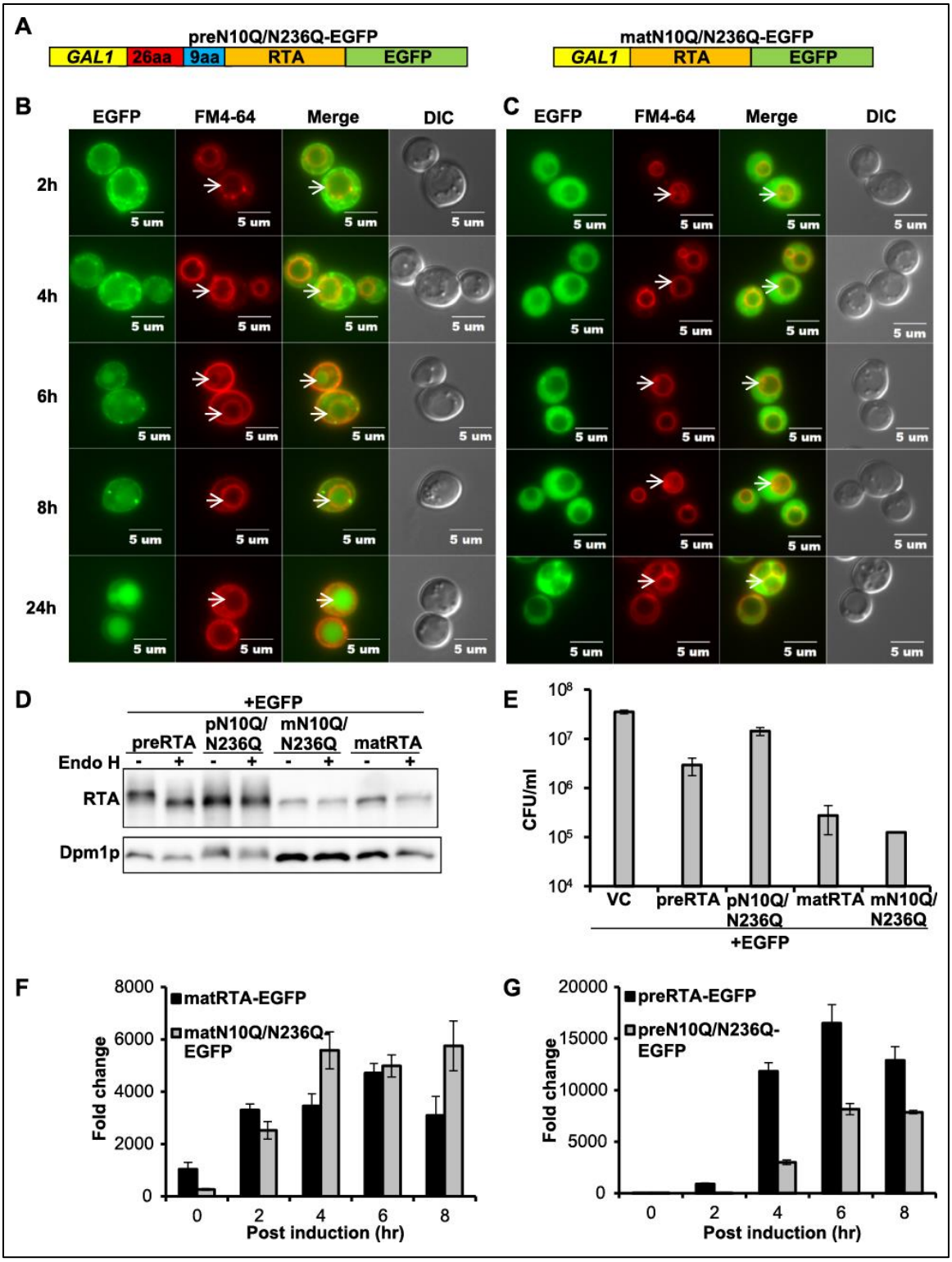

Figure 2.7 Intracellular transport, protein expression, cytotoxicity and depurination activity of the glycosylation mutants. (A) Schematic representation of preN10Q/N236Q-EGFP and matN10Q/N236Q-EGFP. Glycosylation sites at Asn10 and Asn236 were replaced with glutamine in both preRTA-EGFP and mature RTA-EGFP. (B) Trafficking of preN10Q/N236Q-

EGFP and (C) matN10Q/N236Q-EGFP. Yeast cells expressing each construct were grown in SD medium with glucose and induced with galactose. The images were taken at 2, 4, 6, 8 and 24 hpi with an Olympus BX41 fluorescence microscope. Vacuoles were stained with FM4-64. Merged images show localization of each protein relative to the vacuole. The arrows indicate the vacuoles. (D) Immunoblot analysis of membrane fraction isolated from cells expressing each protein at 6 hpi after treatment with (+) or without (-) Endo H to cleave the glycans. Protein (5 µg) was separated on a 10% SDS-polyacrylamide gel and probed with monoclonal anti-RTA (1:5000). The blot was reprobed with the ER membrane marker Dpm1p as a loading control. (E) Viability of yeast expressing each protein and the vector control (VC). (F) Ribosome depurination in yeast expressing matN10Q/N236Q-EGFP compared to matRTA-EGFP by qRT-PCR. (G) Ribosome depurination in yeast expressing preN10Q/N236Q-EGFP compared to preRTA-EGFP by qRT-PCR. Data are mean ± SD from triplicates.

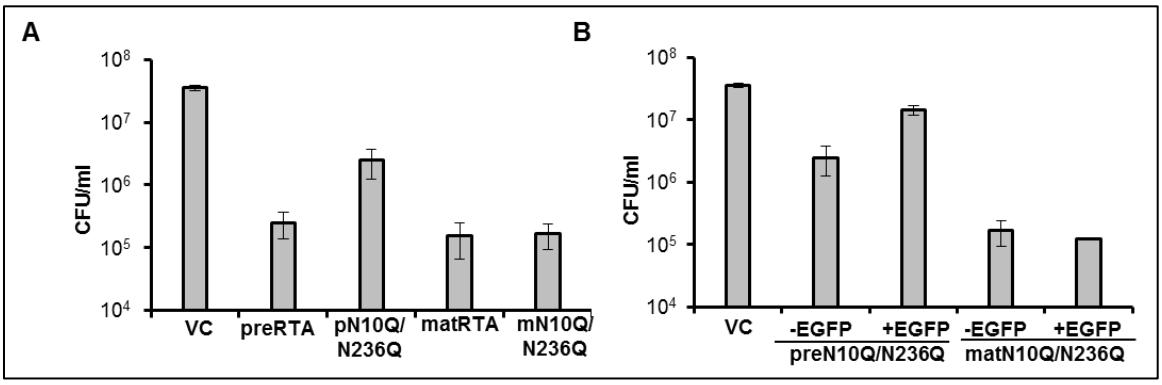

Figure 2.8 Viability of yeast expressing EGFP-tagged or untagged glycosylation mutants of RTA. (A) Viability of yeast harboring the empty vector (VC), preRTA, preN10Q/N236Q, matRTA and matN10Q/N236Q without the EGFP tag. (B) Viability of yeast harboring the empty vector (VC), preN10Q/N236Q, preN10Q/N236Q-EGFP, matN10Q/N236Q and matN10Q/N236Q-EGFP. The CFU/ml was calculated based on at least three different transformants at 10 hpi.

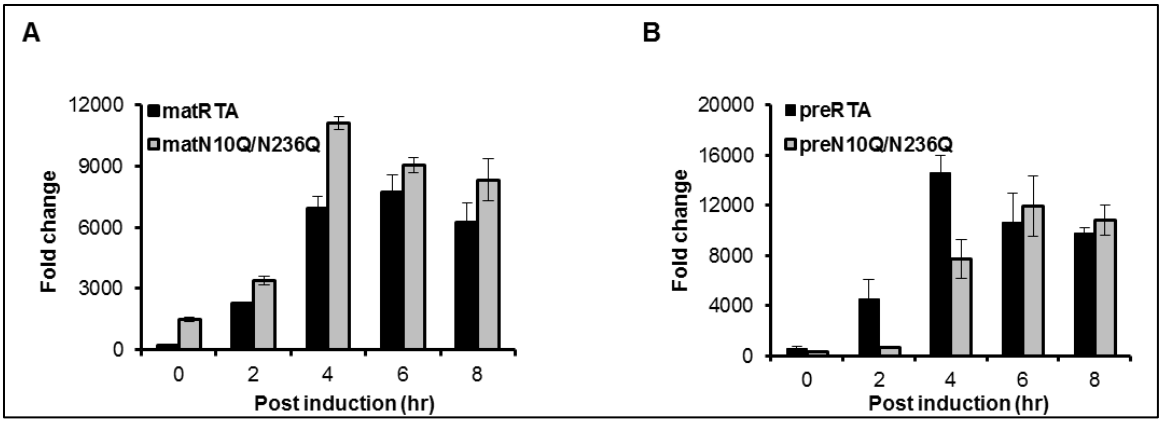

Figure 2.9 Ribosome depurination in yeast expressing untagged glycosylation mutants of RTA. (A) Ribosome depurination in yeast expressing untagged matN10Q/N236Q compared to untagged wild type mature RTA (matRTA) by qRT-PCR (B) Ribosome depurination in yeast expressing untagged preN10Q/N236Q compared to untagged wild type preRTA by qRT-PCR.

The C-terminal hydrophobic region affects transport of RTA beyond the ER

Reduction of the disulfide bond between RTA and RTB in the ER exposes a hydrophobic sequence at the C-terminus of RTA (Val245-Val256), which was proposed to mediate the association of RTA with the ER membrane (3). Mutations in this region do not affect catalytic activity of RTA *in vitro*, but reduce toxicity when the mutated RTA is reassociated with RTB (3). We previously showed that a double mutation, P250L/A253V, in this region eliminated depurination activity and cytotoxicity of RTA in yeast (80). To examine the trafficking of this mutant, we constructed C-terminal EGFP fusions with the precursor and the mature form of P250L/A253V and examined their localization using epifluorescence microscopy. The preP250L/A253V-EGFP showed only perinuclear localization at all time points up to 24 hpi and did not accumulate in the vacuole (Figure 2.10A). The matP250L/A253V-EGFP was observed in the ER and cytosol at 2 hpi and accumulated in the ER after 2 hpi. At 24 hpi it

showed only perinuclear localization (Figure 2.10B). Both preP250L/A253V-EGFP and matP250L/A253V-EGFP co-localized with the ER marker at 6 hpi (Figure 2.3). ER localization of preP250L/A253V was confirmed by indirect immunofluorescence (Figure 2.4).

Immunoblot analysis (Figure 2.10C) showed that preP250L/A253V-EGFP migrated as a single band with a weak slower migrating band, which disappeared after Endo H treatment, suggesting that it was glycosylated. The matP250L/A253V-EGFP migrated as a single band, and did not change in mobility after Endo H treatment, indicating that it was not glycosylated.

The viability of cells expressing preP250L/A253V-EGFP was similar to the viability of cells harboring the vector (Figure 2.10D). Yeast expressing matP250L/A253V-EGFP were slightly less viable than preP250L/A253V-EGFP, but were over 25-fold more viable than yeast expressing wild type matRTA-EGFP. The depurination level of preP250L/A253V-EGFP was barely detectable throughout the time course and 36-fold lower than that of the wild type preRTA-EGFP at 4 hpi (Figure 2.10E). Depurination by matP250L/A253V-EGFP was not detectable at 0 and 2 hpi, but the depurination level increased at 4 hpi and reached the highest level at 6 hpi (Figure 2.10F). Since matP250L/A253V-EGFP depurinated ribosomes, it was slightly more toxic than preP250L/A253V-EGFP (Figure 2.10D). However, it was less toxic than wild type matRTA-EGFP, possibly due to the delay in depurination during the early stages of induction. Cell fractionation analysis confirmed that preP250L/A253V-EGFP was associated primarily with the membrane fraction and migrated slightly faster after

Endo H treatment (Figure 2.6B). In contrast, matP250L/A253V-EGFP was equally distributed between the membrane and the cytosolic fraction, as wild type matRTA-EGFP (81) and did not change in mobility after Endo H treatment. These results demonstrate that the C-terminal hydrophobic stretch is critical for ER exit.

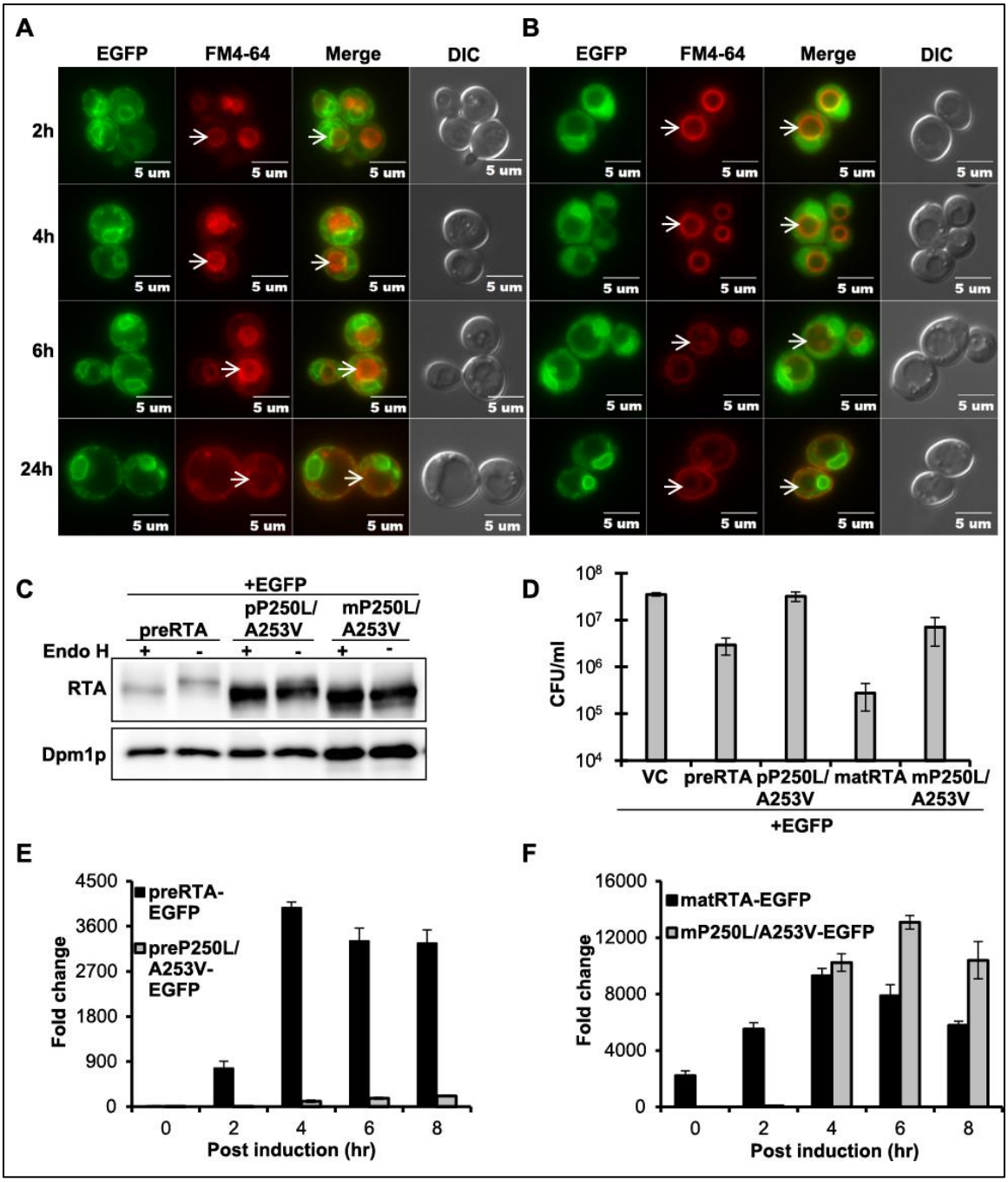

Figure 2.10 Intracellular transport, protein expression, cytotoxicity and depurination activity of preP250L/A253V-EGFP and mature P250L/A253V-EGFP. (A) Trafficking of preP250L/A253V-EGFP and (B) matP250L/A253V-EGFP in yeast. The images were taken at 2, 4, 6 and 24 hpi with Olympus BX41 fluorescence microscope. Merged images show localization of each protein relative to the vacuole. The arrows indicate the vacuoles. (C) Immunoblot analysis of membrane fraction isolated from cells expressing each protein at 6 hpi were treated with (+) or without (-) Endo H to cleave the glycans. The proteins (5 µg) were separated on a 10% SDS-polyacrylamide gel and probed with monoclonal anti-RTA (1:5000). The blot was reprobed with the ER membrane

marker Dpm1p as a loading control. (D) Viability of yeast expressing each protein and the vector control (VC). (E) Ribosome depurination by preP250L/A253V-EGFP and preRTA-EGFP by qRT-PCR. (F) Ribosome depurination by matP250L/A253V-EGFP and matRTA-EGFP by qRT-PCR. Data are mean ± SD from triplicates.

DISCUSSION

RTA is transported from the ER to the vacuole in yeast

In this study, we used EGFP tagged wild type preRTA to examine the time course of intracellular transport and carried out mutation analysis to reveal structural features important for trafficking to the cytosol. We show that plant derived native N-terminal leader sequence directs RTA to the ER membrane in yeast. PreRTA was transported from the ER to the vacuole, while mature RTA without the N-terminal leader stayed in the cytosol. These results demonstrate that RTA is transported from the ER to the vacuole and ER import is necessary for vacuole transport.

To rule out possible artifacts of ER and vacuole localization due to the EGFP tag, we confirmed ER localization by indirect immunofluorescence using untagged preRTA in fixed cells (Figure 2.4). Vacuole localization was confirmed by subcellular fractionation (Figure 2.2D), since vacuoles did not maintain balanced osmolarity and were ruptured during fixation in indirect immunofluorescence (82). These results demonstrated that the EGFP tag does not alter the localization of RTA. The viability of preRTA-EGFP was slightly higher than preRTA, while mature RTA had similar viability with or without the EGFP tag (Figure 2.1B), possibly because the C-terminal EGFP tag caused a

delay in ER export. Similarly, the viability of EGFP tagged preN10Q/N236Q was slightly higher than the untagged form, while the EGFP tagged or untagged mature forms had similar viability (Figure 2.8B). Nevertheless, preRTA-EGFP reduced viability of yeast compared to the vector control 12-fold (Figure 2.1B) and depurinated ribosomes as preRTA without the EGFP tag *in vivo* (Figure 2.1C), indicating that EGFP tagging is a useful strategy to study the time course of intracellular transport of RTA.

Since very little RTA gets into the cytosol, and is impossible to visualize, we used a very sensitive qRT-PCR assay we developed to quantify ribosome depurination (78) as an indicator of RTA trafficking to the cytosol. Ribosomes are depurinated and growth is severely inhibited when wild type preRTA-EGFP is transported to the cytosol in yeast. Mature form of RTA-EGFP was used as a control to detect changes in catalytic activity *in vivo*. Since mature form is localized in the cytosol, changes observed in depurination would be due to its catalytic activity, and not to trafficking. Deletion analysis indicated that only the first 26 residues of the 35-residue N-terminal leader were necessary and sufficient for ER targeting of RTA in yeast as in plants (61). RTA without the nine-residue propeptide was unprocessed, nonglycosylated and was not imported to the ER in tobacco protoplasts (79). However, although in tobacco protoplasts the nine-residue propeptide did not influence vacuolar targeting or the rate of dislocation of RTA to the cytosol (79), we show here that that deletion of the nine-residue propeptide delayed vacuole transport and ribosome

depurination. These results suggested that *N*-glycosylation may promote ER export.

Glycosylation promotes transport of RTA out of the ER

Analysis of the glycosylation mutants indicated that vacuole transport was delayed when the glycosylation sites were mutated in preRTA-EGFP, suggesting that *N*-glycosylation affected transport of RTA from the ER to the vacuole. While mature form of the glycosylation mutant was fully active, ribosome depurination by precursor form was reduced fourfold compared to wild type at 4 hpi, suggesting that the ability to traffic to the cytosol was also impaired in nonglycosylated preN10Q/N236Q-EGFP. Consistent with the depurination data, toxicity of nonglycosylated preN10Q/N236Q-EGFP was reduced over fivefold compared to wild type preRTA-EGFP, while the mature form had similar toxicity as wild type matRTA-EGFP (Figure 2.7E). Similar results were obtained using the precursor and mature forms of non EGFP-tagged glycosylation mutants (Figure 2.8A). Subcellular fractionation indicated that preRTA-EGFP lacking *N*-glycans was associated primarily with the membrane fraction. These results demonstrate that *N*-glycosylation stimulates the cytotoxicity of RTA by promoting its transport to the cytosol.

A previous study concluded that glycosylation is not required for intracellular trafficking, since nonglycosylated proricin ultimately accumulated in the protein bodies as the *N*-glycosylated precursor in the castor bean (62). However, this study did not examine the time course of transport. We demonstrate here that

although both *N*-glycosylated and nonglycosylated RTA are transported to the vacuole, the transport of the nonglycosylated RTA is delayed. This delay appears to be significant, since it results in markedly reduced cytotoxicity. These results suggest that glycosylation is not required for correct targeting of RTA, but allows more efficient intracellular transport to the cytosol and to the vacuole. The timing of trafficking to the cytosol, measured by depurination, coincides with the timing of vacuole transport, indicating that the two processes are coupled. These results suggest that RTA may enter the cytosol during transport through the secretory pathway to the vacuole. This finding is significant because up to now the ERAD pathway is thought to be the only pathway for dislocation of RTA from the ER to the cytosol. We present the first evidence here that RTA may enter the cytosol during transport to the vacuole, suggesting that this may be an alternative mechanism to dislocation from the ER.

Glycosylation in the ER increases hydrophilicity and promotes protein folding (83-85). Discrete foci were observed in yeast expressing the nonglycosylated preN10Q/N236Q-EGFP, but not wild type preRTA-EGFP, suggesting that the nonglycosylated preN10Q/N236Q-EGFP likely aggregated in the ER. Inhibition of glycosylation activates the unfolded protein response (UPR) and triggers ERAD (83, 86, 87). Activation of ERAD prevents toxicity of ricin by reducing its dislocation (4). These results suggest that RTA may need to be properly folded to exit the ER. *N*-glycosylation may promote folding of RTA in the ER to allow efficient transport out of the ER. However, *N*-glycosylation is not

only important for folding of RTA in the ER, since fully folded deglycosylated RTA is less toxic than glycosylated RTA in mice (71).

The pathway that leads to degradation of RTA in the cytosol is unclear. ER import was shown to be a prerequisite for the degradation of a folding competent RTA variant (67). However, this variant was not degraded by the proteasome core and its disappearance in a yeast strain lacking vacuolar proteinase A was similar to that in the wild type (67). These results do not exclude the possibility that vacuolar turnover may be important for degradation of RTA. Our results suggest that ER to vacuole trafficking may reduce cytotoxicity of RTA, possibly by promoting its degradation. Hence, the vacuole may be an alternative compartment for RTA turnover.

C-terminal hydrophobic sequence is critical for transport of RTA out of the ER

Our previous results showed that a double mutation in a hydrophobic sequence at the C-terminus of RTA, P250L/A253V, eliminated toxicity and depurination activity of RTA (80). The P250A mutation alone affected the secondary structure of RTA, reducing its interaction with EDEM1, and transport from the ER to the cytosol in mammalian cells (88). We show here that preP250L/A253V-EGFP was restricted to the ER and was not transported to the vacuole. Ribosome depurination and toxicity of preP250L/A253V-EGFP were almost completely inhibited compared to wild type preRTA-EGFP, suggesting that it was not able to dislocate to the cytosol. Subcellular fractionation

confirmed that this mutant was mainly localized in the membrane fraction. These results indicate that the C-terminal hydrophobic region allows ER exit.

The matP250L/A253V-EGFP was also associated with the ER membrane, even though it did not contain the signal sequence. The matP250L/A253V-EGFP was not glycosylated and thus had not reached the ER by translocation. Toxicity of matP250L/A253V-EGFP was reduced compared to wild type matRTA-EGFP. Depurination was delayed, possibly because the C-terminal mutations allowed insertion of matP250L/A253V-EGFP into the ER membrane, but prevented the release of this mutant from the membrane and inhibited its folding to the native conformation. This mutant likely depurinated ribosomes on the ER membrane, thereby delaying depurination and reducing toxicity.

Glycosylation stimulates toxicity by increasing the rate of transport of RTA into the cytosol

We previously showed that ribosome depurination alone is not sufficient for the cytotoxicity of RTA (80). Factors that contribute to cytotoxicity other than depurination have not yet been identified. We show here that cytotoxicity depends on the timing of depurination. A high depurination level during the early stages of induction implies a high rate of depurination, inducing extensive cell death and degradation of damaged ribosomes. Thus, very little depurinated rRNA accumulates in yeast expressing highly active RTA. Yeast expressing matRTA or matRTA-EGFP were less viable than yeast expressing preRTA or preRTA-EGFP, possibly due to a higher level of depurination during the early

stages of induction. A low level of depurination at the early stages of induction indicates a low rate of depurination. The depurinated rRNA accumulates with time and a higher level of depurination is detected at the later stages of induction since cells do not die. Therefore, a high level of depurination at the later stages of induction does not suggest high catalytic activity.

Depurination is a dynamic process regulated by the rate of dislocation of RTA and its enzymatic activity. The rate of depurination is determined by the rate of dislocation to the cytosol, since dislocation allows exposure of RTA to cytosolic ribosomes. Our results indicate that glycosylation does not affect the catalytic activity of RTA, but affects cytotoxicity by increasing the rate of transport to the cytosol. Although the lack of glycosylation delayed transport to the cytosol by only two hours, it significantly reduced toxicity. Our results are consistent with other studies, which showed that glycosylation is required for efficient intracellular transport of carboxypeptidase Y to the vacuole in yeast (89) and the rate of transport of barley lectin to vacuoles in plants (90).

We propose a model that explains our findings (Figure 2.11). The mature RTA without the 35-residue leader remains in the cytosol and depurinates ribosomes in the cytosol. The preRTA is translocated to the ER, the signal sequence is cleaved and it is *N*-glycosylated. The *N*-glycosylated RTA is transported to the vacuole. Some of it enters the cytosol and depurinates ribosomes. Since RTAΔ26 lacks the signal sequence, it remains in the cytosol and depurinates cytosolic ribosomes. RTAΔ9 is targeted to the ER after synthesis, but remains on the cytosolic face of the ER membrane and

depurinates membrane-bound ribosomes. Some of this protein might be translocated into the ER, but it is not glycosylated and vacuole transport is delayed. The preN10Q/N236Q is translocated to the ER and the signal sequence is processed. It is not glycosylated in the ER. It causes a delay in depurination because ER-cytosol and ER-vacuole transport are delayed. The preP250L/A253V is targeted to the ER after synthesis, and some of it is glycosylated. However, it is not able to exit the ER due to point mutations in the C-terminal hydrophobic sequence. Consequently, it causes a markedly lower level of depurination and is not toxic.

In summary, our results provide the first evidence that *N*-glycosylation stimulates toxicity by increasing the rate of transport of RTA to the cytosol. *N*-glycosylation also affects vacuole transport of RTA, suggesting that it appears to be the driving force for transport of RTA out of the ER. Point mutations in the C-terminal hydrophobic stretch prevent the ability of RTA to get out of the ER and eliminate toxicity and depurination, indicating that this sequence is necessary for ER exit. Our results suggest that RTA may enter the cytosol during transport to the vacuole. These results contribute to our mechanistic understanding of the intracellular transport of ricin and suggest that altering this pathway may have implications for the development of antidotes and vaccines to combat ricin intoxication.

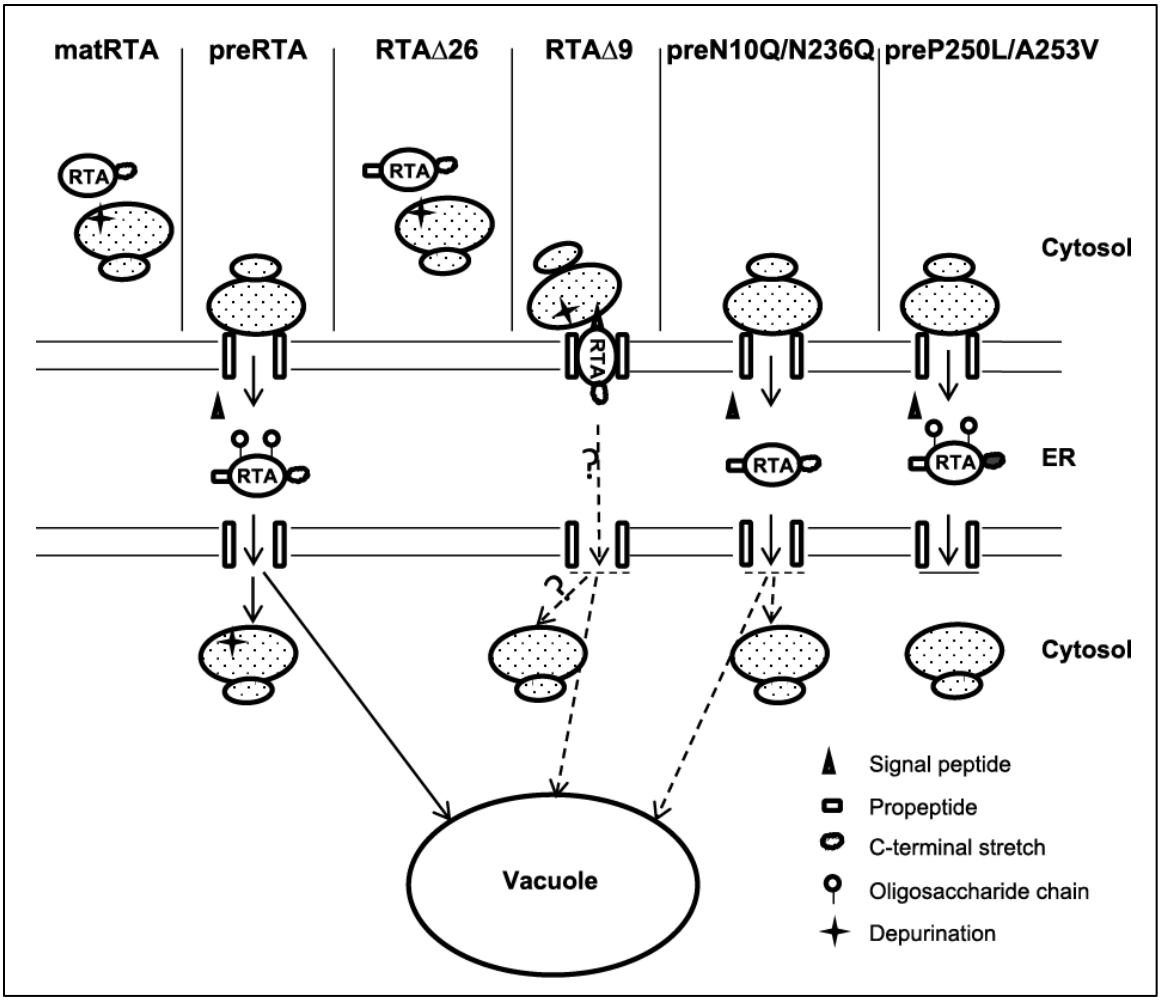

Figure 2.11 A model describing intracellular transport of wild type and mutant forms of RTA. Wild type mature RTA does not contain a 35-residue leader and stays in the cytosol and depurinates ribosomes. Wild type preRTA is targeted to the ER after synthesis, where the signal peptide is cleaved. The preRTA is transported from the ER to the vacuole. Some of it gets into the cytosol and depurinates ribosomes. RTAΔ26 does not contain a signal peptide and remains in the cytosol and depurinates ribosomes. RTAΔ9 is targeted to the ER after synthesis. It may tether to the cytosolic face of the ER membrane and depurinate membrane-bound ribosomes. Some of it may be translocated into the ER lumen. However, it is not glycosylated and the vacuole transport is delayed. The preN10Q/N236Q is targeted to the ER where the signal peptide gets processed. It is not glycosylated in the ER. The depurination in the cytosol is markedly lower because its transport to the cytosol is impaired and its transport to the vacuole is delayed. PreP250L/A253V is targeted to the ER after synthesis. The signal peptide gets processed and some of it gets glycosylated. However, its transport beyond the ER is inhibited.

MATERIALS AND METHODS

Plasmids and yeast strains

The following cDNAs were fused with EGFP tag at the 3' end and cloned into yeast vector containing the *LEU2* marker (NT198) downstream of the galactose-inducible *GAL1* promoter. Wild type preRTA contains a 35-residue signal sequence, followed by 267-residue RTA (preRTA-EGFP, NT1205); wild type mature RTA consists of 267-residue RTA (matRTA-EGFP, NT1206). The first 26 residues of the 35-residue leader was deleted using primer pairs 5'-CCTCTAGAGTCGAGGATGTGGTCTTTCACATTAGAGG-3' and 5'-TAAGAATTCAAACTGTGACGATGGTGGAGG-3'(RTAΔ26-EGFP, NT1493). The 9-residue propeptide was deleted by site directed mutagenesis using the primer 5'-GGATCCACCTCAGGGATATTCCCCAAACAATACC-3' (RTAΔ9-EGFP, NT1494). The glycosylation mutants were generated by substituting Gln at Asn10 and Asn236 using 5'-CCAAACAATACCCAATTATACAATTTACCACAGCGGGTGCC-3' and 5'-CCAATTCAACTGCAAAGACGTCAAGGTTCCAAATTCAGTGTG-3'(preN10Q/N236Q-EGFP, NT1497; matN10Q/N236Q-EGFP, NT1500). The C-terminal mutants contained cDNA with point mutations P250L and A253V (preP250L/A253V-EGFP, NT1253; matP250L/A253V-EGFP, NT1259). The cDNA corresponding to precursor and mature RTA was cloned into NT198 downstream of the *GAL1* promoter to generate preRTA and matureRTA without the EGFP tag (preRTA, NT849; matRTA, NT1456) (80). The plasmids were then transformed into *Saccharomyces cerevisiae* strain W303 (*MAT*a *ade2-1 trp1-1*

ura3-1 leu2-3,112 his3-11,15 can1-100), and transformants were selected on SD-Leu medium containing 2% glucose. The yeast strain, PMY147, containing the ER marker Alg9-RFP (*MATa trp1-Δ901 leu2-3,112 his3-Δ200 ura3-52 lys2-801 suc2-Δ9 can1::hisG ALG9::RFP, TRP1)* was a gift from Dr. Peter Mayinger. PreRTA-EGFP, mature RTA-EGFP, RTAΔ9-EGFP, preN10Q/N236Q-EGFP, preP250L/A253V-EGFP and matP250L/A253V-EGFP were transformed into PMY147 and transformants were selected on SD-Leu,Trp medium containing 2% glucose.

Analysis of protein expression

Yeast cells were grown in SD-Leu supplemented with 2% glucose overnight and then transferred to SD-Leu supplemented with 2% galactose at OD_{600} of 0.3 to induce RTA expression. Cells were collected at 6 hpi and membrane fractions were isolated as previously described (91). Membrane fractions were treated with Endo H using the manufacturer's protocol (New England Biolabs, Ipswich, MA). The protein samples were separated on a 10% SDS-polyacrylamide gel and the blot was probed with monoclonal anti-RTA (1:5000), a gift of Dr. Nicholas J. Mantis. The blot was stripped with 8M guanidine hydrochloride and reprobed with antibody against the ER maker, dolichol phosphate mannose synthase (Dpm1p; Invitrogen, Eugene, Oregon) (1:1000) and developed using ChemiDoc MP imaging system (Bio-Rad, Philadelphia, PA).

Subcellular fractionation

Subcellular fractionation was carried out as previously described (92). Membrane fraction was collected at 6 or 14 hpi by centrifuging at 16,000 x g for 15 min. The supernatant was further centrifuged at 200,000 x g for 1 h to pellet the ribosomes. The membrane fraction and the post ribosomal supernatant were treated with or without Endo H and analyzed by immunoblot analysis using monoclonal anti-RTA followed by anti-Dpm1p as described above. The blot was reprobed using anti-3-phosphoglycerate kinase (Pgk1p; Invitrogen, Eugene, Oregon), as a marker for the cytosol. The vacuole fraction was isolated as described (93). Briefly, cells harvested at 14 hpi were washed with DTT solution (0.1 M Tris pH9.4, 10mM DTT) and lysed by lyticase at 20 U/OD in spheroplasting buffer (0.16 X YPD, 0.4 M sorbitol, 50 mM potassium phosphate, pH 7.5). The spheroplasts were treated with DEAE-Dextran for gentle lysis. Purified vacuoles were obtained by flotation in a 0, 4, 8, 15% Ficoll step gradient. The gradients were centrifuged at 110,000 X g for 90 min in a Beckman L8-70M Ultracentrifuge (Beckman Coulter, Brea, CA) and vacuoles were collected from the 0%-4% interface. The vacuole marker was anti-H^+-ATPase (V-ATPase; Invitrogen, Eugene, Oregon) (1:500). The band intensity was quantified using Quantity One software (Bio-Rad, Philadelphia, PA).

Viability analysis

Yeast were induced as described above and 8 µL of a series of 10-fold dilutions (OD_{600} of 10^{-1} to 10^{-5}) were plated on SD-Leu plates containing 2% glucose at 0, 4, 6 and 10 hpi. Plates were incubated at 30°C for 48 h.

Depurination analysis

For dual primer extension, total yeast RNA from W303 expressing precursor and mature forms of RTA with and without EGFP tag was isolated at 10 hpi and hybridized using a depurination primer and a 25S control primer, as described previously (73). Extension products were separated on a 7M urea-5% polyacrylamide gel and quantified using a PhosphorImager.

The qRT-PCR analysis of depurination was carried out as previously described (78, 94). Cells were harvested at 0, 2, 4, 6 and 8 hpi and total RNA was extracted using the RNeasy Mini Kit (Qiagen, Valencia, CA). Total RNA was converted to cDNA using the High Capacity cDNA Reverse Transcription Kit (Applied Biosystems, Carlsbad, CA). The 25S rRNA was detected using (5'-AGA CCG TCG CTT GCT ACA AT-3'and 5'- ATG ACG AGG CAT TTG GCT AC- 3'). The depurinated rRNA was detected using the forward primer (5'- CTA TCG ATC CTT TAG TCC CTC-3') and the reverse primer (5'- CCG AAT GAA CTG TTC CAC A-3'). Real time PCR was performed using an ABI Prism 7000 Sequence Detection System (Applied Biosystems, Carlsbad, CA). The data was analyzed by the comparative ΔC_T ($\Delta\Delta C_T$) method for quantification (78).

Live cell imaging

Time course of RTA localization was carried out using yeast harboring the precursor and mature RTA with EGFP tag at 2, 4, 6, 8 and 24 hpi. The cells were directly added to 2% agar pads on slides. For ER co-localization, yeast harboring the ER marker, Alg9-RFP was visualized at 6hpi. For vacuole stain,

yeast cells were harvested at 2, 4, 6, 8 and 24 hpi. FM4-64 (Invitrogen, Carlsbad, CA) dissolved in dimethyl sulfoxide (DMSO) was added at a final concentration of 80 µM and cells were incubated in the dark at 30°C for 60 min. Cells were pelleted and washed with YPD media and resuspended in YPD media to chase for 40 min at 30°C. The cell culture was applied to the agar pad and visualized using an Olympus BX41 fluorescence microscope equipped with a CCD camera (Hamamatsu, Bridgewater, NJ) and a 100X oil objective (1.45 N.A. Plan Apo, Olympus). Image acquisition and processing were performed using Metamorph Image Software (7.0; MDS Analytical Technologies). Data analysis was done by pooling images of expressed cells from 3 individual experiments.

Indirect immunofluorescence

Yeast cells harboring preRTA, preN10Q/N236Q and preP250L/A253V were grown in SD-Leu medium supplemented with 2% glucose and induced for RTA production with SD-Leu supplemented with 2% galactose. The cells were collected at 6 hpi and fixed with 4% paraformaldehyde by adding directly to the culture medium and incubated at 30°C for 30 min. The cells were spheroplasted by lyticase and incubated at 30°C for 30 min. The cells were then attached to the 0.1% poly-L-lysine coated Teflon slides. The cells were incubated with primary monoclonal antibody against RTA and then incubated with Alexa Fluor 488 goat anti-mouse antibody (Invitrogen, Carlsbad, CA). DAPI was applied at a concentration of 1µg/ml for 1 min at room temperature to stain the nuclei. The slides were mounted and sealed for observation under an Olympus BX41

fluorescence microscope equipped with a CCD camera (Hamamatsu, Bridgewater, NJ).

In vitro translation

Purified recombinant mature RTA-EGFP and recombinant mature RTA from *E. coli* (21) were added to the Flexi rabbit reticulocyte lysate system (Promega, Madison, WI) at 0, 10, 20, 40, 60, 80, 100, 200, 500 and 1000 pM according to the manufacturer's protocol. The reactions were incubated at 30°C for 30 min and luciferase activity was measured using a luminometer. Data were collected from at least 3 individual experiments.

CHAPTER 3: The effects of mutations on the intracellular transport of ricin A chain in *Saccharomyces cerevisiae*

SUMMARY

Ricin A chain (RTA) has to retrotranslocate across the endoplasmic reticulum (ER) membrane to enter the cytosol by a process termed dislocation to depurinate ribosomes and inhibit protein synthesis. The fate of RTA after dislocation is crucial for RTA mediated cell death. RTA is sorted to its final destination under the scrutiny of the ER quality control (ERQC) system. How the ERQC machinery deciphers the signal elements within RTA is not well understood. To investigate this, we employed a series of nontoxic RTA mutants as well as wild type RTA. The precursor (pre) and mature (mat) forms of the wild type RTA and mutants were tagged with the enhanced green fluorescent protein (EGFP) at their C-termini. I observed two distinct trafficking patterns among the precursor forms of RTA mutants. One group underwent both ER-to-cytosol and ER-to-vacuole transport, like wild type RTA. The other group accumulated in the ER and formed aggregates. The results with the former group suggested that the vacuole transport is a degradation pathway for precursor RTA and possibly contributes to the reduction in depurination. In the cytosol, the dislocated wild type RTA and mutants behaved differently in the absence of the peptide:*N*-glycanase (PNGase; yeast Png1). The wild type preRTA was a substrate for the free pool of Png1 which is only responsible for the deglycosylation of its substrates. One of the RTA mutants, preG83D, which formed aggregates acted

as a substrate for the Png1-Rad23 degradation complex. The ribosome depurination by preG83D increased significantly in response to *PNG1* deletion. These results suggest that the sorting of RTA is sophisticated and diverse. In the ER, it is targeted to the vacuole and/or cytosol transport. In the cytosol, the dislocated RTA is further differentiated by the cytosolic host cellular proteins.

INTRODUCTION

Ricin, from *Ricinus communis*, is a heterodimeric protein that is composed of ricin A chain (RTA) and ricin B chain (RTB). The two subunits play distinct roles in the intoxication process. RTA is catalytically active which inactivates the universally conserved α-sarcin/ricin loop (SRL) of the large 28S ribosomal RNA and inhibits protein synthesis (16). RTB, a cell-binding galactose-specific lectin, promotes the endocytosis of ricin (60). RTA is extremely toxic: a single molecule can inactivate 1500 ribosomes per minute. Because of its high potency, ricin has been used as a bioterrorist weapon and remains a fearful threat worldwide.

Ricin exerts its toxicity by depurinating ribosomes and thus inactivating protein synthesis in the cytoplasm. To enter the cytoplasm in mammalian cells, ricin goes through the retrograde transport pathway after endocytosis with the help of RTB (60). The initial step after endocytosis is the delivery of ricin to the early endosomes. A large amount of ricin in the early endosome is either recycled back to the cell surface or delivered via late endosomes to lysosomes where it is eventually degraded. Only a small portion of ricin follows the retrograde pathway from endosomes to the *trans*-Golgi network (TGN) and

subsequently enters the endoplasmic reticulum (ER) (63). In the ER, RTA is activated through reductive separation from RTB by the protein disulfide isomerase (PDI) (48). RTA then enters the cytosol from the ER by a process termed dislocation or retrotranslocation (56, 64). The dislocation of RTA is of particular importance, since RTA can only depurinate ribosomes once it enters the cytosol. Accumulated evidence suggests that RTA uses the ER associated degradation (ERAD) pathway to reach the cytosol (52). The ERAD components exploited by RTA during its dislocation have been identified using yeast as a model system, because yeast ribosomes are less sensitive to RTA than the mammalian ribosomes (95). Two mutants with attenuated activity, RTA_{E177D} and RTA_{E177A}, have been used as folded proteins. RTA_{Δ}, which denotes RTA with a deletion of five amino acids from the active site, has been used as a misfolded protein (53). It was shown that the folded RTA and misfolded RTA diverged upon entry into the cytosol and were discriminated based on the structural features by the cytosolic ERAD components (53). Among the ERAD components that responded distinctly to the folded RTA and misfolded RTA, a cytosolic peptide: *N*-glycanase (PNGase; yeast Png1) is of particular interest. The yeast Png1 catalyzes the de-*N*-glycosylation activity by hydrolyzing the β-aspartylglycosylamine bond of *N*-linked glycoproteins and glycopeptides (96). The removal of *N*-glycans by Png1 assists the proteasome mediated degradation of misfolded proteins (96). In fact, a subset of Png1 is linked to the 26S proteasome via the DNA repair protein Rad23, thus ensuring the efficient degradation (58). The presence of *N*-linked glycans is an essential signal for

ERAD-L pathway, which is responsible for the degradation of misfolded proteins carrying lesions in the ER luminal domain (97). In addition to the recognition of *N*-glycans by the ER luminal components of the ERAD pathway, a variety of ERAD substrates are implicated to be de-*N*-glycosylated prior to their destruction in the cytosol in an *N*-glycan dependent manner (96). The *N*-glycan dependent Png1 activity suggests the importance of *N*-glycan in signaling the cytosolic side of the ERAD. The yeast Png1 preferred denatured glycoproteins over folded glycoproteins in *in vitro* experiments (98, 99). Structural and mutational analysis of the Png1-Rad23 complex postulated such conformational selectivity of Png1 was derived from the accessibility to its active site (100). The active site of Png1 is buried in a deep cleft which is not accessible to the folded glycoproteins, whereas can be fitted by the more flexible denatured glycoproteins. It was shown that the misfolded RTA_{Δ} and RTL (RTA_{Δ} with a transmembrane domain and the cytoplasmic Leu2) required Png1 for deglycosylation and degradation in yeast (54, 58, 101). In contrast, yeast cells expressing folded form RTA_{E177D} did not show growth defects in response to *PNG1* deletion (53). Although the results supported that Png1 is only involved in the proteasome mediated degradation of the misfolded form RTA_{Δ}, but not the folded form RTA_{E177D}, several studies observed deglycosylation activity of folded form RTA_{E177D} in the cytosol in yeast, tobacco and mammalian cells (46, 57, 102), suggesting that RTA_{E177D} is a substrate for Png1.

In addition to ER-to-cytosol transport through the ERAD pathway (57), wild type RTA also undergoes ER-to-vacuole transport as we showed previously

(103). Similar to the misfolded version of yeast carboxypeptidase yscY (CPY*), vacuole transport might be a degradation pathway that is exploited by RTA (104, 105). When the ERAD capacity is saturated by high concentration of the substrates or the defects in the ERAD pathway occurs, excess ERAD substrates are transported to the vacuole for degradation (106). However, it is not clear how ER-to-vacuole transport contributes to the depurination and toxicity of RTA in yeast. The vacuole transport pathway introduces additional complexity to the understanding of the intracellular transport machineries for proper routing of RTA.

At present, it remains elusive what structural features are critical for ricin induced cell death. To correlate the structural features of RTA with its toxicity, studies involving site-directed mutagenesis and systematic deletion of amino acids were performed. These studies support that most of the mutations that result in nontoxic RTA variants are clustered at the putative active site cleft (6-8). Random mutagenesis using hydroxylamine has identified a series of nontoxic RTA variants, some of which have mutations beyond the active site. The nontoxic RTA variants with certain point mutations away from the active site still depurinate ribosomes (80). Despite the knowledge that the toxicity of RTA is mainly attributed to the depurination of ribosomes, the identification of the active yet nontoxic RTA variants suggests that ribosome depurination is only necessary but not sufficient for RTA cytotoxicity (80). The mutations of RTA could result in structural changes and likely lead to different translocation pathways. The trafficking of RTA affects depurination indirectly, which determines the accessibility of RTA to the ribosomes or the ability to evade degradation

pathways. In the present study, I sought to understand the intracellular trafficking pathways exploited by RTA and their role in toxicity using wild type RTA and nontoxic RTA mutants with varied depurination activities. These RTA mutants carrying altered sequence motifs were sorted out under the scrutiny of the ER quality control (ERQC) system. The precursor and mature forms of RTA variants (G83D, G212E, S215F and P95L/E145K) and the wild type were fused with the EGFP tag at the C-termini to track their intracellular trafficking *in vivo*. The precursor form contains the signal peptide, which allows the co-translational import of RTA into the ER and subsequent dislocation to the cytosol. The mature forms do not have the signal peptide and propeptide at the N-termini and remain in the cytosol, allowing examination of their catalytic activity *in vivo*. The results show that wild type RTA and nontoxic RTA mutants were sorted differently by the transport machinery. Based on their trafficking pattern, they were divided into two major groups. One contained RTA mutants that underwent ER-to-cytosol and ER-to-vacuole transport, similar to wild type RTA. The other group contained mutants that had defects in ER-to-vacuole transport. With the former group, the results suggested that vacuole transport is a degradation pathway for RTA. After dislocation to the cytosol, the wild type RTA and RTA variants had different requirements for the cytosolic ERAD component Png1. The deglycosylation and degradation of misfolded preG83D were impaired in response to *PNG1* deletion. In the presence of Png1, preG83D was led to the proteasomal degradation machinery. However, Png1 only affected the deglycosylation but not degradation of wild type preRTA. Since wild type preRTA is the substrate for the free Png1

which is separated from the degradation machinery, it evades the proteasomal degradation and remains potent. *PNG1* deletion had no effects on the misfolded preS215F, or folded preG212E and preS215F. The results suggest that mutations in the RTA could result in distinct intracellular trafficking pathways and provide insights into the final step of RTA transport important for its toxicity.

RESULTS

RTA variants have different intracellular trafficking

To investigate the intracellular trafficking of RTA variants, precursor and mature forms of RTA variants and wild type RTA were fused to the EGFP tag at the C-terminal end (preG83D-EGFP, preG212E-EGFP, preS215F-EGFP, preP95L/E145K-EGFP, preRTA-EGFP; matG83D-EGFP, matG212E-EGFP, matS215F-EGFP, matP95L/E145K-EGFP, matRTA-EGFP). The expression was under the control of the *GAL1* promoter to permit growth under non-inducing conditions and induce expression under inducing conditions. The viability assay (Figure 3.1) with the EGFP tagged RTA variants was performed and showed that the precursor forms and the mature forms of RTA variants with the EGFP tag were nontoxic when expressed in the yeast cells. The results agreed with the previous non-tagged RTA variants (80).

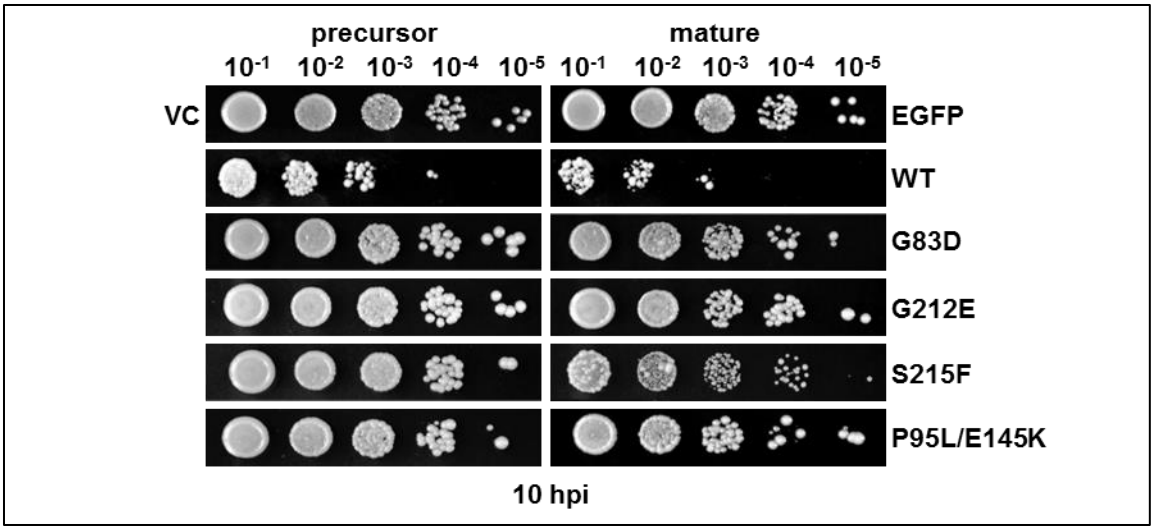

Figure 3.1 The viability of yeast cells expressing the precursor and mature forms of wild type RTA-EGFP, RTAG83D-EGFP, RTAG212E-EGFP, RTAS215F-EGFP and RTAP95L/E145K-EGFP. Yeast cells were first grown in SD-Leu supplemented with 2% glucose and then transferred to SD-Leu supplemented with 2% galactose. At 10 hpi, a series of ten-fold dilutions were plated on media containing 2% glucose and grown at 30ºC for approximately 48 h. The precursor forms are shown on the left and the mature forms are shown on the right. The mutations of RTA are indicated on the right. VC represents empty vector. EGFP represents EGFP open reading frame in the empty vector.

The EGFP tag does not affect the sorting and activity of wild type preRTA as shown previously (2). The yeast cells were observed at 2, 4, 6 and 24 h post-induction (hpi) using the epifluorescence microscope. As shown in Figure 3.2A, wild type preRTA-EGFP was localized to the ER at 2 hpi, and accumulated into the vacuole at 4 hpi (2). At 24 hpi, 100% of the cells showed colocalization of preRTA-EGFP with the vacuole marker FM4-64 (2). PreG212E-EGFP and preP95L/E145K-EGFP were both transported to the vacuole as wild type. PreG212E-EGFP colocalized with the ER at 2 hpi, and with the vacuole at 4 hpi and thereafter. However, the transport of preP95L/E145K-EGFP to the vacuole was delayed by 2 hours. As shown in Figure 3.2B, the wild-type mature RTA,

which did not have the 35-residue leader, was localized in the cytosol after synthesis (103). Similarly, matG212E-EGFP and matP95L/E145K-EGFP remained in the cytosol overtime.

In contrast to the wild type and preG212E-EGFP and preP95L/E145K-EGFP mutants, preG83D-EGFP and preS215F-EGFP were not transported to the vacuole even at 24 hpi (Figure 3.3A). They localized to the ER due to the signal peptide (2) and formed large punctate structures on the ER and cell periphery, suggesting that they formed aggregates and might be transported to the cell periphery from the ER instead of being sorted to the vacuole. Correspondingly, matG83D-EGFP and matS215F-EGFP also localized differently compared with wild type matRTA-EGFP. Besides the cytosolic localization, matG83D-EGFP and matS215F-EGFP co-localized with the nuclei, which was defined by Hoechst 33342 stain (Figure 3.3B). The nucleus localization implicated the destruction of proteins in the proteasome which resides in the nucleus in the case of yeast (107).

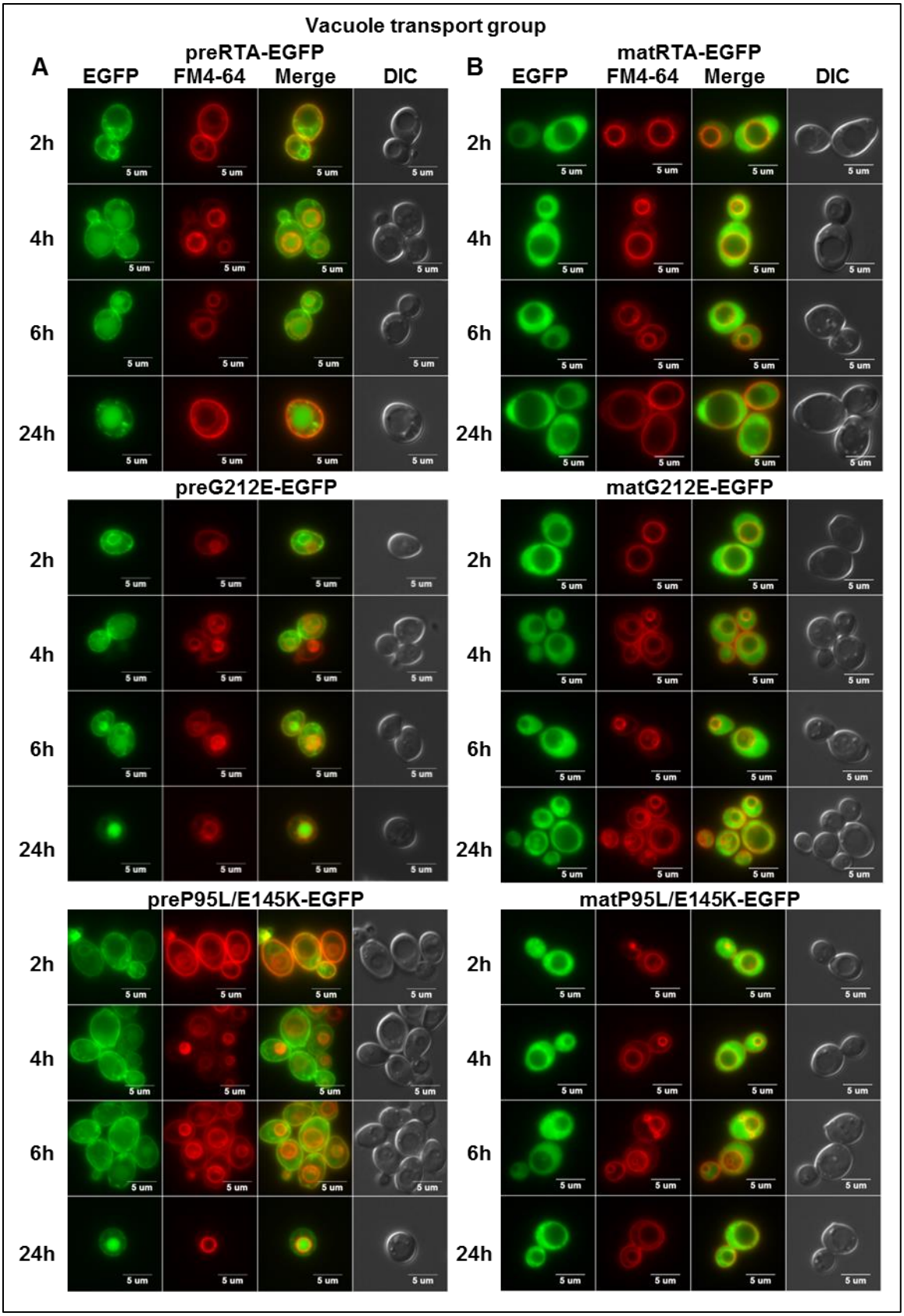
Vacuole transport group
A
preRTA-EGFP
EGFP
FM4-64
Merge
DIC
2h
4h
6h
24h
B
matRTA-EGFP
EGFP
FM4-64
Merge
DIC
2h
4h
6h
24h
preG212E-EGFP
2h
4h
6h
24h
matG212E-EGFP
2h
4h
6h
24h
preP95L/E145K-EGFP
2h
4h
6h
24h
matP95L/E145K-EGFP
2h
4h
6h
24h
5 um

Figure 3.2 Wild type preRTA-EGFP, preG212E-EGFP and preP95L/E145K-EGFP were transported to the vacuole. The images of yeast cells harboring the precursor forms (A) and mature forms (B) of wild type RTA, G212E and P95L/E145K were taken at 2, 4, 6 and 24 hpi with an Olympus BX41 fluorescence microscope. Yeast cells were treated with FM4-64 to stain the vacuole. Merged images show localization of each protein relative to the vacuole.

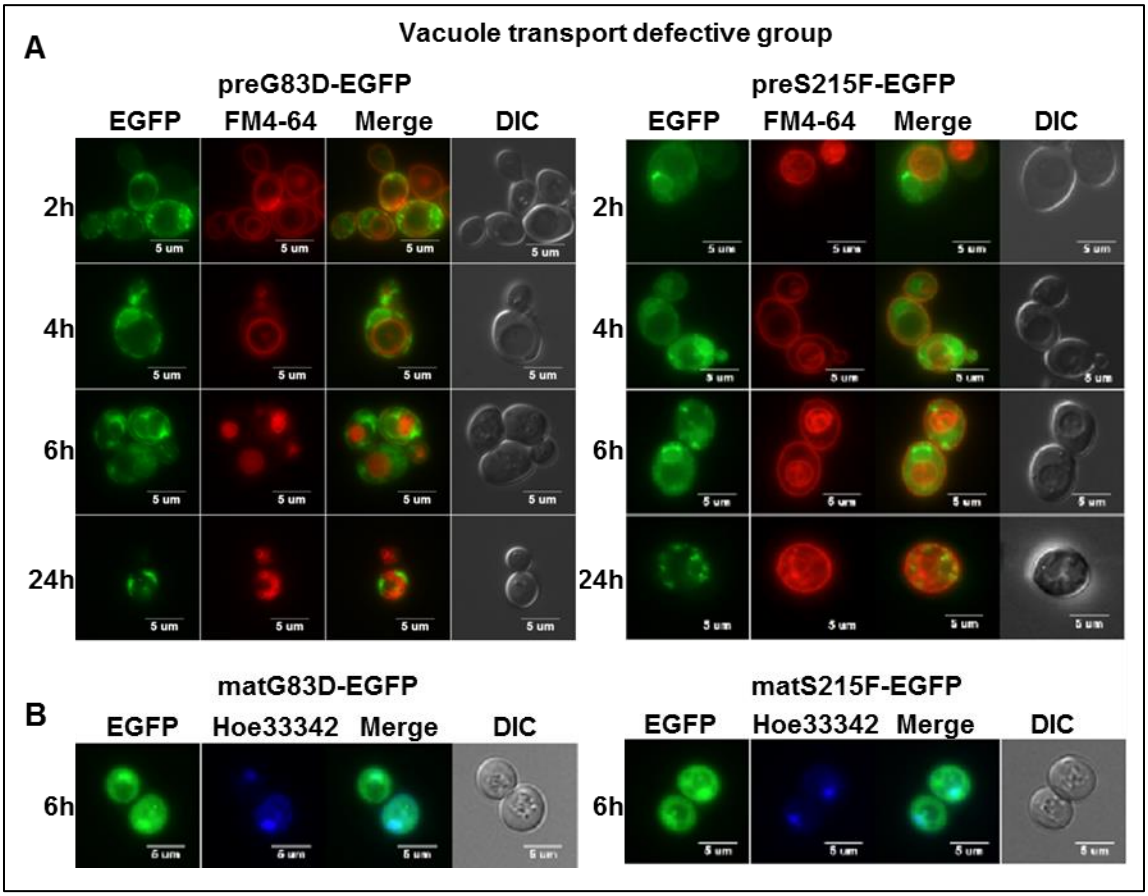

Figure 3.3 PreG83D-EGFP and preS215F-EGFP had defects in vacuole transport and formed big punctate structures. (A) The images of yeast cells harboring the precursor forms of G83D and S215F were taken at 2, 4, 6 and 24 hpi with an Olympus BX41 fluorescence microscope. Yeast cells were treated with FM4-64 to stain the vacuole. Merged images show no colocalization of preG83D-EGFP and preS215F-EGFP with the vacuole. (B) The images of yeast cells harboring the mature forms of G83D and S215F were taken at 6 hpi. The nuclei were stained with Hoechst 33342. The merged images show colocalization of matG83D-EGFP and matS215F-EGFP with the nuclei.

RTA variants have different depurination kinetics

I detected ribosome depurination of EGFP tagged precursor and mature forms of RTA variants *in vivo* with quantitative RT-PCR (108) as readouts for enzymatic activity of RTA in the cytosol. The depurination of wild type RTA was examined as a standard with each nontoxic RTA mutant. The depurination kinetics rather than the end point cell viability is a more sensitive measurement to assess the effects of RTA on the yeast ribosomes and the dislocation of the precursor forms. The depurination of the mature forms of RTA were cytosolic controls to indicate the enzymatic activity, whereas the depurination of the precursor forms were affected by both entry to the cytosol and the enzymatic activity. As shown in Figure 3.4A, wild type matRTA-EGFP depurinated from 0 hpi and the depurination reached a peak at 4 hpi. All the nontoxic mature RTA-EGFP mutants had delayed depurination and the levels were much lower than that of the wild type at the early time points, but all rose to the similar depurination levels as the wild type at 6 and 8 hpi. Because we have demonstrated that the depurination at early stage of induction was essential to the toxicity of RTA and represented its activity (103), the results suggested that all the nontoxic matRTA-EGFP mutants were less active than the wild type. The depurination levels up until 4 hpi will be used to determine their activity.

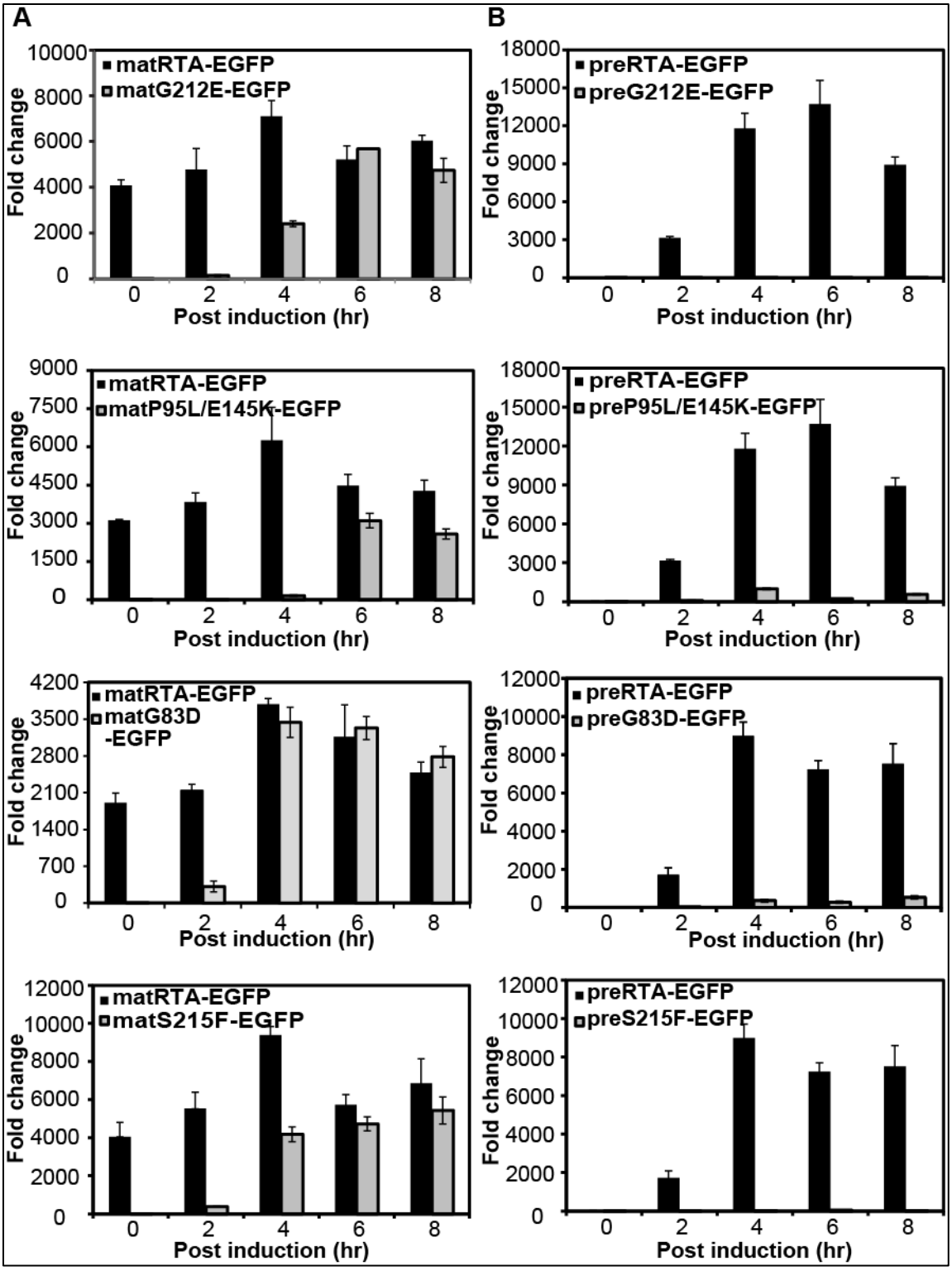

Figure 3.4 Ribosome depurination of mature (A) and precursor (B) forms of RTA mutants compared with wild type RTA-EGFP *in vivo* by qRT-PCR. The ribosomes of yeast cells expressing wild type RTA and each mutant were extracted at 0, 2, 4, 6 and 8 hpi. Two pairs of primers were designed to amplify the target amplicon (depurinated SRL) and the reference amplicon (25S rRNA).

The data was analyzed by comparative ΔC_T method ($\Delta\Delta C_T$). The y-axis indicates the fold change in depurination in yeast harboring the precursor and mature forms of wild type RTA and each mutant over yeast harboring the empty vector.

The RTA mutants that had similar trafficking pattern as observed with the fluorescence microscope were investigated together. As shown in Figure 3.4A, the depurination of matG212E-EGFP was negligible at 2 hpi and was three-fold less than that of matRTA-EGFP at 4 hpi. The depurination of matP95L/E145K-EGFP was only detectable until 4 hpi and was 38-fold less than that of wild type, indicating a greater reduction in enzymatic activity compared with matG212E-EGFP. The results suggested that matG212-EGFP was more active than matP95L/E145K-EGFP. Although the higher *in vivo* depurination level of matG212E-EGFP might be attributed to the higher expression level compared with that of matP95L/E145K-EGFP (Figure 3.5A), I further confirmed that matG212E was more active than matP95L/E145K by treating yeast ribosomes with wild type matRTA, matG212E and matP95L/E145K purified from *E. coli* in an *in vitro* depurination assay (Figure 3.6). To assess the effects of the mutations on the dislocation of RTA, the *in vivo* depurination of the precursor forms was tested (Figure 3.4B). PreRTA-EGFP started to depurinate from 2 hpi, which was delayed compared with matRTA-EGFP, suggesting that ER-to-cytosol dislocation was not a rapid process (2). The depurination of preG212E-EGFP was negligible throughout the time course. However, the depurination of preP95L/E145K-EGFP was only about 12-fold less than that of preRTA-EGFP at 4 hpi. The results suggested that the precursor form of P95L/E145K-EGFP had higher depurination

level than G212E-EGFP, although it was not as catalytically active as G212E. The difference in the depurination was not due to the amount of the proteins, since the expression levels of preG212E-EGFP and preP95L/E145K-EGFP were equal (Figure 3.5B). The rapid vacuole transport of preG212E-EGFP could result in the greater reduction in depurination compared with preP95L/E145K-EGFP. Because vacuole degradation is faster than the multistep ERAD (104). The results suggested that ER-to-vacuole transport may be an alternative degradation pathway for RTA and affect the depurination by diverting RTA to a more efficient degradation mechanism.

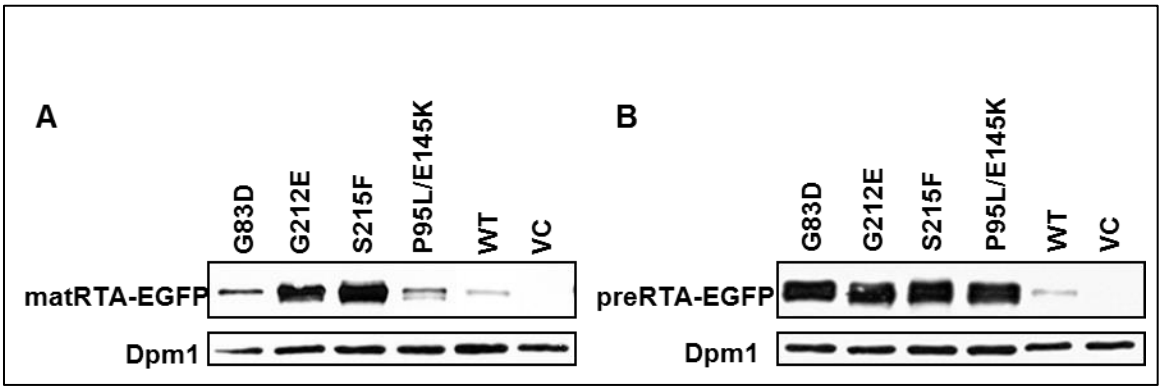

Figure 3.5 Immunoblot analysis of RTA expression. Membrane fractions isolated from cells expressing the EGFP tagged mature (A) and precursor (B) forms of wild type RTA and RTA mutants were separated on a 12% SDS-polyacrylamide gel and probed with polyclonal anti-RTA (1:5000). The blot were exposed for 30sec, except for wild type mature RTA, which was exposed for 2 min. The blot was reprobed with the ER membrane marker Dpm1p as a loading control.

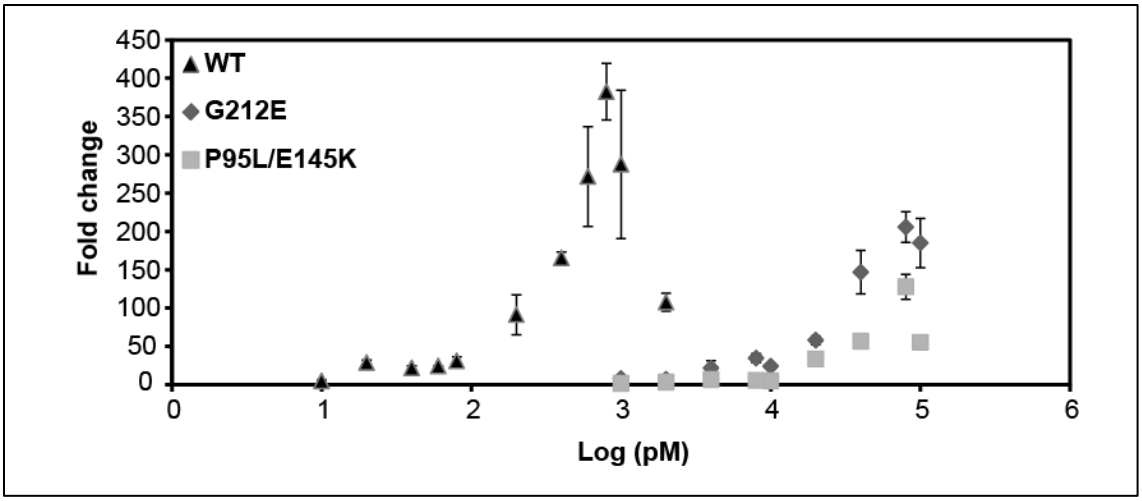

Figure 3.6 *In vitro* depurination of wild type matRTA, matG212E and matP95L/E145K. Ribosomes were incubated for 10 minutes at 30°C with purified wild type RTA at final concentrations of 10, 20, 40, 80, 100, 200, 400, 800, 1000 and 2000 pM. The mutants matG212E and matP95L/E145K were used at final concentrations of 1, 2, 4, 8, 10, 20, 40, 80 and 100 nM.

For the subset of RTA mutants that formed aggregates on the ER membrane, the *in vivo* depurination was detected to examine how the distinct transport pattern affected the depurination. The matG83D-EGFP was the most active among all the RTA mutants tested. The depurination of matG83D-EGFP at 2 hpi was about seven-fold less than that of the wild type matRTA-EGFP and was similar to the wild type at 4 hpi and thereafter (Figure 3.4A). The depurination of preG83D-EGFP could be detected from 4 hpi and the level was 25-fold less than that of the preRTA-EGFP (Figure 3.4B). Compared with the matG83D-EGFP, the trafficking of preG83D-EGFP had a significant effect on its depurination. The other mutant in this group, matS215F-EGFP, depurinated 15-fold less than matRTA-EGFP at 2 hpi (Figure 3.4A). At 4 hpi, the depurination rose up to a peak and was around twofold less than that of matRTA-EGFP. However, the depurination of preS215F-EGFP was significantly reduced and was

about 300-fold less than that of the wild type (Figure 3.4B). The results suggested that preG83D-EGFP and preS215F-EGFP had ER-to-cytosol transport, although their dislocation was reduced and affected their depurination as a consequence.

RTA variants fold and are processed differently

Immunoblot analysis (Figure 3.7) was performed with both membrane fraction and cytosol fraction of yeast cells expressing wild type RTA and each nontoxic RTA mutant without the EGFP tag to better resolve the migrating species on the SDS-PAGE. The proteins were either treated with (+) or without (-) endoglycosidase H (Endo H) to cleave the mannose rich *N*-linked oligosaccharides. With this treatment, the *N*-glycosylation profile of the proteins was determined. PreRTA migrated as three species in the membrane fraction. The differences in the migrating rates were results of the nine-amino acid propeptide (p) and the glycosylation (g). The top two slower migrating bands represented the glycosylated form with (g+p) and without the nine-amino acid propeptide ($g+p_0$). They migrated faster and corresponded to the top and bottom bands respectively after Endo H treatment. The fastest migrating form represented the nonglycosylated and propeptide attached form (g_0+p), since it corresponded to the band of the same size after Endo H treatment. The results suggested that the propeptide of a fraction of preRTA is removed in the ER. The existence of glycosylated forms either with or without propeptide indicated that the propeptide cleavage of wild type preRTA is preceded by its *N*-glycosylation.

In the cytosol fraction, the majority of preRTA was in glycosylated form without propeptide ($g+p_0$) which reduced the size after Endo H treatment. The less abundant faster migrating band was deglycosylated form (g_0+p_0), which did not change in size after Endo H treatment. It suggests that dislocation to the cytosol occurs only with the propeptide cleaved forms. The nontoxic RTA mutant preG212E migrated as four species in the membrane fraction. Besides the g+p, $g+p_0$ and g_0+p forms that were also present with the wild type, it had a major g_0+p_0 band, which was not apparent in the membrane fraction of cells expressing wild type preRTA. The g_0+p_0 band might be derived from deglycosylation of the $g+p_0$ form. In addition, among the migrating species of preG212E in the membrane fraction, the glycosylated forms accounted for a minor fraction compared with nonglycosylated forms, suggesting that *N*-glycosylation was not efficient for preG212E or the deglycosylation of the ER associated preG212E was rapid. In the cytosol, the majority of the protein was in g_0+p_0 form. Similarly, preP95L/E145K migrated as four bands in the membrane fraction. In the cytosol fraction, the $g+p_0$ form had slightly higher amount than the g_0+p_0 form.

RTA mutants preG83D and preS215F that formed punctate structures on the ER both had similar migrating pattern on SDS-PAGE (Figure 3.7). They had g+p, $g+p_0$, g_0+p and a minor g_0+p_0 form in the membrane fraction. Although the amount of protein in the membrane fraction was high for both preG83D and preS215F, they were not detectable in the cytosol, suggesting the proteins may form aggregates, which agreed with the punctate structures observed with the EGFP tagged fusions under the fluorescence microscope (Figure 3.3A).

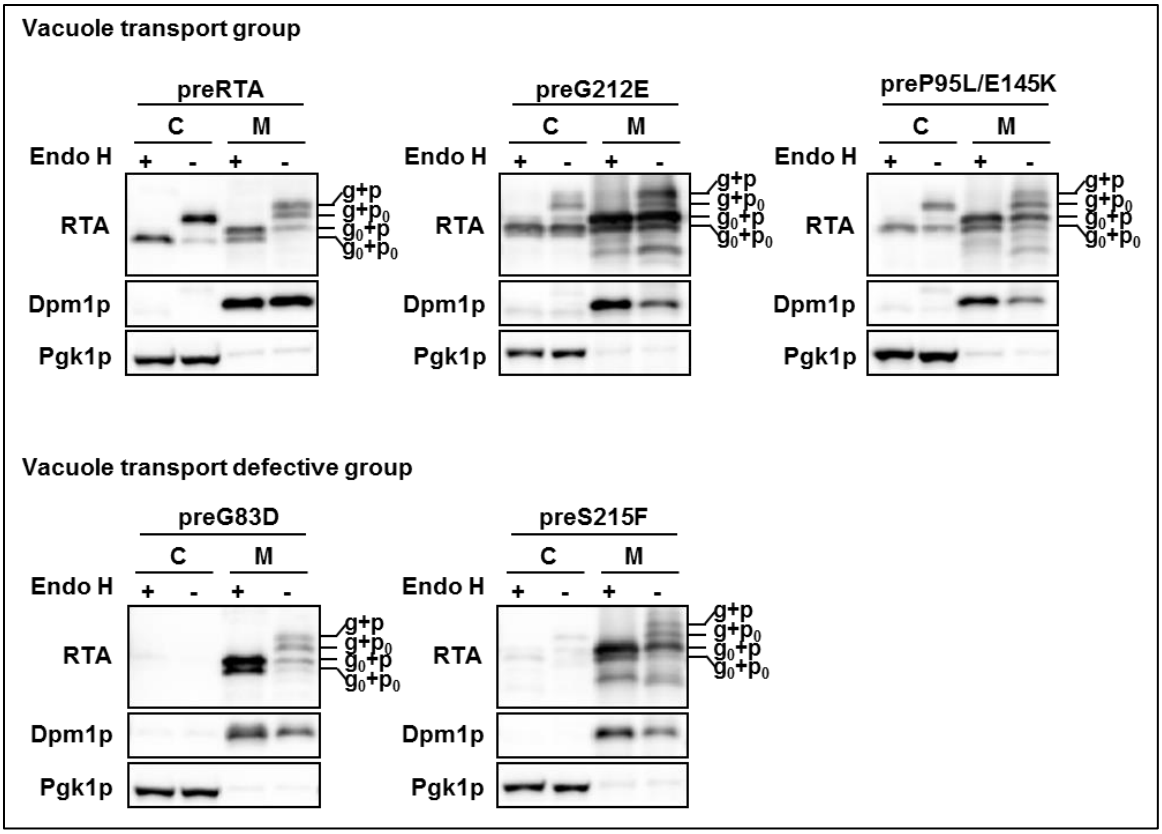

Figure 3.7 Protein expression of the precursor forms of wild type RTA and RTA mutants. Membrane (M) and cytosol (C) fractions isolated at 6 hpi were treated with (+) or without (-) Endo H to cleave the *N*-glycans. The proteins (5 µg) were separated on a 10% SDS-polyacrylamide gel and probed with monoclonal anti-RTA (1:5000). The blot was reprobed with the ER membrane marker Dpm1p and cytosolic marker Pgk1p as loading controls. The group that is capable in vacuole transport has soluble proteins in the cytosol, whereas RTA mutants that are defective in vacuole transport form aggregates.

To confirm the vacuole transport of wild type preRTA, preG212E and preP95L/E145K without the EGFP tag, the vacuole fraction was isolated from yeast expressing preRTA, preG212E and preP95L/E145K, as well as preG83D and preS215F as negative controls at 6 hpi (Figure 3.8). Immunoblot analysis showed that preRTA, preG212E and preP95L/E145K were all present in the vacuole fraction at 6 hpi, whereas preG83D and preS215F were absent, consistent with the microscopic images with the EGFP fusions. Although the

vacuole fraction contained some ER membrane contamination based on the loading control Dpm1, the amount was less than that in the membrane fraction and the distributions of the migrating species of RTA in the vacuole fraction and in the membrane fraction were different, suggesting that the proteins present in the vacuole fraction were not from the contamination. The vacuole marker, Vph1p, encoding the Vacuolar H^+-ATPase was 100 kDa in the membrane fraction, but partially reduced to 75 kDa in the vacuole fraction, due to proteolysis during vacuole isolation (103). In the vacuole fraction of the yeast expressing wild type preRTA, preRTA migrated as four species, including g+p, g+p_0, g_0+p and g_0+p_0. The results suggested that the propeptide attached forms are exclusively sorted to the vacuole fraction from the ER, whereas the dislocation to the cytosol only occurs with the propeptide cleaved forms as described above. The vacuole fractions of cells expressing preG212E and preP95L/E145K also contained all four migrating species. However, the migrating species of each mutant and wild type RTA are not the same, suggesting that preG212E, preP95L/E145K and wild type RTA are processed differently. The yeast cells expressing RTA mutants preG83D and preS215F had insignificant amount of proteins in the vacuole fraction, which could be due to the contamination from the ER membrane. The results suggested that preG83D and preS215F are defective in vacuole transport and the proteins are only associated with the ER.

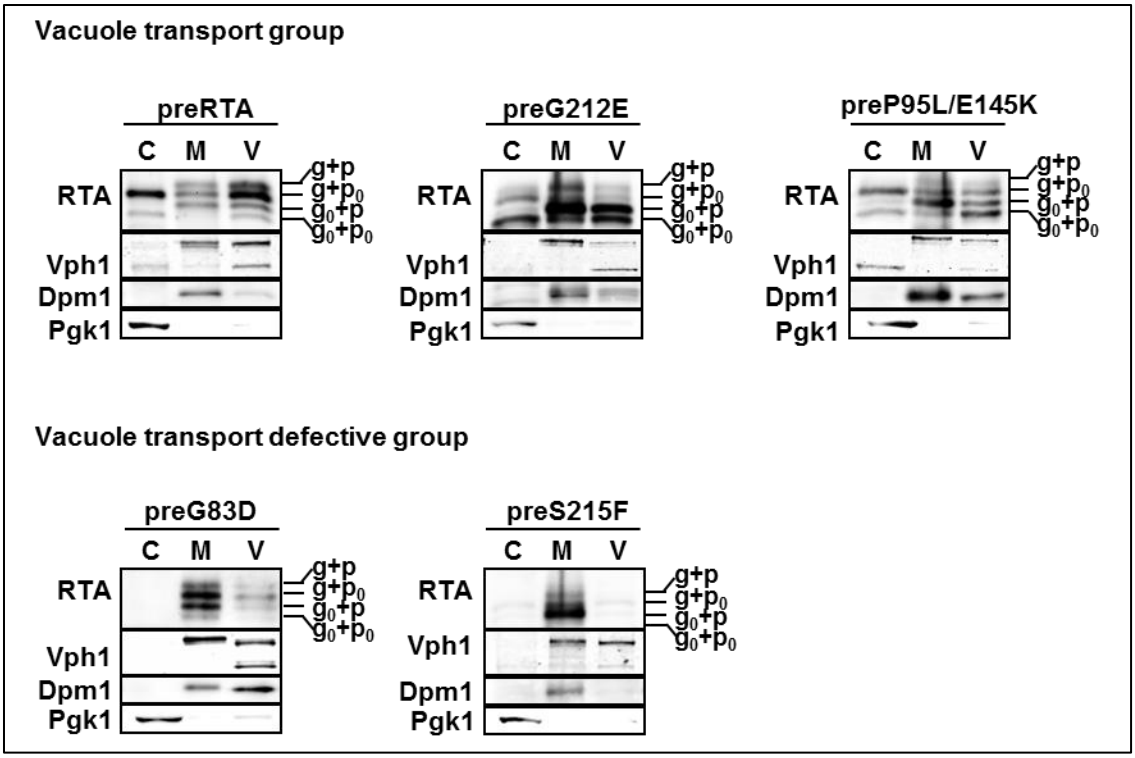

Figure 3.8 Protein expression of wild type RTA and RTA mutants in vacuole (V), membrane (M) and cytosol (C) fractions. The Vacuole, membrane and cytosol fractions were isolated at 6 hpi. The proteins (5 µg) were separated on a 10% SDS-polyacrylamide gel and probed with monoclonal anti-RTA (1:5000). The blot was reprobed with vacuole membrane marker, Vph1p, ER membrane marker, Dpm1p and cytosol marker, Pgk1p.

Based on the intracellular localization, depurination and subcellular fractionation, wild type RTA and its variants were divided into two groups. One group contained RTA competent in both ER-to-cytosol and ER-to-vacuole trafficking, including wild type RTA, preG212E and preP95L/E145K. The other group contained RTA mutants that only had ER-to-cytosol transport and formed aggregates, including preG83D and preS215F.

Png1 affects the toxicity and depurination activity of RTA variants differently

It was shown that Png1 was responsible for the deglycosylation of RTA_{Δ} and RTL and further assisted in the degradation of them by proteasome (54, 58), and that yeast Png1 can distinguish the native form and the unfolded form of the glycoprotein (98). The structural selectivity of Png1 raises the question of how the Png1 deciphers the structural elements in RTA variants. The intracellular localization of RTA variants clearly suggests that the vacuole transport defective mutants preG83D and preS215F form aggregates and are folding defective proteins. In contrast, preG212E and preP95L/E145K closely resemble wild type preRTA.

I transformed the precursor forms of wild type RTA as well as nontoxic RTA variants into the parental BY4743 and *png1*Δ strains to determine if *PNG1* deletion altered the deglycosylation and the degradation of these proteins. The cell viability, deglycosylation or depurination level of vacuole transport competent mutants preG212E and preP95L/E145K (Figure 3.9A-C), and vacuole transport defective mutant preS215F (Figure 3.10A-C) were similar in *png1*Δ strain and the parental BY4743 strain, suggesting that they were not substrates for Png1. The effects of Png1 on viability, deglycosylation and depurination of wild type preRTA and preG83D are described below.

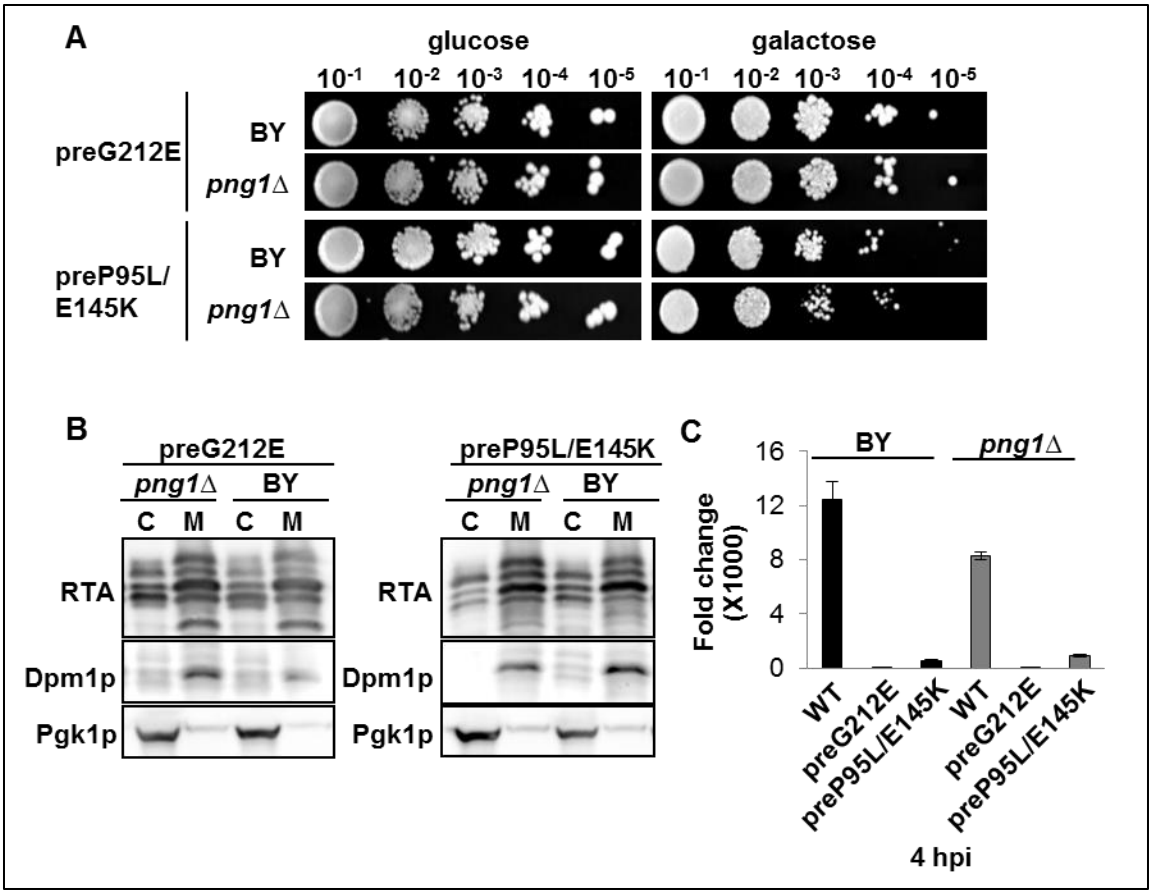

Figure 3.9 RTA mutants preG212E and preP95L/E145K were not substrates for Png1. (A) The viability of BY and *png1*Δ strains expressing preG212E or preP95L/E145K. A series of ten-fold dilutions were spotted on glucose and galactose plates after overnight growth in glucose. (B) Protein expression of BY and *png1*Δ strains expressing preG212E and preP95L/E145K. The membrane fraction (M) and cytosol fraction (C) isolated at 6 hpi were separated on a 10% SDS-polyacrylamide gel and probed with monoclonal anti-RTA (1:5000). The ER membrane marker Dpm1p and cytosolic marker Pgk1p were used as loading controls. (C) Ribosome depurination by wild type preRTA, preG212E and preP95L/E145K expressed in BY and *png1*Δ strains *in vivo* by qRT-PCR. Yeast ribosomes were extracted at 4 hpi.

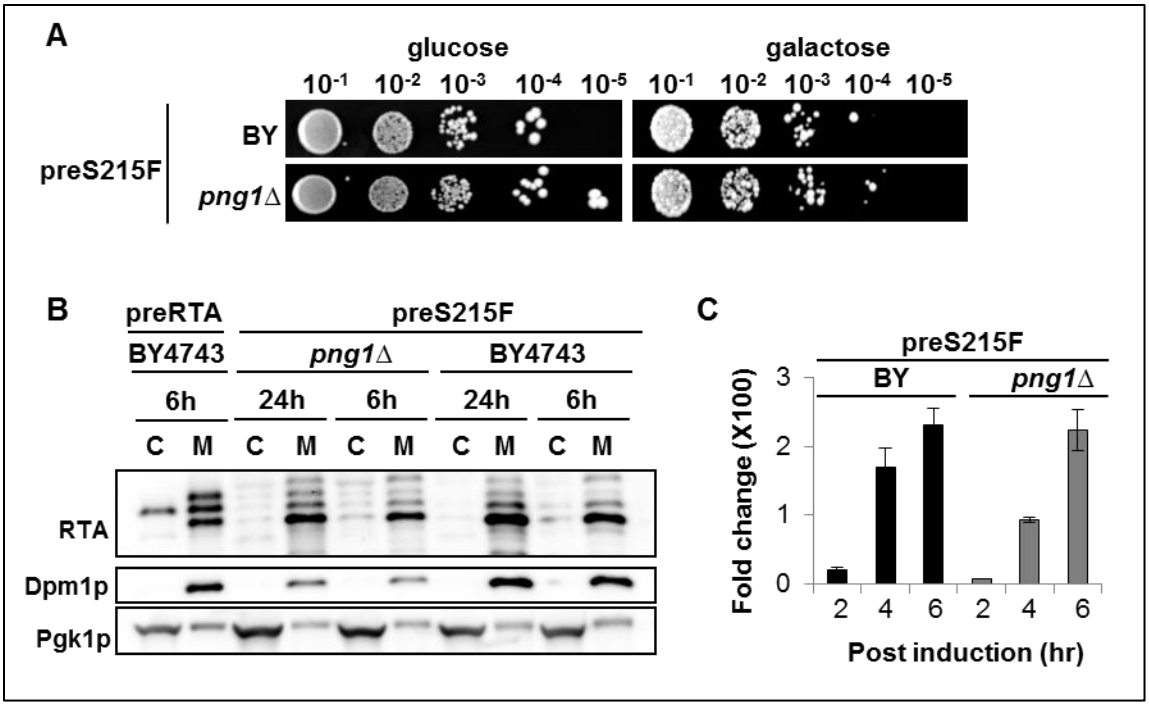

Figure 3.10 RTA mutant preS215F was not a substrate for Png1. (A) The viability of BY and *png1*Δ strains expressing preS215F. A series of ten-fold dilutions were spotted on glucose and galactose plates after overnight growth in glucose. (B) Protein expression of BY and *png1*Δ strains expressing preS215F. The membrane fraction (M) and cytosol fraction (C) isolated at 6 hpi and 24 hpi were separated on a 10% SDS-polyacrylamide gel and probed with monoclonal anti-RTA (1:5000). The ER membrane marker Dpm1p and cytosolic marker Pgk1p were used as loading controls. (C) Ribosome depurination by preS215F expressed in BY and *png1*Δ strains *in vivo* by qRT-PCR. Yeast ribosomes were extracted at 2, 4, 6 hpi.

Viability analysis was performed by spotting ten-fold serial dilutions on plate. The viability of wild type preRTA was tested on glucose plate at 0 h and 24 h after galactose induction. The viability was also tested on galactose plate for continuous induction, but preRTA were too toxic to grow under this condition. It showed (Figure 3.11A) that preRTA had similar toxicity in BY4743 and *png1*Δ strain based on the cell viability on glucose plate at 24 hpi. The result is consistent with the cell survival by using RTA_{E177D} as a folded form of RTA (53).

The viability of preG83D was tested on galactose plate after overnight growth in non-inducing medium containing glucose. Because preG83D was less enzymatically active, the galactose plate introduced more growth pressure due to the continuous induction condition after spotting. Therefore, the differences in the viability of BY4743 and *png1*Δ strains expressing preG83D would be more evident. In contrary to wild type preRTA, the viability of *png1*Δ strain expressing preG83D was significantly reduced compared with that of BY4743 expressing preG83D (Figure 3.11A), suggesting that Png1 is involved in the degradation of preG83D. The viability result of preG83D agrees with the result using RTA_{Δ} as a folding defective form (53).

Immunoblot analysis (Figure 3.11B) of preG83D and preRTA was performed with both membrane and cytosol fractions and treated with (+) and without (-) Endo H to distinguish the glycosylated forms. In the BY4743 strain, preRTA had three bands in the membrane fraction representing g+p, g+p_0 and g_0+p forms as described above. In the cytosol, there were g+p_0 and deglycosylated form g_0+p_0, suggesting that the dislocated glycosylated preRTA with the propeptide was deglycosylated in the cytosol. In the *png1*Δ strain, the migrating species did not change in the ER membrane. However, in the cytosol, the deglycosylated form of RTA became less abundant. The results suggested that the deglycosylation activity of preRTA in the cytosol was compromised without Png1. preG83D migrated as four bands in the membrane fraction. As described above, they were g+p, g+p_0, g_0+p and g_0+p_0 forms. PreG83D cannot be detected in the cytosol fraction as shown above. In the *png1*Δ strains, the

deglycosylated form without propeptide (g_0+p_0) disappeared from the membrane fraction. The g_0+p form which contained the nonglycosylated and deglycosylated preG83D became less abundant. The results suggested that Png1 was involved in the deglycosylation of the membrane associated preG83D.

Depurination examined with quantitative RT-PCR was used as a sensitive method to indicate the catalytic activity in the cytosol (Figure 3.11C). When expressed in the parental BY4743 strain, preRTA had a negligible amount of depurination at 2 hpi. At 4 hpi, the depurination increased significantly and was about 27-fold higher than that at 2 hpi and further increased at 6 hpi to about 38-fold more than that at 2 hpi. However, with *PNG1* deletion, the depurination of preRTA increased slowly and was about 2.8 and 3.6 times lower than that in the wild type BY4743 at corresponding time points. The decrease in the depurination level of preRTA in *png1*Δ strain was not a global effect, since the depurination level of the nonglycosylated preN10Q/N236Q, which was not a substrate for Png1 (54), was not affected upon *PNG1* deletion (Figure 3.12A-B). The reduced depurination of wild type preRTA in *png1*Δ strain suggests that Png1 affects the dislocated preRTA, but is not responsible for the degradation of preRTA. In contrast, PreG83D expressed in *png1*Δ strain had about three-fold and five-fold higher depurination than that in the BY4743 at 4 and 6 hpi. The increased depurination of preG83D in *png1*Δ strain suggests that Png1 is involved in degradation of the folding defective preG83D, which agrees with the viability results.

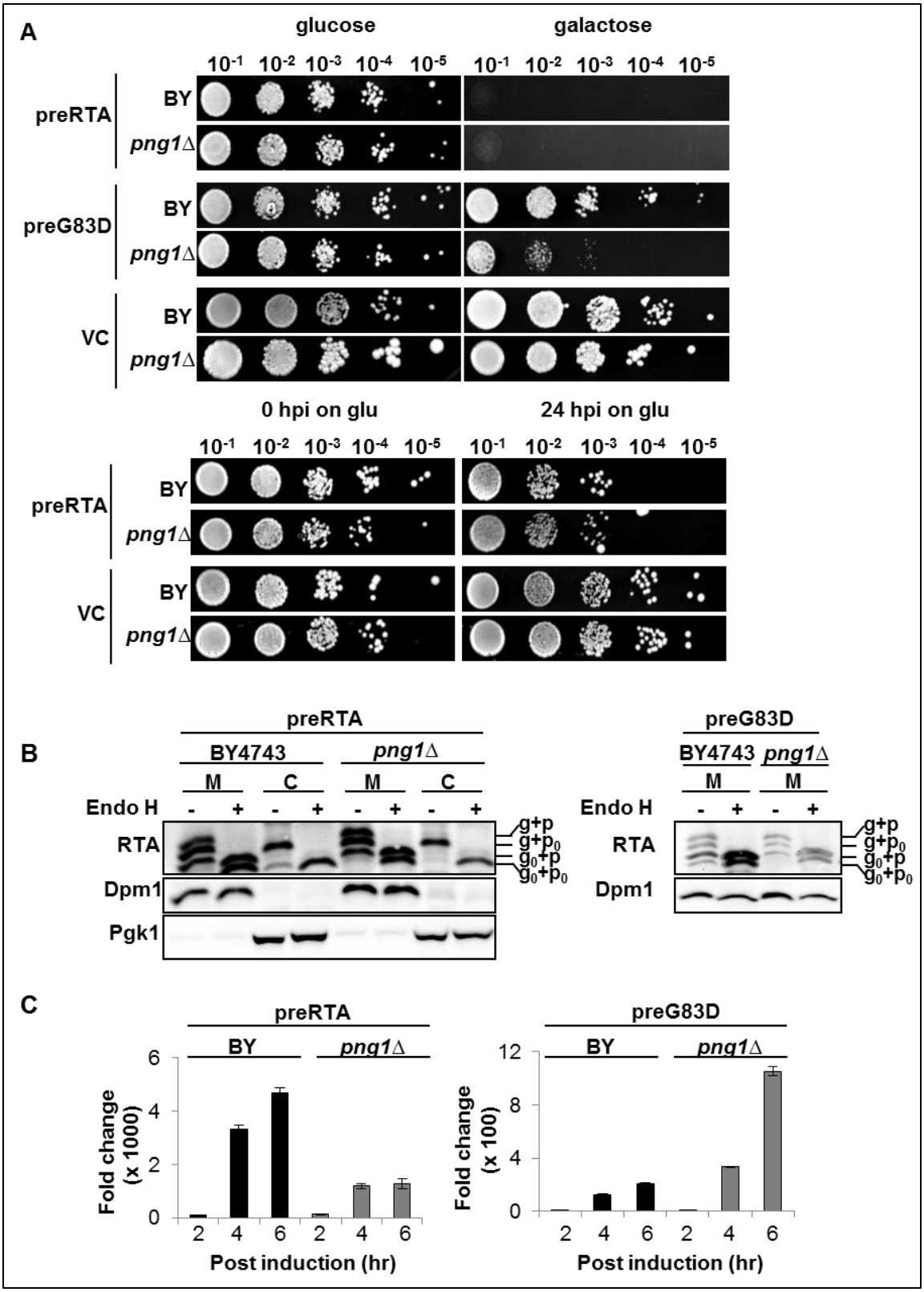

Figure 3.11 Wild type preRTA and preG83D had different responses to *PNG1* deletion. (A) The viability of BY and *png1*Δ strains expressing preRTA or preG83D. A series of ten-fold dilutions were spotted either on galactose plate

after overnight growth in glucose media or plated on glucose plate at 0 and 24 h after galactose induction. (B) Immunoblot analysis of membrane and cytosol fractions of BY and *png1*Δ strains expressing preRTA or preG83D. The proteins (5 µg) were treated with (+) or without (-) Endo H. (C) Ribosome depurination by preRTA or preG83D expressed in BY and *png1*Δ strains *in vivo* by qRT-PCR. Yeast ribosomes were extracted at 2, 4, 6 hpi.

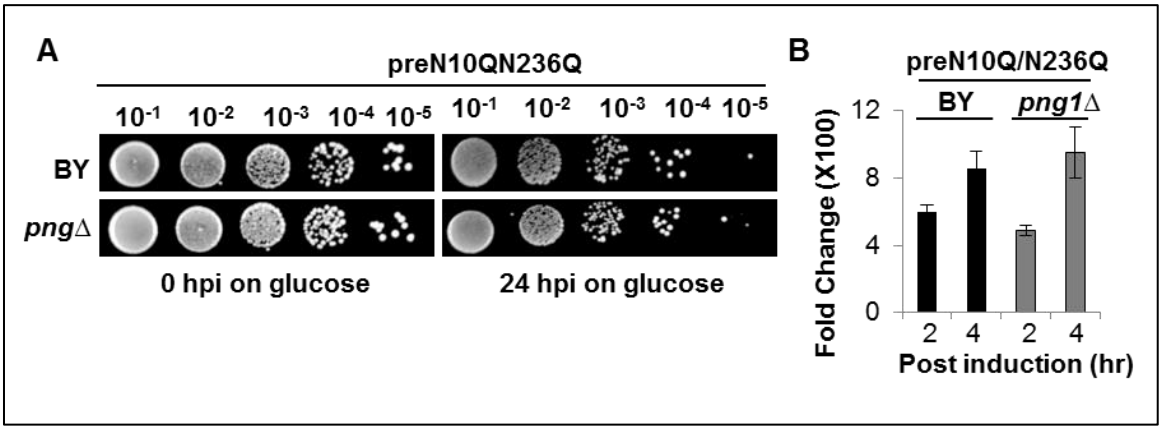

Figure 3.12 The nonglycosylated RTA mutant was not a substrate for Png1. (A) The viability of BY and *png1*Δ strains expressing the nonglycosylated RTA mutant preN10Q/N236Q. A series of ten-fold dilutions were spotted on glucose plate at 0 and 24 h post induction. (B) Ribosome depurination by preN10Q/N236Q expressed in BY and *png1*Δ strains *in vivo* by qRT-PCR. Yeast ribosomes were extracted at 2 and 4hpi.

I then asked whether the vacuole transport of wild type preRTA was affected in the *png1*Δ strain. As observed by the epifluorescence microscope (Figure 3.13), the majority of preRTA-EGFP was localized to the ER at 2 and 4 hpi in BY4743 strain. At 4 hpi, preRTA-EGFP in only 3% (*n*=100) of the cells were localized to the vacuole. Vacuole transport was detected at 6 hpi when preRTA-EGFP was localized in the vacuole in 34% (*n*=100) of the cells. In *png1*Δ strain, the vacuole transport of preRTA occurred at the same time. At 4 hpi 2% (*n*=100) and at 6 hpi 37% (*n*=100) of the cells had preRTA-EGFP in the vacuole in *png1*Δ strain. The results suggest that the vacuole transport of preRTA is not

affected by *PNG1* deletion, in agreement with the previous study in which CPY* was used as a substrate and no differences were observed in the vesicular transport in *png1*Δ and in the isogenic wild type strain (109).

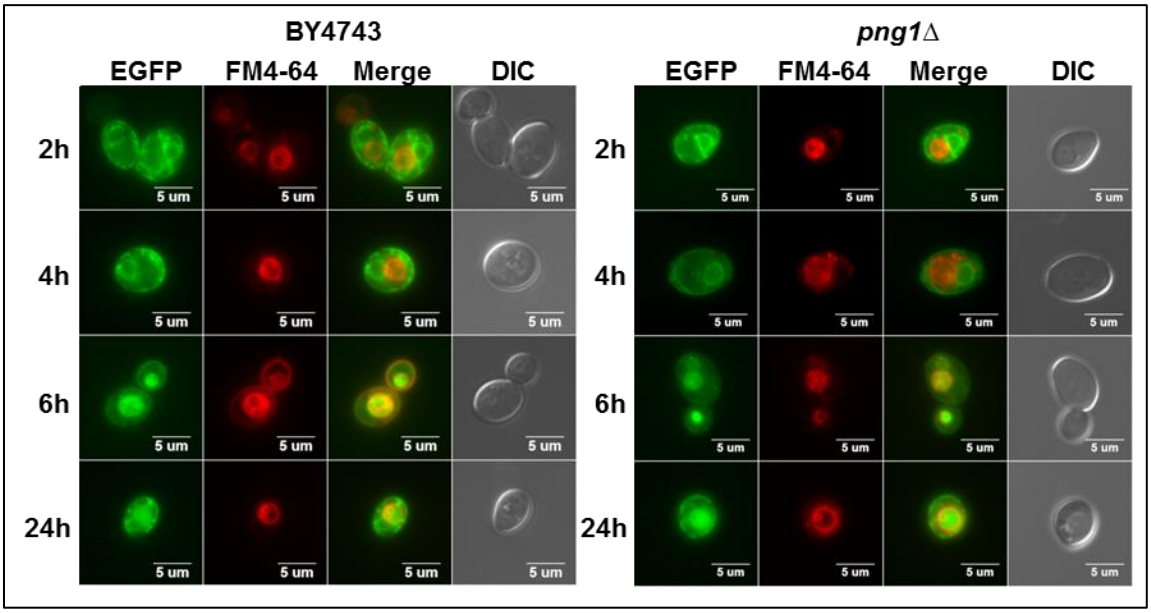

Figure 3.13 The intracellular trafficking of preRTA-EGFP in BY4743 and *png1*Δ strains. The images of yeast cells harboring the preRTA-EGFP were taken at 2, 4, 6 and 24 hpi with an Olympus BX41 fluorescence microscope. Yeast cells were treated with FM4-64 to stain the vacuole. Merged images show localization of preRTA-EGFP relative to the vacuole.

I then examined whether the expression of Png1 driven by the constitutive promoter *GPD1* could complement the degradation defect in *png1*Δ strain expressing preG83D. As shown in Figure 3.14, the expression of Png1 recovered the growth of *png1*Δ strain expressing preG83D (Figure 3.14A). The expression of the preG83D and the transformed *PNG1* was confirmed by detecting the total protein extracts (Figure 3.14B). The depurination level was also reduced to the same level of BY4743 expressing preG83D (Figure 3.14C). For wild type preRTA

(Figure 3.15), the viability of cells expressing preRTA was not affected by Png1 (Figure 3.15A). The expression of Png1 in the *png1*Δ strain was confirmed with the total protein extracts (Figure 3.15B) and it restored the depurination level (Figure 3.15C).

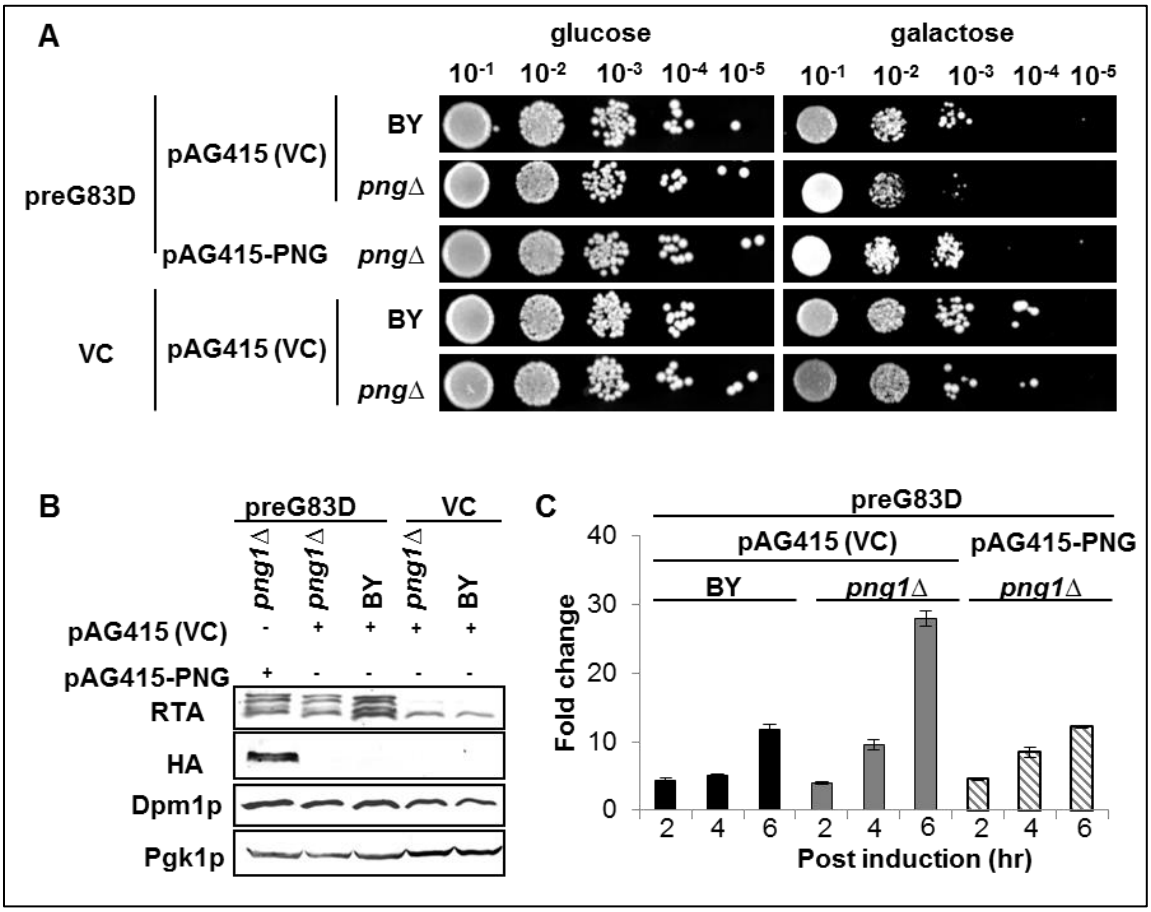

Figure 3.14 Expression of Png1 in the *png1*Δ strain restored the viability and depurination of preG83D in yeast cells. (A) The viability of BY and *png1*Δ strains co-expressing preG83D and *PNG1* or its vector driven by a constitutive promoter *GPD1*. A series of ten-fold dilutions were spotted on galactose plate and glucose plate after overnight growth in glucose media. (B) Protein expression of BY and *png1*Δ strains co-expressing preG83D and *PNG1* or its vector. Whole protein extracts isolated at 6 hpi were separated on a 10% SDS-polyacrylamide gel and probed with monoclonal anti-RTA (1:5000). The blot was reprobed with anti-HA (1:1000) to detect the expression of C-terminal HA tagged Png1. The ER membrane marker Dpm1p and cytosolic marker Pgk1p were used as loading controls. (C) Ribosome depurination by preG83D expressed in BY

and *png1*Δ strains transformed with *PNG1* or its vector *in vivo* by qRT-PCR. Yeast ribosomes were extracted at 2, 4, 6 hpi.

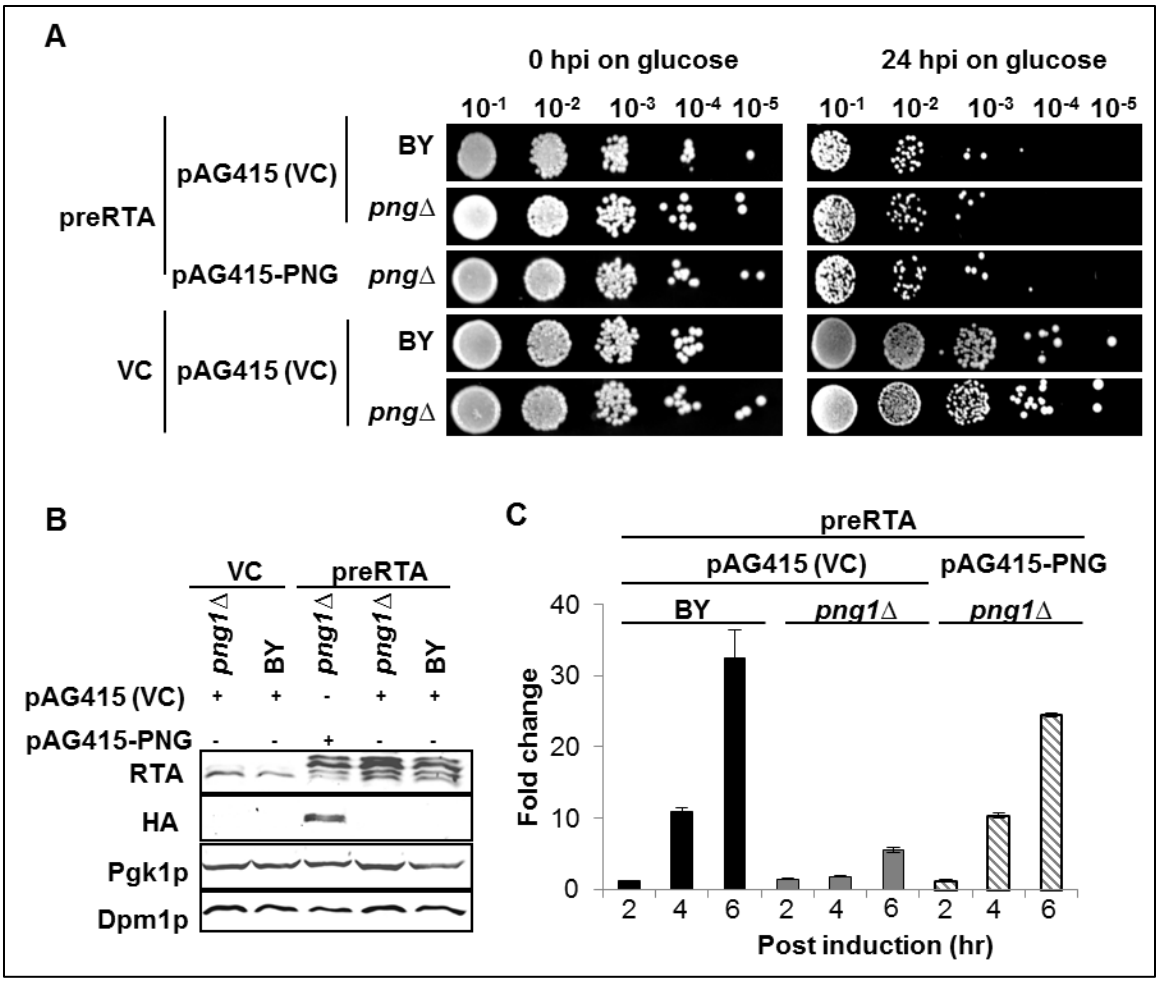

Figure 3.15 Expression of Png1 in the *png1*Δ strain restored the depurination of preRTA in yeast cells. (A) The viability of BY and *png1*Δ strains co-expressing preRTA and *PNG1* or its vector driven by a constitutive promoter *GPD1*. A series of ten-fold dilutions were spotted on glucose plate at 0 and 24 h post induction in galactose media. (B) Protein expression of BY and *png1*Δ strains co-expressing preRTA and *PNG1* or its vector. Whole protein extracts isolated at 6 hpi were separated on a 10% SDS-polyacrylamide gel and probed with monoclonal anti-RTA (1:5000). The blot was reprobed with anti-HA (1:1000) to detect the expression of C-terminal HA tagged Png1. The ER membrane marker Dpm1p and cytosolic marker Pgk1p were used as loading controls. (C) Ribosome depurination by preRTA expressed in BY and *png1*Δ strains transformed with *PNG1* or its vector *in vivo* by qRT-PCR. Yeast ribosomes were extracted at 2, 4, 6 hpi.

DISCUSSION

The mutations in RTA result in multiple trafficking pathways

Because ribosomes are sensitive to the depurination by the wild type RTA, RTA variants with reduced catalytic activity are often used to study the trafficking pathway exploited by RTA. Compared with wild type RTA, however, RTA mutants do not only have altered structures and activities, they may also follow different intracellular trafficking pathways as a result of changed structural motifs as important sorting determinants. To unravel the structure of RTA related to its trafficking, the folding competent form RTA_{E177D} and the folding defective form RTA_{Δ} were tested on their requirements for the known ERAD components. The results showed that different sets of cytosolic components in yeast were involved in the degradation and toxicity of RTA_{E177D} and RTA_{Δ} after their dislocation (53). The model represented by the folded and misfolded forms of RTA provided insights into the structural requirements for sorting in the ERAD pathway. However, it remains elusive whether RTA under the sophisticated scrutiny of the ERQC machinery is recognized only by the general unfolding of RTA_{Δ} for routing to distinct ERAD machinery or the sorting signals may be diverse and lead to multiple pathways. Moreover, the discovery of vacuole transport (103) adds to the complexity of the intracellular trafficking of RTA. In the present study, I substantiate the knowledge of how the sequence motifs affect the intracellular trafficking of RTA by investigating a series of nontoxic RTA mutants. Because the ribosome depurination level alone does not count entirely for the cytotoxicity of these mutants (80), the intracellular trafficking should be a contributor which

indirectly affects the ribosome depurination by diverting RTA from the ribosomes or targeting RTA for degradation. I showed that RTA mutants with reduced toxicity had different localizations and varied in their requirements for the cytosolic ERAD component Png1. Wild type preRTA-EGFP, preG212E-EGFP and preP95L/E145K-EGFP were all sorted to the vacuole besides dislocation to the cytosol, but transport to the vacuole was delayed in cells expressing preP95L/E145K-EGFP. The dislocated wild type RTA was deglycosylated by the cytosolic Png1, but preG212E and preP95L/E145K were not. The other group of RTA mutants, PreG83D-EGFP and preS215F-EGFP had defects in the vacuole transport. They formed large punctate structures on the ER and cell periphery. Their corresponding mature forms were enriched in the nuclei, suggestive of the proteasome degradation in the nuclei (107). These results suggest that the mutations of G83D and S215F lead to an altered targeting signal that affects both precursor and mature forms. The preG83D was demonstrated to be deglycosylated by Png1 and the subsequent degradation by the proteasome was facilitated. In contrast, although preS215F was also a misfolded RTA form, neither the deglycosylation nor degradation of preS215F was affected by Png1. Taken together, the wild type and nontoxic RTA mutants all behaved differently in response to *PNG1* deletion. The results provide evidence that the sorting mechanisms of RTA are sophisticated and diverse. In the ER, RTA is subjected to the vacuole transport and/or the cytosol dislocation. Even if RTA variants are sorted similarly in the ER, subsequently, in the cytosol, the dislocated RTA is

further differentiated by the cytosolic host factors. The differences in their oligosaccharide modifications may act as a sorting signal.

Vacuole transport is an alternative degradation pathway for RTA

It was demonstrated that RTA undergoes ERAD pathway for cytosolic entry, but can competently evade the proteasome degradation, because it carries only a few lysine residues as sites for ubiquitin tagging (59). I found that besides ER-to-cytosol transport via the ERAD, preRTA-EGFP had ER-to-vacuole transport. I hypothesized that vacuole transport may be an alternative degradation pathway for preRTA. Several lines of evidence have demonstrated that RTA has anterograde trafficking from the ER to the Golgi (53, 58, 110). Golgi apparatus is part of the ERQC machinery and contains anterograde transport and retrograde transport dynamics (111). Therefore, the delivery of preRTA to the vacuole may be preceded by the transport to the Golgi. Similarly, The canonical ERAD substrate CPY* was also shown to be sorted to two competing pathways within the ER, which were ERAD and ER exit followed by vacuole delivery. The CPY* mutant carrying ER exit signal to the vacuole had a faster degradation rate than the CPY* mutant acting only as an ERAD substrate, since the rate of vacuole turnover is higher than that of the ERAD (99). In the case of RTA mutants, the precursor forms of P95L/E145K depurinated at a higher level in the cytosol than G212E, although G212E was more catalytically active. The lower *in vivo* depurination of preG212E might be due to the faster degradation which is a result of the faster vacuole delivery of preG212E than that of preP95L/E145K.

Although preRTA has two parallel pathways, the three migrating species of wild type preRTA in the membrane fraction undergo different pathways following ER export. The propeptide attached glycosylated and nonglycosylated forms of preRTA was detected exclusively in the vacuole fraction (103) (Figure 3.8), suggesting that these species do not go through the ERAD pathway but are transported to the vacuole. In contrast, the propeptide cleaved glycosylated form dislocated to the cytosol. These observations suggest that the propeptide of preRTA is an important sorting signal. This is in agreement with our previous study that showed deletion of the propeptide delayed vacuole delivery of preRTA. The propeptide may influence the vacuole transport by facilitating the folding of preRTA as was suggested with the CPY in *in vitro* experiments (112, 113).

RTA variants have differential requirements for Png1

RTA dislocates to the cytosol from the ER through the ERAD-L pathway. One crucial structural element required for substrate recognition in the ERAD pathway is *N*-linked glycans. In the ER luminal side, two ERAD components, Htm1 (the yeast homolog of mammalian EDEM) and Yos9 (the yeast homolog of mammalian OS-9), are both required for RTA dislocation and their functions are *N*-glycan dependent (54). In the cytosol, PNGase in the ERAD pathway catalyzes the de-*N*-glycosylation of unfolded glycoproteins and assists its degradation by the proteasome. PNGase seems to have stringent structural constraints for substrates deglycosylation. It is suggested that yeast Png1 prefers high mannose type oligosaccharides over complex type (114). It has higher

affinity for $GlcNAc_2Man_9$ than $GlcNAc_2$. The truncated glycoproteins lacking terminal mannose residues do not act as substrates for Png1 (115). In addition to the structure of the oligosaccharide chains, Png1 could distinguish the folded glycoprotein and the denatured glycoproteins *in vitro* (98). However, the structural determinants of RTA for Png1 recognition are ambiguous. A recent study in yeast showed that *PNG1* deletion did not affect the growth of cells expressing RTA_{E177D} (53), but decreased the viability of cells expressing a folding defective RTA_{Δ} (58). It seemingly suggests that Png1 could discriminate the folded form and the unfolded form of RTA. However, it was contradicted by the observations that the folded form RTA_{E177D} is deglycosylated in the cytosol in yeast, plant and mammalian cells (46, 57, 102). One theory to explain the conflicting observations is that in both mammalian and yeast systems, PNGase is proposed to exist as a free pool and a pool in complex with Rad23/HR23B which functions in releasing the glycan chains from the proteins to meet the conformational constrains in protein degradation by the proteasomes (58, 116). It is possible that the folded RTA_{E177D} is only deglycosylated by the free pool of Png1 in the cytosol, so that its degradation is not affected. Our results supported this possibility. I showed that Png1 deglycosylated the wild type preRTA in the cytosol fraction, but not in the membrane fraction. The viability of cells expressing wild type preRTA was not altered with *PNG1* deletion, which is consistent with previous results using RTA_{E177D} as the folded form (53), suggesting that Png1 does not affect the degradation of wild type preRTA. The results fit in the model (Figure 3.16) in which Png1 is situated in the cytosol as a free pool which is

separated from the proteasomal degradation machinery (58, 97, 116). Because wild type preRTA is not a substrate for Png1 mediated proteasomal degradation, *PNG1* deletion will not confer depurination increase of preRTA, rather, from our results, the depurination by preRTA was reduced. Because the glycosylated and nonglycosylated forms of RTA took different degradation pathways (58), one explanation is that the deglycosylated form has a lower degradation rate, therefore in the absence of deglycosylation, when only glycosylated form exists, the degradation rate is elevated. On the other hand, the structurally distinctive RTA mutant preG83D increased ribosome depurination and toxicity in response to *PNG1* deletion, suggestive of a decrease in the degradation. The deglycosylation happened on the membrane associated preG83D. The results fit in another model (Figure 3.16) in which Png1 is situated in the ER membrane and deglycosylates glycoproteins in a co-retrotranslocational manner (116). The binding to the ER is possibly through the N-terminal helix that associates with Rad23 (100)**.** The deglycosylated preG83D are then sent to the proteasome linked with the Png1 for destruction (97). It should be noted that since preG83D does not have the alternative vacuole degradation pathway, the defects in the ERAD pathway tend to have a global effect to compromise cell survival (105, 117). Therefore, the end point cell viability is not sufficient to indicate Png1 mediated degradation of preG83D. To complement this, I also detected depurination and demonstrated that the increased toxicity of preG83D to *png1*Δ strain was not a result of its inability to utilize the alternative vacuole degradation pathway and loss of ERAD simultaneously (105), instead was caused by the

increased depurination in response to Png1 depletion. The results also suggest that the reduction in the toxicity of preG83D mutant is partially because it is a substrate for the Png1-Rad23 degradation complex. Although preS215F forms aggregates like preG83D and is obviously a misfolded protein, it does not respond to *PNG1* deletion. It is possible that this mutant is not a substrate for Png1 or is not dislocated through the ERAD-L pathway at all. Although preG212E and preP95L/E145K closely resemble wild type preRTA in the retrotranslocation, their deglycosylation or the depurination is not affected by Png1 depletion, indicating that they evade Png1 in the ERAD pathway completely.

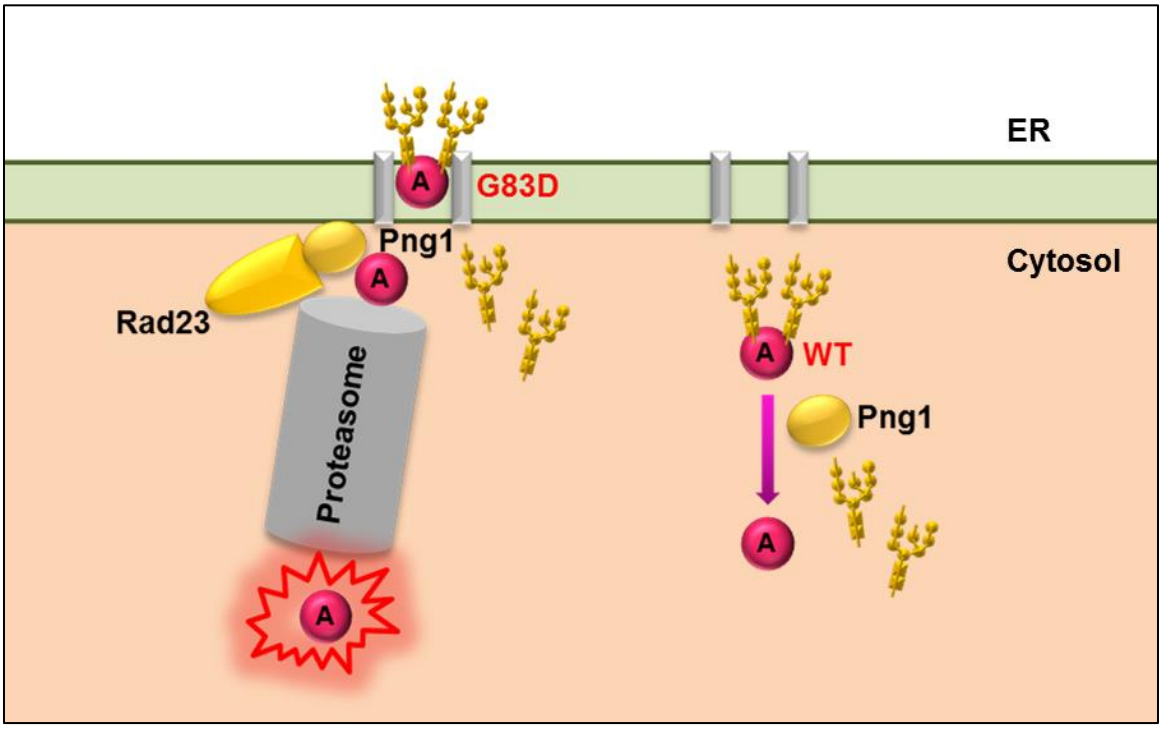

Figure 3.16 Schematic representation of different subsets of Png1 involved in the deglycosylation of preG83D and wild type preRTA. preG83D is deglycosylated by the Png1 in complex with proteasome for degradation. Wild

type preRTA is deglycosylated by free pool of Png1, which is separated from the proteasomal degradation.

MATERIALS AND METHODS

Plasmids and yeast strains

Wild type preRTA contains a 35-residue N-terminal extension, followed by 267-residue RTA (preRTA-EGFP, NT1205); wild type mature RTA consists of 267-residue RTA (matRTA-EGFP, NT1206). The precursor and mature forms of G83D, S215F, G212E and P95L/E145K with EGFP tag contained cDNAs with point mutations G83D, S215F, G212E and P95L/E145K respectively The above cDNAs were fused with EGFP tag at the 3' end and cloned into yeast vector containing LEU2 marker (NT198) downstream of the galactose-inducible GAL1 promoter (preG83D-EGFP, NT1248; matG83D, NT1254; preS215F-EGFP, NT1251; matS215F-EGFP,NT1257; preG212E-EGFP,NT1250; matG212E-EGFP, NT1256; preP95L/E145K-EGFP, NT1252; matP95L/E145K-EGFP,NT1258). The cDNAs corresponding to precursor forms of RTA and RTA mutants were cloned into NT198 downstream of the *GAL1* promoter to generate preRTA and matRTA without the EGFP tag as described previously (preRTA, NT849; preG83D, NT1031; preS215F, NT1038; preG212E, NT1037; preP95L/E145K, NT1039)(80). The plasmids were then transformed into *Saccharomyces cerevisiae* strain W303 (*MATa ade2-1 trp1-1 ura3-1 leu2-3,112 his3-11,15 can1-100*), and transformants were selected on SD-Leu medium containing 2% glucose. The yeast deletion strains *png1*Δ, *usa1*Δ, *hrd1*Δ and the parental BY4743 (*MATa/a his3D1/his3D1 leu2D0 /leu2D0 lys2D0/LYS2*

MET15/met15D0 ura3D0 /ura3D0) were derived from yeast genome homozygous diploid gene deletion collection (Open Biosystems, Huntsville, AL). To investigate the effect of Png1, Usa1 and Hrd1 on preRTA, preG83D, preG212E, preS215F and preP95L/E145K, NT849, NT1031, NT1037, NT1038 and NT1039 were transformed into each deletion strains as well as the parental BY4743. The transformants were selected on SD-Leu medium containing 2% glucose. For complementation experiment, PNG1 ORF (YPL096W) were from yeast ORF library (Open Biosystems, Huntsville, AL) (118). The PNG1 ORF were cloned into vector pAG415GPD-ccdB-HA (Addgene plasmid 14242) (119) with *LEU2* marker using Gateway recombination cloning technology (Invitrogen, Eugene, Oregon). The preRTA and preG83D plasmids co-transformed with the PNG ORF were cloned under the *GAL1* promoter in a single copy CEN plasmid pRS416 (120) with *URA3* marker (preRTA, NT1403; preG83D, NT1541). The transformants were selected on SD-Leu, Ura medium containing 2% glucose.

Analysis of protein expression

Yeast cells were grown in dropout medium without the appropriate amino acid supplemented with 2% glucose overnight and then transferred to dropout medium supplemented with 2% galactose at OD_{600} of 0.3 to induce RTA expression. For yeast cells expressing precursor forms of RTA and mutants, the dropout medium lacks Leucine for selection. For yeast cells co-expressing pAG415GPD-PNG or vector and pRS416Gal1-PreRTA or pRS416Gal1-preG83D, the dropout medium lacks Leucine and Uracil. Cells were collected at 6 hpi and

membrane fractions were isolated as previously described (91). The supernatant was further centrifuged at 200,000 x g for 1 h to pellet the ribosomes. The membrane fraction and the post ribosomal supernatant were treated with or without Endo H using the manufacturer's protocol (New England Biolabs, Ipswich, MA). The protein samples were separated on a 10% SDS-polyacrylamide gel and the blot was probed with monoclonal anti-RTA (1:5000), a gift of Dr. Nicholas J. Mantis. The blot was stripped with 8M guanidine hydrochloride and reprobed with antibody against the ER maker, dolichol phosphate mannose synthase (Dpm1p; Invitrogen, Eugene, Oregon) (1:1000). The blot was also reprobed using anti-3-phosphoglycerate kinase (Pgk1p; Invitrogen, Eugene, Oregon), as a marker for the cytosol. The blots were developed using ChemiDoc MP imaging system (Bio-Rad, Philadelphia, PA). The vacuole fraction was isolated as described (93). Briefly, cells harvested at 6 hpi were washed with DTT solution (0.1 M Tris pH9.4, 10mM DTT) and lysed by lyticase at 20U/OD in spheroplasting buffer (0.16 X YPD, 0.4 M sorbitol, 50 mM potassium phosphate, pH 7.5). The spheroplasts were treated with DEAE-Dextran for gentle lysis. Purified vacuoles were obtained by flotation in a 0, 4, 8, 15% Ficoll step gradient. The gradients were centrifuged at 110,000 X g for 90 min at 4 ^{o}C in a Beckman L8-70M Ultracentrifuge (Beckman Coulter, Brea, CA) and vacuoles were collected from the 0%-4% interface. The vacuole marker was anti-H^{+}-ATPase (V-ATPase; Invitrogen, Eugene, Oregon) (1:500). The total protein extracts were isolated as described (121). Briefly, the 5 OD_{600} cells were washed with water. The cells

were resuspended in 2 M LiAc and kept on ice for 5 min, followed by treating with 0.4 M NaOH and incubated on ice for 5 min.

Analysis of growth rate

Yeast cells harboring precursor and mature RTA and precursor and mature RTA mutants with the EGFP tag were grown in SD-Leu medium containing 2% glucose overnight and then transferred to SD-Leu medium containing 2% galactose at OD_{600} of 0.3. Aliquots were taken every hour up to 10 hours and OD_{600} was recorded to generate growth curve. Doubling times were calculated based on OD_{600} at 4-10 h time point within the exponential growth phase.

Cell viability analysis

Yeast cells carrying precursor and mature forms of RTA and nontoxic RTA mutants with the EGFP tag were induced as described above. Tenfold serial dilutions of 15 µL from OD_{600} of 10^{-1} to 10^{-5} were plated on SD-Leu plates containing 2% glucose at 10 hpi. BY4743 and *png1*Δ strains expressing preRTA or co-expressing pAG415GPD-PNG or vector and pRS416Gal1-preRTA were induced as described above. A series of 10-fold dilutions of 10 µL from OD_{600} of 10^{-1} to 10^{-5} were plated on dropout plates containing 2% glucose at 0 and 24 hpi. The plates were incubated at 30 °C for approximately 48 h. BY 4743 and *png1*Δ strains expressing preG83D or co-expressing pAG415GPD-PNG or vector and pRS416Gal1-preG83D were grown overnight in glucose as described above. The non-induced overnight culture were collected and plated on dropout plate with 2%

galactose in a series of 10-fold dilutions of 10 µL from OD_{600} of 10^{-1} to 10^{-5}. The plates were incubated at 30 °C for 4 days.

Depurination analysis

For *in vivo* depurination, cells were harvested at time points indicated and total RNA was extracted using the RNeasy Mini Kit (Qiagen, Valencia, CA). For *in vitro* depurination, yeast ribosomes were isolated as previously described (22). Ribosomes were incubated for 10 minutes at 30°C with purified wild type RTA at final concentrations of 10, 20, 40, 80, 100, 200, 400, 800, 1000 and 2000 pM or with G212E or P95L/E145K mutants at elevated final concentrations of 1, 2, 4, 8, 10, 20, 40, 80 and 100 nM. The qRT-PCR analysis of depurination was carried out as previously described (78, 94).Total RNA was converted to cDNA using the High Capacity cDNA Reverse Transcription Kit (Applied Biosystems, Carlsbad, CA). The 25S rRNA was detected using (5'-AGA CCG TCG CTT GCT ACA AT-3'and 5'- ATG ACG AGG CAT TTG GCT AC- 3'). The depurinated rRNA was detected using the forward primer (5'- CTA TCG ATC CTT TAG TCC CTC-3') and the reverse primer (5'- CCG AAT GAA CTG TTC CAC A-3'). Real time PCR was performed using an ABI Prism 7000 Sequence Detection System (Applied Biosystems, Carlsbad, CA). The data was analyzed by the comparative ΔC_T ($\Delta\Delta C_T$) method for quantification (78).

Live cell imaging

Time course of RTA localization was carried out using yeast harboring the precursor and mature RTA with EGFP tag at indicated time points. The cells were directly added to 2% agarose pads on slides. For vacuole stain, yeast cells were harvested at 2, 4, 6 and 24 hpi. FM4-64 (Invitrogen, Carlsbad, CA) dissolved in dimethyl sulfoxide (DMSO) was added at a final concentration of 80 µM and cells were incubated in the dark at 30°C for 60 min. Cells were pelleted, washed and resuspended with YPD media containing 2% galactose to chase for 40 min at 30°C. For nuclear stain, Hoechst 33342 (Invitrogen, Carlsbad, CA) was added at a final concentration of 10 µM to the cell culture and incubated at 37 °C for 60 min. The cell culture was applied to the agar pad and visualized using an Olympus BX41 fluorescence microscope equipped with a CCD camera (Hamamatsu, Bridgewater, NJ) and a 100X oil objective (1.45 N.A. Plan Apo, Olympus). Image acquisition and processing were performed using Metamorph Image Software (7.0; MDS Analytical Technologies).

Strain verification

The *png1*∆ strain was verified by PCR using knockout cassette specific primers (primers “A” and “KanB”) (yeastdeletion.stanford.edu). The PCR was also conducted with the same primer pair for the parental strain BY4743 as a control. The amplification product was separated on a 1% agarose gel.

CHAPTER 4: Characterization of the cellular proteins identified from the genome-wide screen in the retrotranslocation of ricin A chain in *Saccharomyces cerevisiae*

SUMMARY

In an effort to systematically investigate the host factors involved in ricin A chain (RTA) intracellular trafficking, a genome-wide screen of yeast nonessential gene knockout library against RTA has identified genes potentially involved in RTA intracellular trafficking pathway. In this study, I focused on the Hrd1p complex and the AP-2 complex whose deletions provided protective hits. The Hrd1p and Der1p subunits of the Hrd1p complex were the main components and indispensable for the dislocation of the precursor forms of wild type RTA (preRTA) and a misfolded RTA mutant (preG83D). The Usa1p subunit of the Hrd1p complex was only required for the dislocation of the misfolded preG83D, but not wild type preRTA, suggesting a structural role of Usa1p in the Hrd1p complex. The vacuole transport of wild type preRTA was independent of the Hrd1p complex. In the AP-2 complex, the depletion of Apl3p subunit completely impaired the vacuole transport of preRTA. The depurination of preRTA was not reduced in the *apl3*Δ strain, suggesting that the dislocation to the cytosol was not affected. These results suggested that ER-to-cytosol and ER-to-vacuole are two parallel pathways and provided insights into the mechanisms of the intracellular trafficking of RTA.

INTRODUCTION

Ricin is an A/B toxin, which is composed of ricin A chain (RTA) and ricin B chain (RTB). The binding subunit, RTB binds to the cell surface galactose receptors and promotes the endocytosis of the active subunit, RTA. RTA is an *N*-glycosidase, which depurinates an adenine residue from the universally conserved α-sarcin/ricin loop (SRL) of the 28S rRNA and inhibits protein synthesis (17). Besides the ribosome depurination, the intracellular trafficking is also an integral part of the intoxication mechanisms of RTA. The interactions of RTA with the cellular components in the intracellular trafficking pathway determine its accessibility to the substrate ribosomes in the cytosol and the ability to evade ubiquitin-proteasome degradation or vacuolar proteolysis. The intracellular trafficking pathway for ricin has been studied in yeast and in mammalian cells. In mammalian cells, ricin enters the cells by endocytosis with the help of RTB. After endocytosis, ricin follows the retrograde transport pathway passing along the early endosomes, *trans*-Golgi network (TGN) and the endoplasmic reticulum (ER). In the ER, RTA is reduced from RTB by the protein disulfide isomerase (PDI) and thus being activated (48). RTA is delivered through the ER-associated degradation (ERAD) pathway from the ER to the cytosol where it exerts the depurination activity and leads to cell death (57). This process is termed dislocation or retrotranslocation. Because the dislocation and the subsequent fate of RTA are especially crucial to the understanding of the RTA intoxication mechanisms, the ERAD components required for RTA toxicity have been studied. The engagement of the ERAD components in the dislocation of RTA was primarily studied in yeast, because the basic ERAD machinery is

completely conserved from yeast to mammalian cells, and the genetic analyses of yeast are easily manipulated. In yeast, in the ER luminal side of the ERAD, the α-mannosidase activity of Htm1 (the yeast homolog of mammalian EDEM) and the subsequent substrate recognition by Yos9 (the yeast homolog of mammalian OS-9) are required for RTL (RTA with five amino acids deletion within the active site cleft linked to a transmembrane domain and a cytoplasmic Leu2 protein) dislocation. However, unlike the canonical ERAD substrates, RTL does not require Mns1, which is an ER luminal α1,2-mannosidase, for dislocation (54). RTA was reported to use the Hrd1p ubiquitin ligase complex as the protein conducting channel for ER export (53, 54). Both the folded RTA mutant RTA_{E177D} and the misfolded RTA mutant RTA_{Δ} (RTA with five amino acids deletion within the active site cleft) dislocated via the Hrd1p ubiquitin ligase complex. The dislocation of RTA required prior ER-Golgi transport, since both forms could be stabilized in pulse-chase analysis with defective ER to Golgi transport COPII vesicles. After entry into the cytosol, the pathways for the folded and the misfolded RTA mutants diverged. RTA_{Δ} showed strong requirement for Cdc48 (53), which possibly provided the extraction force for the dislocation of RTA_{Δ} (122). RTA_{Δ} also required a subunit of the 19S proteasomal regulatory particle (RP) Rpt2p AAA ATPase activity. In contrast, the folded RTA_{E177D} did not require Cdc48 for dislocation, but instead depended on the 19S proteasome cap protein Rpt4p for extraction (53). Although the studies provided insights into the ERAD machineries responsible for the RTA intoxication mechanisms, they were focused on testing the effects of the known ERAD components on the toxicity of

RTA. Moreover, up to this point, the ER export of RTA has been considered only as the ER-to-cytosol transport. However, my work showed that RTA was also observed to be transported to the vacuole (103), where the proteolytic degradation occurs. The cellular proteins required for the vacuole transport of RTA remain elusive. The ER-to-vacuole transport pathway for RTA introduces additional complexity to the understanding of the cellular machinery for proper routing of RTA.

To systematically elucidate the involvement of the genes in toxin trafficking, genome-wide RNAi screens against ricin and Pseudomonas exotoxin (PE) were employed to identify genes required for intoxication in mammalian cells (123). The screens identified a large number of genes related to the membrane compartments or membrane transport processes based on gene ontologies (GOs), indicating a significant importance of intracellular trafficking in the intoxication mechanisms of ricin and PE. The host gene requirements for ricin and PE are drastically different, with only 13% overlap. A recent genome-wide shRNA screen against ricin, aimed at generating a genetic interaction map, also identified host factors greatly enriched in the retrograde transport pathway as either sensitizing or protective hits, further raised the importance of the intracellular trafficking in the intoxication mechanisms of ricin (110). In yeast, a genome wide screen against an A/B toxin K28 “killer” toxin yielded 176 mutations causing K28 resistance and 189 mutants causing K28 hypersensitivity. Because this toxin closely resembles ricin in the intracellular trafficking pathway, the components involved in the K28 trafficking may have implications on ricin(124).

Current knowledge on the post-ER events in the intracellular trafficking of RTA in yeast is inadequate with relatively few genes identified. Limited studies address the specific proteins, mechanisms required for the trafficking and toxicity of RTA in yeast systematically. The complete set of approximately 5,000 yeast non-essential gene knockout strains were screened against precursor form of RTA (preRTA) and mature form of RTA (matRTA). PreRTA was synthesized endogenously and co-translationally transported to the ER in each strain, so that only the events after ER import were focused. The genes whose deletions conferred resistance to preRTA but not to matRTA were potentially involved in the intracellular trafficking pathway of preRTA. This provided a global view of the non-essential genes required for the intoxication mechanisms of RTA. Among these genes, the ones had a cellular component GO related to the membrane compartments or a biological process GO related to transport were studied in detail. Uncovering the genes involved in the intracellular trafficking of RTA is essential to the development of antidotes by altering the function of these host proteins.

RESULTS

A genome-wide screen identified genes related with the intracellular trafficking of RTA

A genome-wide screen to identify yeast deletion strains that conferred resistance to RTA was performed in our laboratory. The yeast non-essential gene knockout library containing approximately 5,000 strains was transformed

with preRTA or matRTA in a high-throughput manner. The preliminary screen yielded 137 deletion strains that conferred resistance to preRTA but not to matRTA. The yeast cellular proteins encoded by these genes implied potential roles in the intracellular trafficking of preRTA and their functions might be broadly applied to the transport of other cargo proteins. The rationale behind this was that the deletion of a gene important for the trafficking of preRTA will impair the accessibility of preRTA to cytosolic ribosomes and increase cell survival, but will not affect the viability of cells expressing the cytosol localized matRTA. In this study, I focused on genes whose annotated biological functions are directly related to transport processes or to subcellular compartments in the retrograde or anterograde transport pathways by gene ontology (GO) tool. I subdivided these genes into four categories based on their GO functions. The genes related with the Golgi include *MNN9*, *GLO3*, *COY1*, *GRX6* and *GRX7*; The genes functioning in the ERAD pathway include *USA1* and *SSE1*; The genes related with the clathrin mediated vesicle transport include *APL3* and *APM4*; The genes related with vacuole transport include *VTC4*, *VPS72*, *VPS73* and *CPS1*.

In order to confirm the viability of these protective hits from the high throughput screen, I transformed preRTA and matRTA into individual strains with deletions of genes mentioned above and spotted a series of ten-fold dilutions of transformed yeast cells on non-inducing glucose plates at 24 h post induction (hpi). In agreement with the screen results, most of the deletion strains expressing matRTA had similar viability as the wild type BY4743. However, the corresponding strains expressing preRTA were more viable than the wild type

BY4743. The results suggested that the deletions affected preRTA dislocation to the cytosol to depurinate rRNA rather than affecting the ribosome depurination activity itself. As an exception, *sse1*Δ strain was hypersensitive to both endogenously expressed preRTA and matRTA (Figure 4.1).

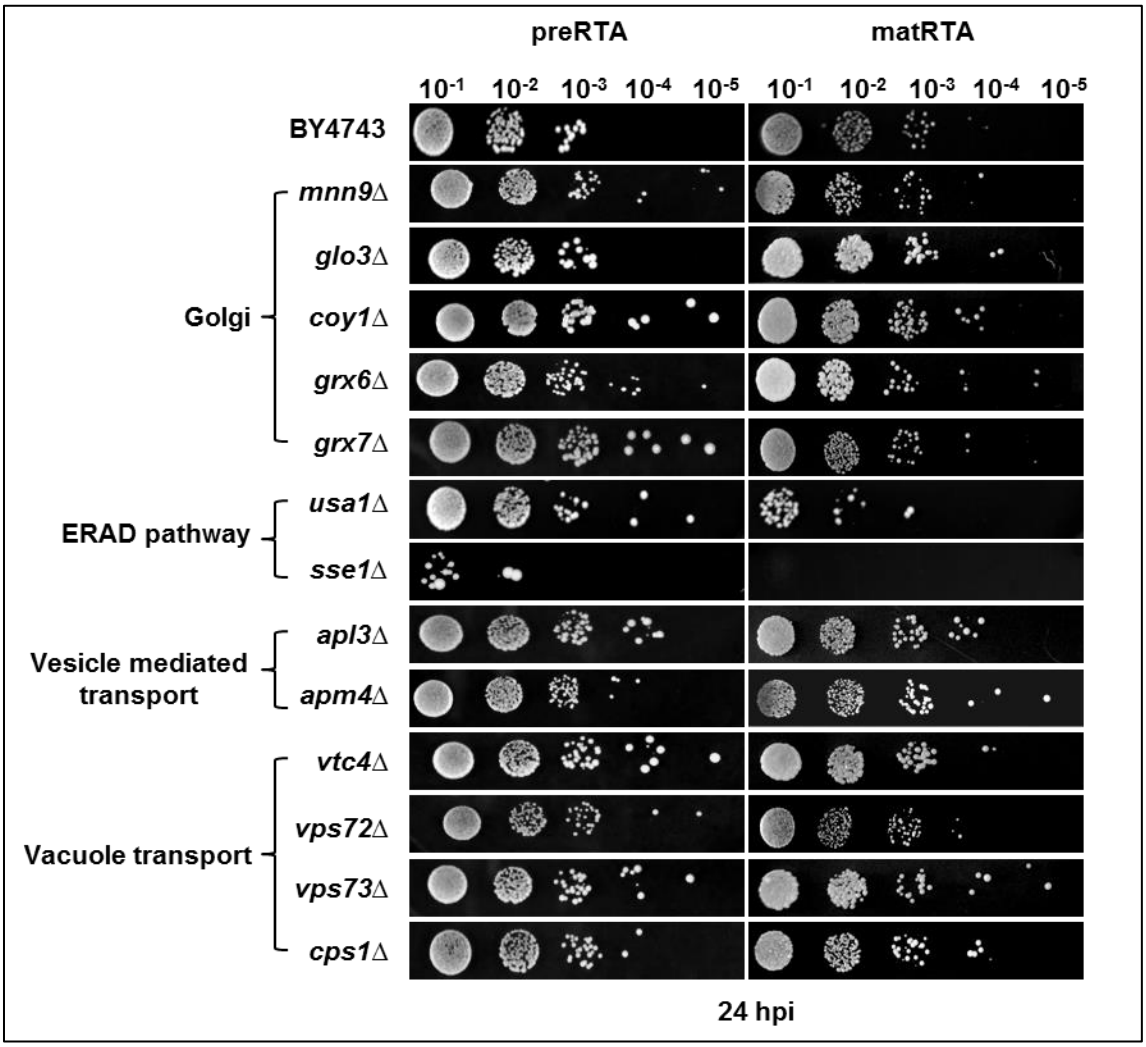

Figure 4.1 The viability of parental BY4743 and yeast homozygous deletion strains expressing the precursor and mature forms of wild type RTA (preRTA and matRTA). Yeast cells were first grown in SD-Leu supplemented with 2% glucose and then transferred to SD-Leu supplemented with 2% galactose. At 24 hpi, a series of ten-fold dilutions were plated on media containing 2% glucose and incubated at 30 ºC for approximately 48 h.

Hrd1p ubiquitin ligase complex is involved in the dislocation of RTA, but not vacuole transport

The Hrd1p ubiquitin ligase complex is a heterotetrameric membrane protein complex functioning in the ERAD-L pathway, which is responsible for degradation of misfolded proteins carrying lesions in the luminal domain (125). It is comprised of the E3 ubiquitin ligase Hrd1p, as well as Hrd3p, Usa1p and Der1p. Hrd1p is the key component in the Hrd1p ubiquitin ligase complex. Its oligomerization is required for the retrotranslocation of the substrates. Although Hrd1p has the potential to spontaneously form oligomers, Usa1p facilitates this process by interacting with Hrd1p through its one domain and oligomerizes with another Usa1p through another domain (126). Hrd3p and Der1p function upstream of Hrd1p to recruit substrates and deliver them to the Hrd1p (127).

Previous studies showed the involvement of Hrd1p ubiquitin ligase complex in the dislocation of a folded RTA mutant RTA_{E177D} and a misfolded RTA mutant RTA_{Δ} (53, 54). I further investigated the involvement of Hrd1p ubiquitin ligase complex in detail to reveal the roles of its individual components in the trafficking, depurination and toxicity of wild type preRTA and a folding defective RTA mutant preG83D. The evidence that preG83D is a folding defective form of RTA was provided by microscopic images (Figure 4.2). PreG83D as well as preRTA were fused with the enhanced green fluorescent protein (EGFP) tag at the C-termini. The expression was under the control of the *GAL1* promoter to permit growth under non-inducing condition and provoke expression under inducing condition. The EGFP tag does not affect the sorting and activity of wild type preRTA as

demonstrated previously (103). As shown with the confocal images (Figure 4.2), at 6 hpi, wild type preRTA-EGFP was localized to the perinuclear structure defined by the Hoechst 33342 nuclear stain, which is indicative of the ER, and accumulated into the vacuole, consistent with the previous observations (103). However, preG83D-EGFP was not transported to the vacuole. It formed big punctate structures on the ER and cell periphery, suggesting that preG83D-EGFP is a folding defective form of RTA and it is unable to utilize the vacuole transport pathway.

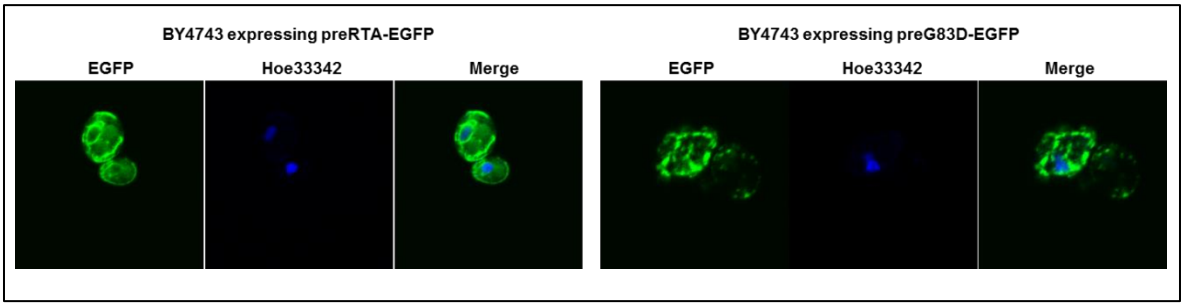

Figure 4.2 The localization of preRTA-EGFP and preG83D-EGFP in the parental BY4743 strain at 6 hpi by confocal microscope. The images of BY4743 harboring preRTA-EGFP and preG83D-EGFP were taken at 6 hpi. The live cells were stained with Hoechst 33342 to show the nuclei. The merged images show the perinuclear structure of preRTA-EGFP and preG83D-EGFP.

One subunit of the Hrd1p ubiquitin ligase complex, Usa1p, was identified as a protective hit from the screen. As was shown in Figure 4.1, the deletion of *USA1* conferred mild protection to cells expressing preRTA. The result agreed with the previous experiment using RTA_{E177D} to represent the native form (53) and suggested a subsidiary role of Usa1p in the Hrd1p ubiquitin ligase complex.

Usa1p is a scaffold subunit of the Hrd1p complex (128). It promotes the oligomerization of the Hrd1p, but the need for Usa1p can be bypassed by overexpression of Hrd1p (126). Hrd1p is the central component of the Hrd1p ubiquitin ligase complex. Its oligomerization is required to dislocate protein flux (126). Der1p functions upstream of Hrd1p, the precise role remains unknown (127). In order to get a complete picture of the Hrd1p ubiquitin ligase complex in the translocation pathway of RTA, the effects of Hrd1p and Der1p in the toxicity of preRTA and preG83D were examined. The cell viability was tested with BY4743, *hrd1*Δ and *der1*Δ strains expressing preRTA or preG83D. The cell cultures were grown in glucose overnight, and a serial of ten-fold dilutions was plated on inducing galactose plates as a way to induce continuous expression of RTA. The same dilutions were replica plated on non-inducing glucose plates as controls. As shown in Figure 4.3, the parental BY4743, *hrd1*Δ and *der1*Δ expressing preRTA were too toxic to grow on the inducing galactose plates. The cell cultures should be plated on glucose plate instead at 24 hpi to better compare the viability. In contrast, BY4743, *hrd1*Δ and *der1*Δ strains expressing preG83D were viable and they did not show significant differences in toxicity.

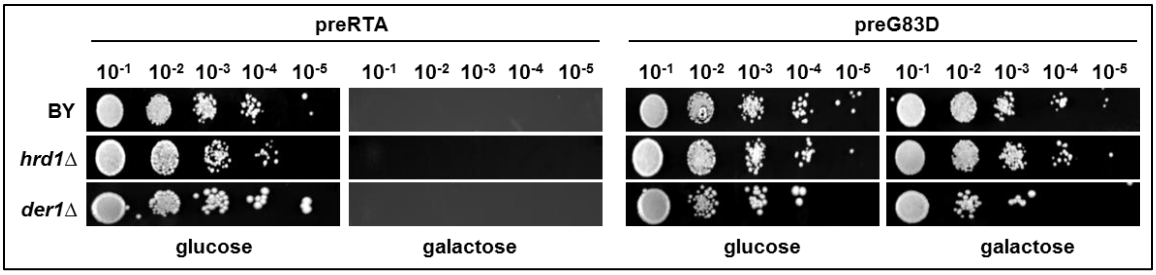

Figure 4.3 The viability of BY4743, *hrd1*Δ and *der1*Δ strains expressing preRTA or preG83D. A series of ten-fold dilutions were spotted either on galactose plate after overnight growth in glucose media or on glucose plate at 0 hpi.

In order to understand the role of Hrd1p ubiquitin ligase complex in the trafficking of preRTA, I examined the subcellular localization of preRTA-EGFP in *hrd1*Δ and *usa1*Δ strains by fluorescence microscope and stained the cells with lipophilic dye FM4-64 to visualize the vacuole (Figure 4.4). These two components were chosen, because Hrd1p and Usa1p were necessary for the structure of the Hrd1p complex which was required for the dislocation of RTA (53). In the wild type BY4743, preRTA-EGFP was localized to the ER at 2 h and 4 hpi, and it accumulated to the vacuole from 6 hpi. However, in *usa1*Δ strain, preRTA-EGFP was localized to the ER at 2 hpi, but was transported to the vacuole at 4 hpi, which occurred at an earlier time point than in the BY4743. Similarly, in *hrd1*Δ strain, preRTA-EGFP was transported to the vacuole as early as 2 hpi. The results suggested that the vacuole transport of preRTA-EGFP is independent of the Hrd1p ubiquitin ligase complex. Most importantly, loss of Hrd1p or Usa1 promoted vacuole transport, possibly because the vacuole degradation pathway for preRTA-EGFP became dominant when the ERAD degradation pathway was compromised (104). The earlier onset of vacuole

transport may contribute to the reduced cytotoxicity, since vacuole turnover is faster than the multi-step ERAD (104).

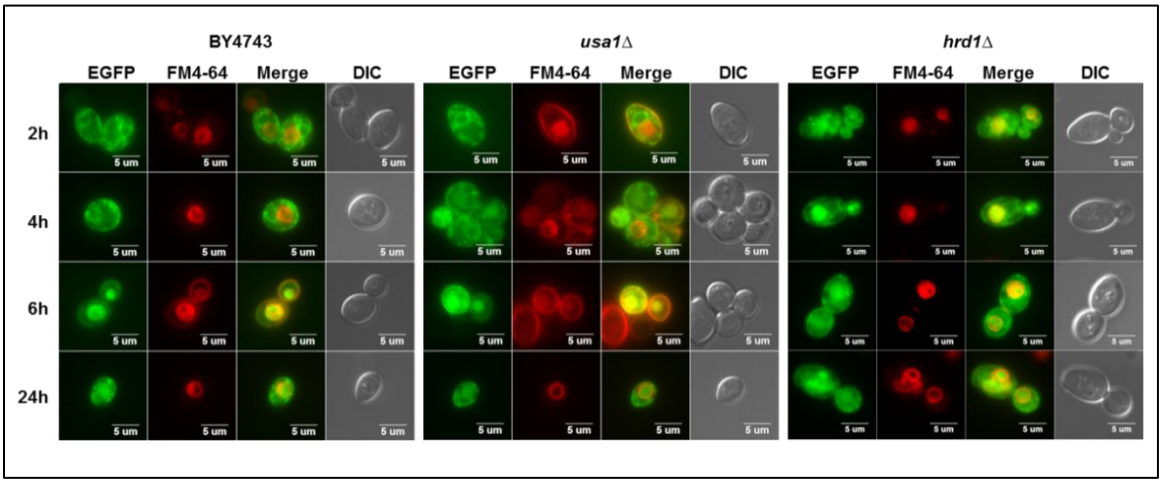

Figure 4.4 The intracellular trafficking of preRTA-EGFP in BY4743, *usa1*Δ and *hrd1*Δ strains. The images of parental BY4743 and deletion strains harboring preRTA-EGFP were taken at 2, 4, 6 and 24 hpi with an Olympus BX41 fluorescence microscope. Yeast live cells were treated with FM4-64 to stain the vacuole. Merged images show localization of preRTA-EGFP relative to the vacuole.

Western blot analysis was performed to examine the effect of *USA1* deletion on the membrane fraction of preRTA. The membrane fraction was extracted from parental BY4743 and *usa1*Δ strains expressing preRTA at 6 hpi. The proteins were treated with (+) or without (-) endoglycosidase H (Endo H) to identify the glycosylated form and the nonglycosylated form. It shows in Figure 4.5A that preRTA expressed in the parental BY4743 migrated as three bands. The differences in migrating rate were results of the nine-amino acid propeptide (p) and glycosylation (g). The top two slower migrating bands represented the glycosylated forms with (g+p) and without the nine-amino acid propeptide ($g+p_0$).

They corresponded to the two deglycosylated bands with and without propeptide after Endo H treatment. The fastest migrating band was the nonglycosylated form with the propeptide (g_0+p), and it migrated at the same rate after Endo H treatment. In *usa1*Δ strain, the glycosylated form without the propeptide (g+p_0) and the nonglycosylated form with the propeptide (g_0+p) became more abundant in the membrane fraction. However, the glycosylated form with the propeptide (g+p) was not evident from the membrane fraction in the *usa1*Δ strain. The results suggested that the different migrating species of preRTA underwent different intracellular trafficking pathways. The protein level of glycosylated form without propeptide (g+p_0) and nonglycosylated form with propeptide (g_0+p) of preRTA in the membrane fraction in the *usa1*Δ strain increased compared with that in the BY4743, suggesting that Usa1p was involved in the dislocation of these two forms, agreed with the suggested role of Hrd1p ubiquitin ligase complex in the dislocation of preRTA (53, 54). Previous results showed that the glycosylated form with propeptide (g+p) did not appear in the cytosol fraction, but only appeared in the membrane and vacuole fractions (103), suggesting the glycosylated form with propeptide (g+p) did not go through the ERAD pathway, but was transported to the vacuole after ER exit. Therefore, a plausible explanation is that the deletion of *USA1* promoted the vacuole transport, therefore the glycosylated form with the propeptide (g+p) disappeared from the membrane fraction faster. This result was consistent with our observation that the onset of vacuole transport was earlier in the *usa1*Δ strain (Figure 4.4).

Protein expression of preRTA and preG83D in *hrd1*Δ and *der1*Δ strains was analyzed with western blot in both membrane and cytosol fractions to investigate the role of Hrd1p and Der1p in the dislocation of preRTA and preG83D (Figure 4.5B-C). The membrane fraction and the cytosol fraction were extracted from cells expressing preRTA or preG83D at 6 hpi. In the membrane fraction, the top band of preRTA, which represented the glycosylated form with the propeptide (g+p), became less abundant in both *hrd1*Δ and *der1*Δ strains compared with that in the BY4743. The glycosylated band without the propeptide ($g+p_0$) and the nonglycosylated band with propeptide (g_0+p) became more abundant in *hrd1*Δ and *der1*Δ strains than in the BY4743. The results were similar with those in the *usa1*Δ strain. In the cytosol fraction, preRTA migrated as two forms in BY4743. The top band represented the glycosylated form without propeptide ($g+p_0$) and the lower band represented the deglycosylated band (g_0+p_0) derived from the top glycosylated form. In both *hrd1*Δ and *der1*Δ strains, the cytosolic protein decreased in amount, which can be explained by the defects in the dislocation of preRTA without a functional Hrd1p ubiquitin ligase complex. Moreover, in the *hrd1*Δ and *der1*Δ strains, the nonglycosylated form with the propeptide (g_0+p) was released to the cytosol. This form was not detected in the cytosol fraction in the parental BY4743, suggesting that the Hrd1p ubiquitin ligase complex may be responsible for the proper sorting of the substrates in the ERAD pathway. In agreement with this, it was shown that Hrd1p is able to retain misfolded proteins in the ER (129). The folding defective mutant preG83D migrated as four species in the membrane fraction in the BY4743. They represented the glycosylated

forms with (g+p) and without propeptide (g+p_0), nonglycosylated forms with (g_0+p) and without propeptide (g_0+p_0). PreG83D could not be detected in the cytosol fraction, since it formed aggregates as was observed with the confocal microscope (Figure 4.2). The deletion of *HRD1* and *DER1* intensified the amount of all migrating species of preG83D in the membrane fraction, suggesting that the dislocation of preG83D was also inhibited in the *hrd1*Δ and *der1*Δ strains. Unlike preRTA, the glycosylated form with propeptide (g+p) of preG83D also increase the amount in the membrane fraction in *hrd1*Δ and *der1*Δ strains, suggesting that the trafficking pathways of preG83D and preRTA were different. Since preG83D was defective in vacuole transport, which was responsible for the faster ER export of glycosylated with propeptide (g+p) form of preRTA (103), all four migrating species of preG83D required Hrd1p ubiquitin ligase complex for ER export. Taken together, the western blot analysis with *hrd1*Δ, *der1*Δ and *usa1*Δ strains all showed similar results, suggesting that these components were involved in the dislocation of preRTA and folding defective preG83D.

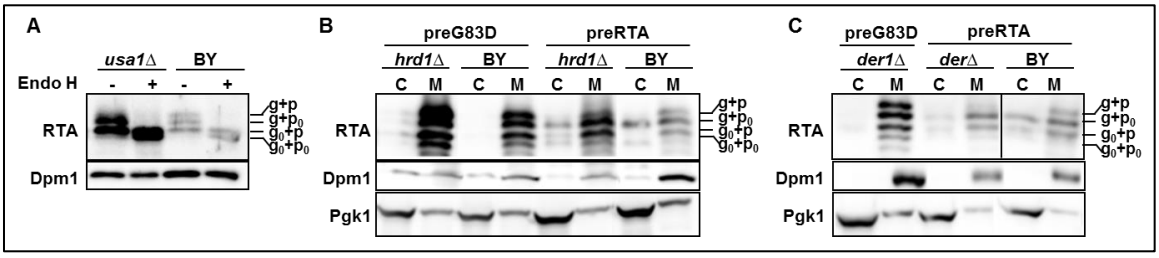

Figure 4.5 Immunoblot analysis of BY4743 (BY), *usa1*Δ, *hrd1*Δ and *der1*Δ strains expressing preRTA or preG83D. The proteins were extracted at 6 hpi. (A) Membrane fraction of BY and *usa1*Δ strains expressing preRTA. The proteins (5 μg) were treated with (+) or without (-) Endo H to distinguish the glycosylated forms. (B-C) Membrane (M) and cytosol (C) factions of BY and *hrd1*Δ strains (B) or *der1*Δ strain (C) expressing preRTA and preG83D.

RTA catalyzed ribosome depurination was tested as readout for the entry of preRTA into the cytosol. To quantitatively measure the depurination levels of yeast strains expressing preRTA and preG83D, a qRT-PCR method designed for yeast was used (108). As shown in Figure 4.6, the parental BY4743 expressing preRTA resulted in a 230-fold increase in the depurination at 2 hpi. The depurination level increased significantly to about 4000-fold increase at 4 hpi. In *usa1*Δ strain, preRTA did not have significantly different depurination levels at both time points examined. In contrast, preG83D expressed in the *usa1*Δ strain had a 20-fold lower depurination than in the BY4743 at 4 hpi, which was drastically different from the wild type preRTA. The results suggested that Usa1p affected the dislocation of the folding defective form, but not the native form of RTA. To further understand if other components of the Hrd1p ubiquitin ligase complex would have different effects on the dislocation of preRTA and preG83D, the depurination was tested with *hrd1*Δ and *der1*Δ strains expressing preRTA and preG83D at 4 hpi. This time point was chosen because wild type BY4743 harboring preRTA had a low level of depurination at 2 hpi and only until 4 hpi there was a significant increase in the depurination. It was shown that at 4 hpi, both *hrd1*Δ and *der1*Δ strains expressing preRTA had a significant decrease in the ribosome depurination. The fold change of depurination in BY4743 expressing preRTA was about five-fold of that in the *hrd1*Δ strain, and about an order of magnitude of that in the *der1*Δ strain. The folding defective preG83D had similar effect on the depurination with *HRD1* and *DER1* deletion. The parental BY4743 strain expressing preG83D had about five-fold higher depurination level

than that in *hrd1*Δ strain and about 11-fold higher than that in the *der1*Δ strain. Taken together, the results suggested that Hrd1p and Der1p are important for the dislocation of both preRTA and preG83D, whereas Usa1p is critical for the dislocation of preG83D, but not for wild type preRTA.

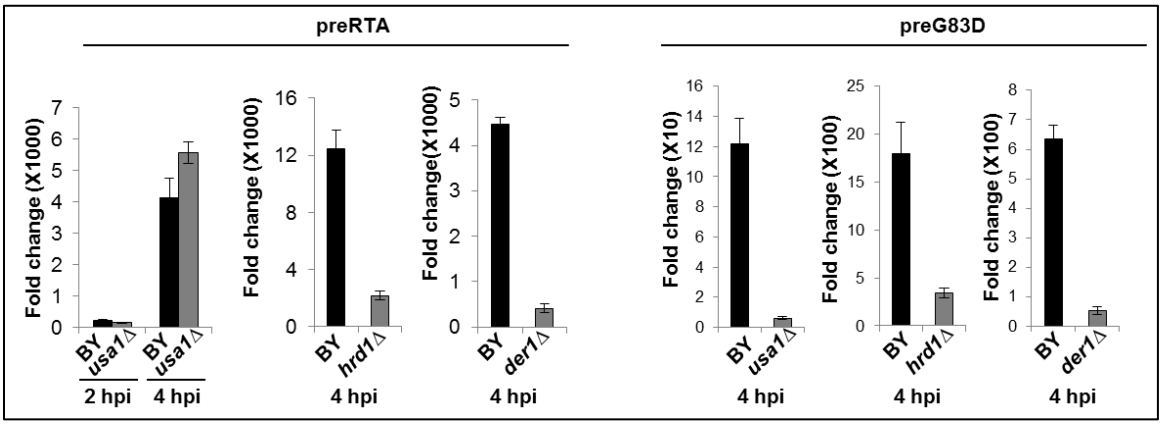

Figure 4.6 Ribosome depurination by preRTA or preG83D expressed in BY, *usa1*Δ, *hrd1*Δ and *der1*Δ strains *in vivo* by qRT-PCR. Yeast ribosomes were extracted at time points indicated after galactose induction.

The fact that Usa1p, but not Hrd1p or Der1p, affected the ER-to-cytosol dislocation of preRTA and preG83D differently could be explained as follows. Although Usa1p promotes the oligomerization of Hrd1p which is required for the substrates flux, Hrd1p has the propensity to form oligomers by itself (130). The folding defective form preG83D forms large aggregates on the ER and possibly requires protein conduits with larger dimensions to dislocate. In this case, Usa1p is required to facilitate the formation of higher order oligomers of Hrd1p. However, native form is able to dislocate through the lower degree of spontaneous oligomerization of Hrd1p. With *USA1* deletion, preRTA was more abundant in the

membrane fraction, but the protein was associated with the cytosolic side of the ER and still depurinated ribosomes in the cytosol. In contrast, the depletion of Hrd1p or Der1p would greatly reduce the dislocation of preRTA and preG83D, suggesting that both components are indispensable for the dislocation of RTA.

The Hrd1p ubiquitin ligase complex may be involved in the proper sorting of the preRTA. When the function of Hrd1p ubiquitin ligase complex was compromised, nonglycosylated form with propeptide (g_0+p) of preRTA was detected in the cytosol, suggesting that propeptide of preRTA acts as a sorting determinant and the presence of Hrd1p ubiquitin ligase complex impairs the dislocation of propeptide attached form of RTA. The Hrd1p ubiquitin ligase complex is involved in the ERAD pathway of preRTA, but not in the vacuole transport. Previous study also suggested that ER to Golgi anterograde trafficking which precedes vacuole transport is independent of the Hrd1p function (131). However, the defects in the Hrd1p complex can facilitate the vacuole transport. This is an indirect effect mediated by the unfolded protein response (UPR). The defects in the ERAD would induce UPR which upregulates the expression of genes involved in the vesicular transport and vacuolar protein targeting (117). When the vacuole transport was stimulated by depletion of subunits in the Hrd1p complex, the propeptide attached glycosylated form of preRTA, which destined to the vacuole (103), disappeared from the membrane fraction more efficiently. Since preG83D did not have the vacuole transport pathway as preRTA, all migrating species in the membrane fraction were affected similarly in the Hrd1p complex deletion strains. These results confirmed that defects in Hrd1p complex

would activate vacuole transport, and preRTA and preG83D underwent different intracellular trafficking pathways. In spite of the similarities of the components of Hrd1p complex in the dislocation of preRTA and preG83D, they have respective roles. Hrd1p is the main component. Its oligomerization acts as a retrotranslocon for the dislocation of the substrates. Usa1p has a secondary role in the Hrd1p complex. Usa1p determines the extend of the oligomerization of the Hrd1p (126). It affected the depurination of the folding defective form preG83D, but not the wild type preRTA, indicating that Usa1p is a scaffold protein and is required for the dislocation of proteins having big dimensions. The deletion of *DER1* also conferred profound deficiency to the dislocation of both preRTA and preG83D. It was demonstrated that mammalian Derlin, which is the homolog of yeast Der1p, links the PNGase to the ER membrane in mammalian system and potentially promotes the substrate degradation through the ERAD pathway (132). Although the mammalian PNGase are distinct from yeast Png1, whether Der1p affects the yeast Png1 is still an open question.

Adaptor protein (AP) complex is involved in the RTA transport

From our screen, ***apl3***Δ and ***apm4***Δ strains carrying deletions from the same protein complex were identified as two protective hits. Apl3p and Apm4p all belong to the clathrin associated protein complex AP2. AP2 adaptor complex links cargo to the clathrin-coated pits. AP2 is involved in the internalization of the cargo on the plasma membrane for endocytosis and transport to early endosomes (133, 134). AP2 consists of four subunits. Apl3p is the large subunit,

or α subunit. Apm4p is the μ2 subunit. During the clathrin mediated transport, the trunk domain which contains Apm4p binds to the membrane and to the cargo. Apl3p recruits the accessory proteins and is implicated in the binding to the target membrane (135).

Because *apl3*Δ and *apm4*Δ strains expressing preRTA were more viable than the parental BY4743 strain (Figure 4.1), I examined if the trafficking of preRTA was affected by transforming preRTA-EGFP into *apl3*Δ and *apm4*Δ strains. As shown in Figure 4.7, in *apl3*Δ strain, preRTA-EGFP was localized to the ER, but the delivery to the vacuole was completely abolished even after tracking for an extended 24 hpi. In *apm4*Δ strain, preRTA-EGFP was first localized to the ER and transported to the vacuole at 6 hpi, the same as in the parental BY4743 strain (Figure 4.4).

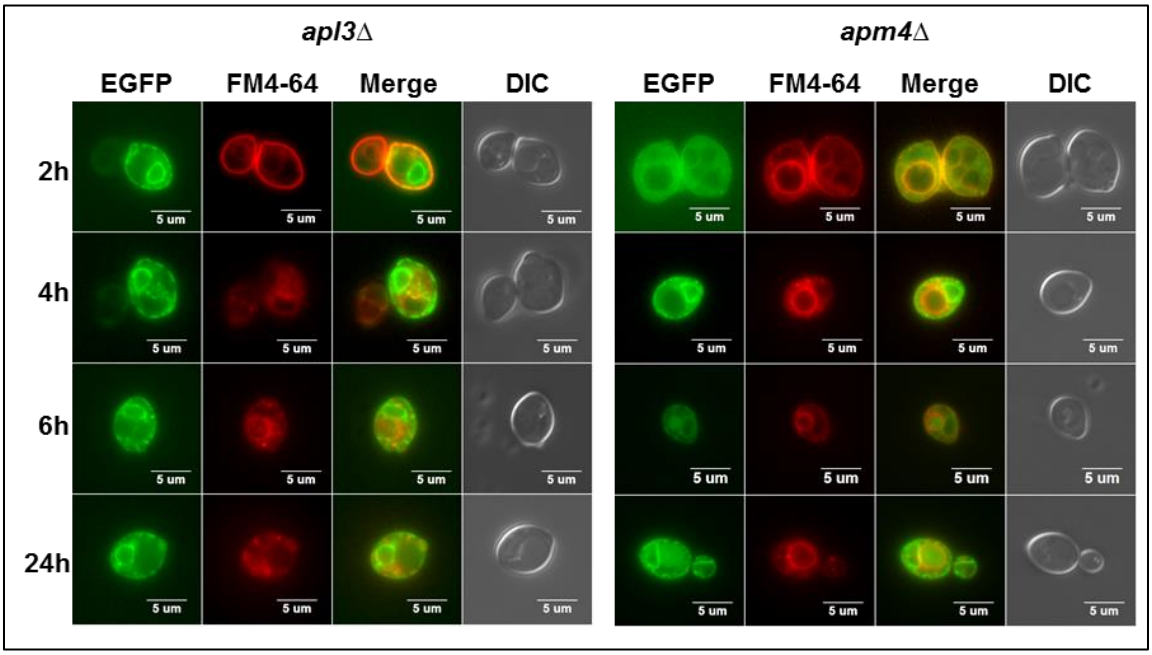

Figure 4.7 The intracellular trafficking of preRTA-EGFP in *apl3*Δ and *apm4*Δ strains. The images of *apl3*Δ and *apm4*Δ strains harboring preRTA-EGFP were

taken at 2, 4, 6 and 24 hpi with an Olympus BX41 fluorescence microscope. Yeast cells were treated with FM4-64 to stain the vacuole. Merged images show localization of preRTA-EGFP relative to the vacuole.

Since there was a dramatic inhibition in the vacuole transport of preRTA-EGFP in the *apl3*Δ but not in *apm4*Δ strain, I asked whether the dislocation of preRTA to the cytosol was affected differently in these two deletion strains. Depurination was tested at 2 and 4 hpi with BY4743, *apl3*Δ and *apm4*Δ strains expressing preRTA or matRTA. In Figure 4.8A, wild type BY4743 expressing preRTA had a low depurination level at 2 hpi. The depurination level increased significantly to about 4000-fold increase at 4 hpi. BY4743 expressing matRTA had equal depurination levels at 2 and 4 hpi, which was about 2000-fold increase. The preRTA expressed in *apl3*Δ strain depurinated at a much higher level at 2 hpi, which was about 1500-fold increase. The depurination increased to about 3000-fold at 4 hpi. The matRTA expressed in the *apl3*Δ strain depurinated at 2800- and 2100-fold increase at 2 and 4 hpi, which was slightly higher than that in the wild type BY4743. The results suggested that preRTA in *apl3*Δ strain still retrotranslocated to the cytosol, and the depurination proceeded, although the cells were more viable. In *apm4*Δ strain, the depurination level of preRTA had 1500-fold increase at 2 hpi and rose up to 3000-fold increase at 4 hpi, which was similar to the depurination in the *apl3*Δ strain. The depurination level of matRTA in *apm4*Δ strain had about 700- and 1700-fold increase at 2 and 4 hpi. The results suggested that the deletion of *APM4* and *APL3* did not inhibit ribosome depurination. This supported that the causes of toxicity are not limited to the

ribosome depurination. Especially, with *APL3* deletion, preRTA still dislocated to the cytosol, although the vacuole transport was inhibited. This suggested that the ER-to-vacuole and ER-to-cytosol transport are two independent pathways.

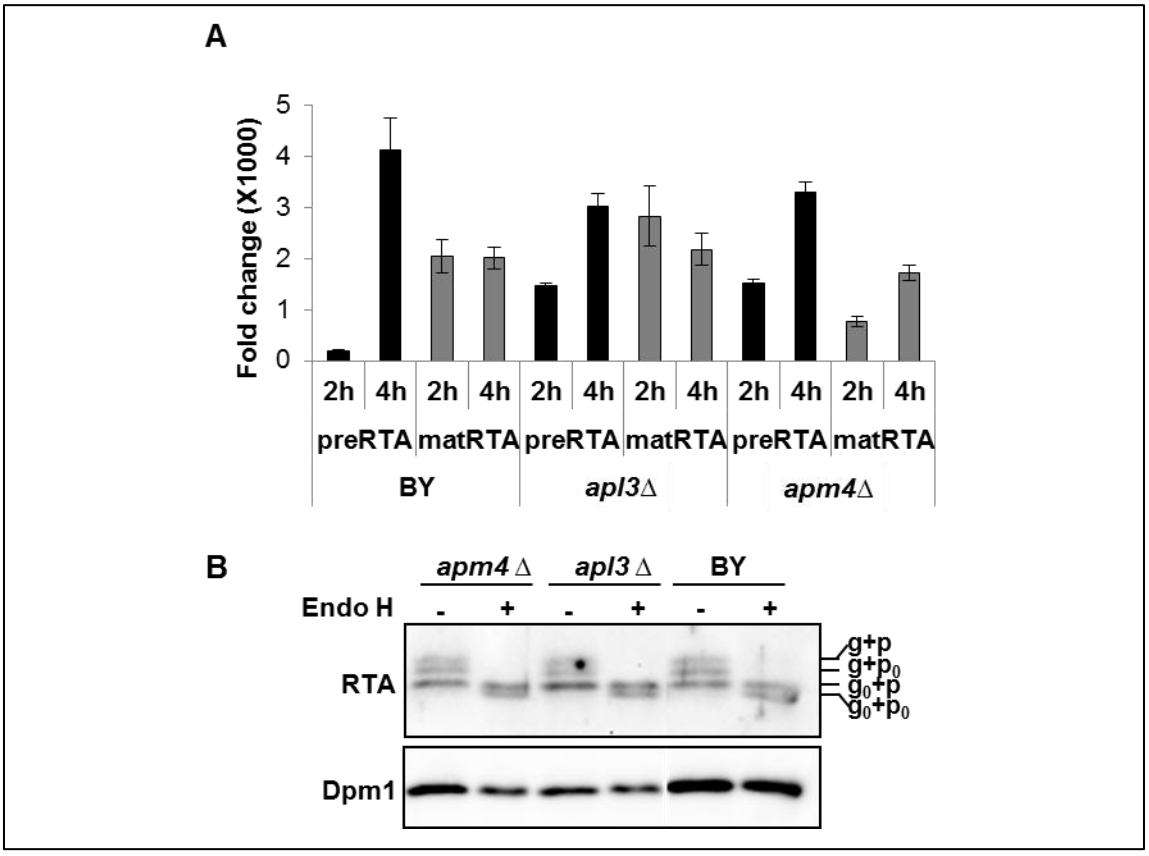

Figure 4.8 The effects of Apl3p and Apm4p on the depurination and expression of preRTA. (A) Ribosome depurination by preRTA and matRTA in BY4743, *apl3*Δ and *apm4*Δ *in vivo* by qRT-PCR. Yeast ribosomes were extracted at 2 and 4 hpi. The data was analyzed by comparative ΔC_T method ($\Delta\Delta C_T$). The y-axis indicates the fold change in depurination in yeast harboring preRTA-EGFP and matRTA-EGFP over yeast harboring the empty vector. (B) Immunoblot analysis of membrane fractions of BY4743, *apl3*Δ and *apm4*Δ strains expressing preRTA. The proteins (5 µg) were treated with (+) or without (-) Endo H to identify the glycosylated forms. Dpm1 was probed as a loading control.

Western blot analysis was performed with membrane fraction of BY4743, *apl3*Δ and *apm4*Δ strains expressing preRTA (Figure 4.8B). The proteins were treated with (+) and without (-) Endo H to distinguish the glycosylated bands. The BY4743, *apl3*Δ and *apm4*Δ strains expressing preRTA did not have differences in the migrating forms. The top two bands are the glycosylated forms with (g+p) and without the nine-amino acid propeptide ($g+p_0$). They corresponded to the two bands after Endo H treatment. The fastest migrating form is the nonglycosylated band with the propeptide (g_0+p). It migrated at the same rate and corresponded to the top band after Endo H treatment.

Although the deletions of *APL3* and *APM4* all conferred more resistance to cells expressing preRTA, they differed in the intracellular trafficking of preRTA-EGFP, suggesting the two genes involved in different transport pathways of RTA. To better understand the role of the AP complex in the toxicity and trafficking of preRTA, I tested the other two components in the AP2 complex, Apl1p and Aps2p. Apl1p is another large subunit of AP2 complex besides Apl3p. Aps2p is the small subunit of the AP2 complex. Wild type preRTA-EGFP and matRTA-EGFP were transformed into *apl1*Δ and *aps2*Δ strains and the deletions did not confer growth advantages to cells expressing preRTA-EGFP and matRTA-EGFP at 10 hpi (Figure 4.9). The localization of preRTA-EGFP in live yeast cells was observed with epifluorescence microscope at 2, 4, 6 hpi (Figure 4.10). In both strains, preRTA-EGFP was localized to the ER at 2 hpi, and was transported to the vacuole at 4 and 6 hpi, indicating that Apl1p and Aps2p did not affect the vacuole transport.

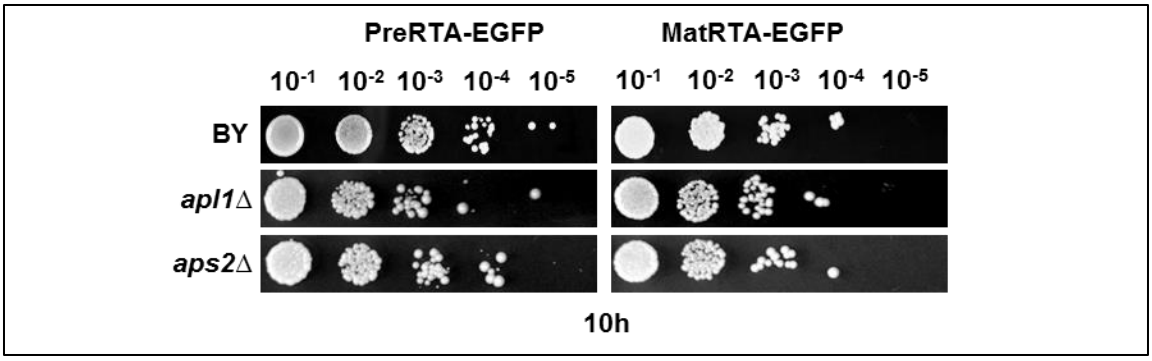

Figure 4.9 The viability of parental BY4743, *apl1*Δ and *aps2*Δ strains expressing preRTA-EGFP and matRTA-EGFP. Yeast cells were first grown in SD-Leu supplemented with 2% glucose and then transferred to SD-Leu supplemented with 2% galactose. At 10 hpi, a series of ten-fold dilutions were plated on media containing 2% glucose and grown at 30ºC for approximately 48 h.

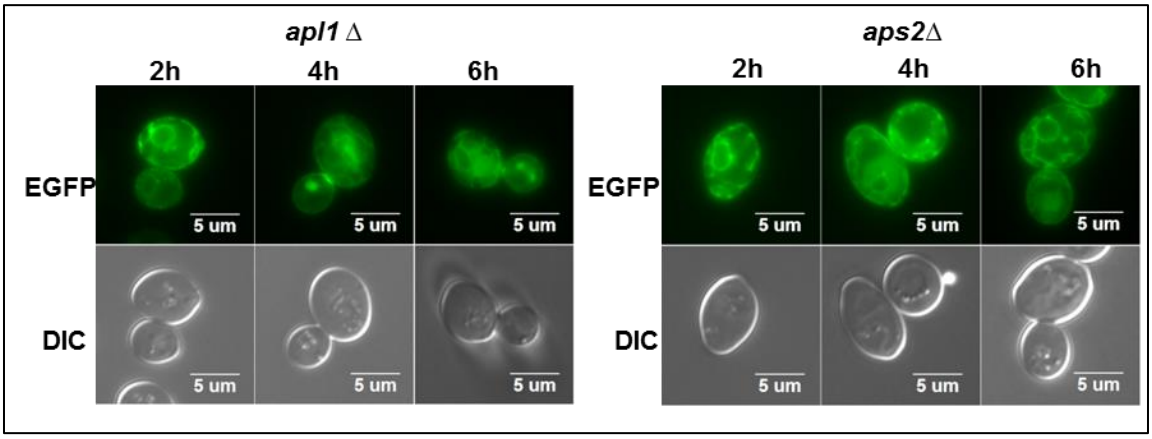

Figure 4.10 Wild type preRTA-EGFP was transported to the vacuole in *apl1*Δ and *aps2*Δ strains. The images of yeast cells harboring preRTA-EGFP were taken at 2, 4 and 6 hpi with an Olympus BX41 fluorescence microscope.

The depurination was tested at 6 and 24 hpi with *apl1*Δ and *aps2*Δ strains expressing preRTA-EGFP and matRTA-EGFP (Figure 4.11). At 6 hpi, the depurination levels of matRTA-EGFP in *apl1*Δ and *aps2*Δ strains were not significantly different than that in the parental BY4743 strain, suggesting that Apl1p and Aps2p did not affect the cytosolic depurination. However, the

depurination levels of preRTA-EGFP in *apl1*Δ and *aps2*Δ strains were about three times less than that in the BY4743 strain. At 24 hpi, the depurination levels of matRTA-EGFP in *apl1*Δ and *aps2*Δ strains were still similar to that in the BY4743. The depurination levels of preRTA-EGFP in *apl1*Δ and *aps2*Δ strains were about three-fold less than that in the BY4743 strain. The results indicated that deletion of Apl1p and Aps2p reduced the dislocation to the cytosol. However, to better understand the dislocation of preRTA in these deletion strains, a time course of depurination by preRTA without the EGFP tag should be followed and the early time points after induction should be emphasized.

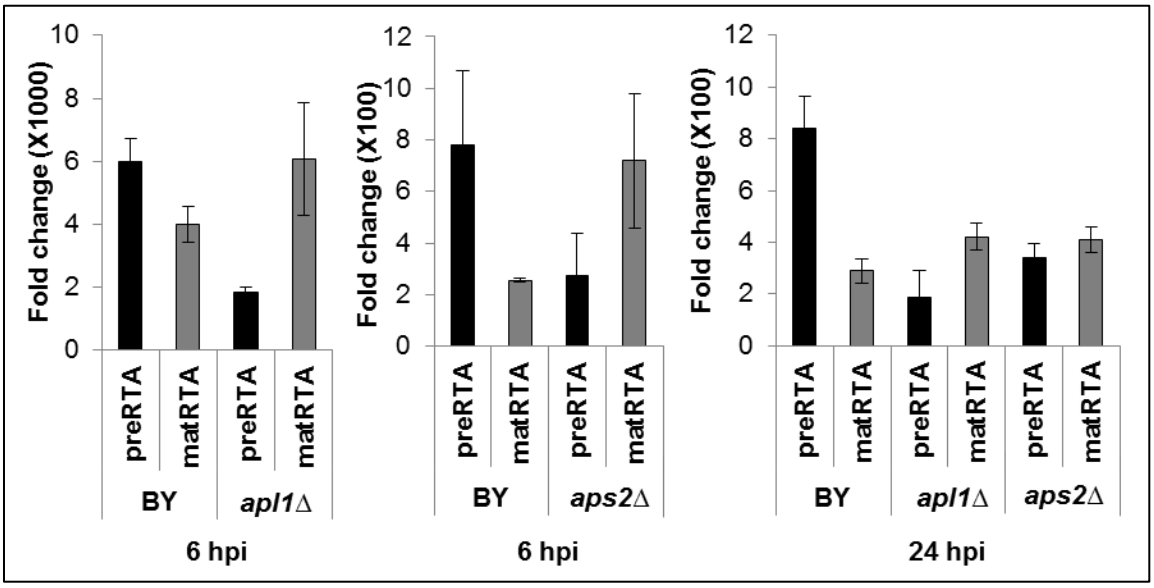

Figure 4.11 Ribosome depurination by preRTA-EGFP and matRTA-EGFP in BY4743, *apl1*Δ and *aps2*Δ strains *in vivo* by qRT-PCR. Yeast ribosomes were extracted at 6 and 24 hpi. Two pairs of primers were designed to amplify the target amplicon (depurinated SRL) and the reference amplicon (25S rRNA). The data was analyzed by comparative ΔC_T method ($\Delta\Delta C_T$). The y-axis indicates the fold change in depurination in yeast harboring the preRTA-EGFP and matRTA-EGFP over yeast harboring the empty vector.

AP1 is another adaptor protein complex in yeast. It is involved in the clathrin mediated transport at the late Golgi or TGN. Since preRTA has anterograde transport to the Golgi from the ER (53), it is possible that AP1 is involved in the trafficking pathway of preRTA. I next tested the effects of the four components of the AP1 complex on the trafficking of preRTA. I transformed preRTA-EGFP into the deletion strains of AP1 complex. The deletion did not confer growth advantages to yeast cells expressing preRTA-EGFP or matRTA-EGFP (Figure 4.12). In Figure 4.13, in all four *apm1*Δ, *apl4*Δ, *aps1*Δ and *apl2*Δ strains, preRTA-EGFP was localized to the ER at 2 hpi and started to transport to the vacuole at 4 hpi. The results suggested that by deleting any one of the subunits of the AP1 complex, the vacuole transport was not prevented as in *apl3*Δ strain, but was shifted up 2 hours than that in the BY4743.

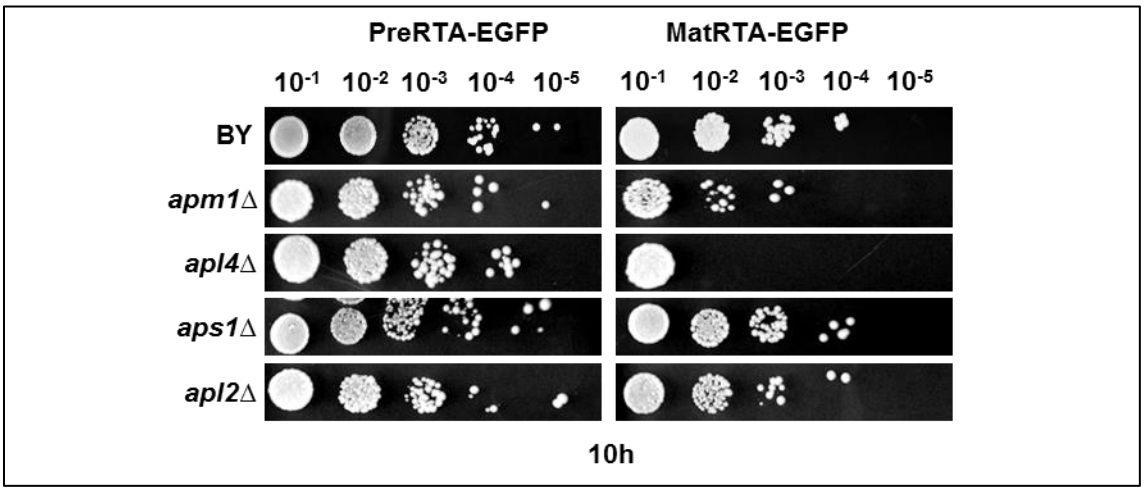

Figure 4.12 The viability of parental BY4743 and yeast deletion strains of the AP1 complex expressing preRTA-EGFP and matRTA-EGFP. Yeast cells were first grown in SD-Leu supplemented with 2% glucose and then transferred to SD-Leu supplemented with 2% galactose. At 10 hpi, a series of ten-fold dilutions were plated on media containing 2% glucose and grown at 30ºC for approximately 48 h.

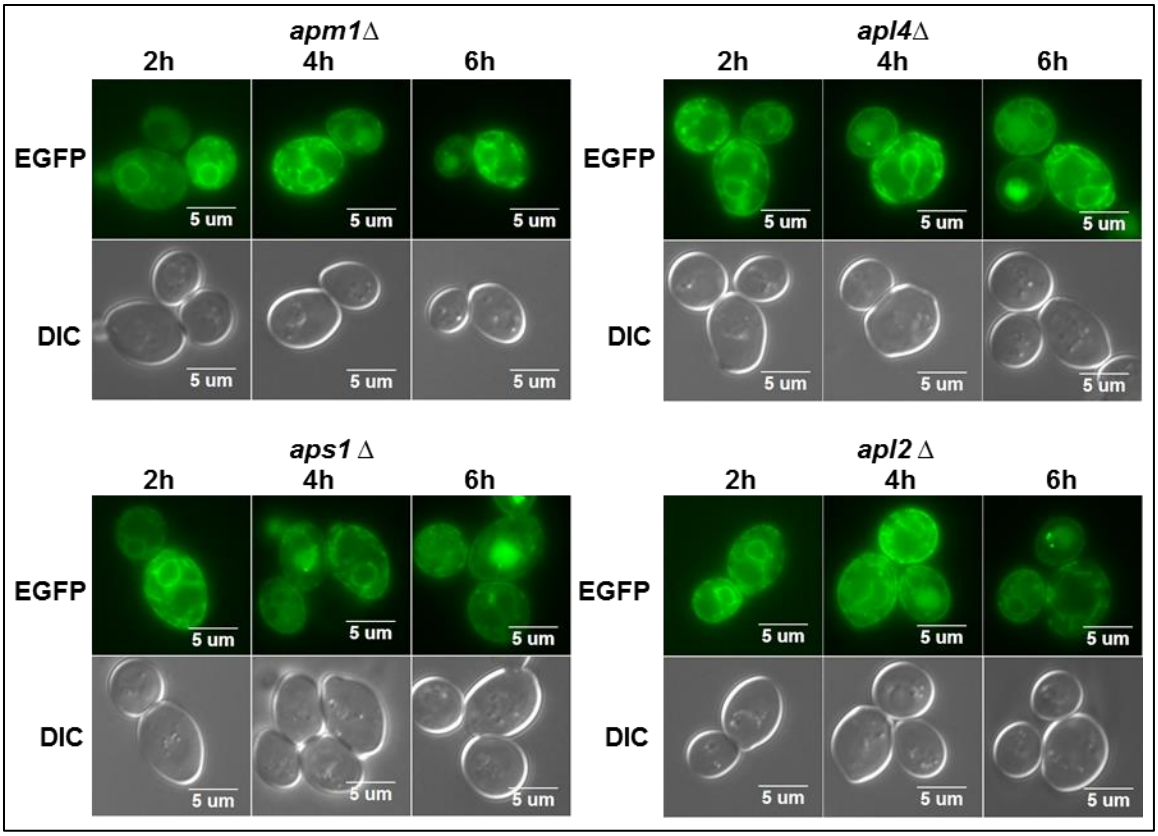

Figure 4.13 Wild type preRTA-EGFP was transported to the vacuole in *apm1*Δ, *apl4*Δ, *aps1*Δ and *apl2*Δ strains. The images of yeast cells harboring preRTA-EGFP were taken at 2, 4 and 6 hpi with an Olympus BX41 fluorescence microscope.

The depurination was examined with *apm1*Δ, *apl4*Δ, *aps1*Δ and *apl2*Δ strains expressing preRTA-EGFP and matRTA-EGFP (Figure 4.14). At 6 hpi, the depurination by matRTA-EGFP in all four AP1 deletion strains had similar depurination levels as in the parental BY4743, indicating that the AP1 complex was not involved directly in the ribosome depurination in the cytosol. The depurination of preRTA-EGFP in the AP1 deletion strains were all around two to three-fold less than that in BY4743, suggesting that AP1 complex was involved in the preRTA-EGFP export from the ER to the cytosol. At 24 hpi, the AP1 complex deletion strains expressing matRTA-EGFP still had similar depurination levels as

in the BY4743. The depurination by preRTA-EGFP in *apl2*Δ, *apl4*Δ and *aps1*Δ strains was around two-fold less than that in the BY4743. Whereas preRTA-EGFP expressed in *apm1*Δ was depurinating at similar level as that in the BY4743. Our results further demonstrated that the vacuole transport of RTA was prevented by deleting Apl3p, but was not perturbed by deleting any of the other subunits in the AP1 or AP2 complex. However, further experiment should examine the time course of depurination by preRTA without the EGFP tag to better understand the dislocation of preRTA to the cytosol.

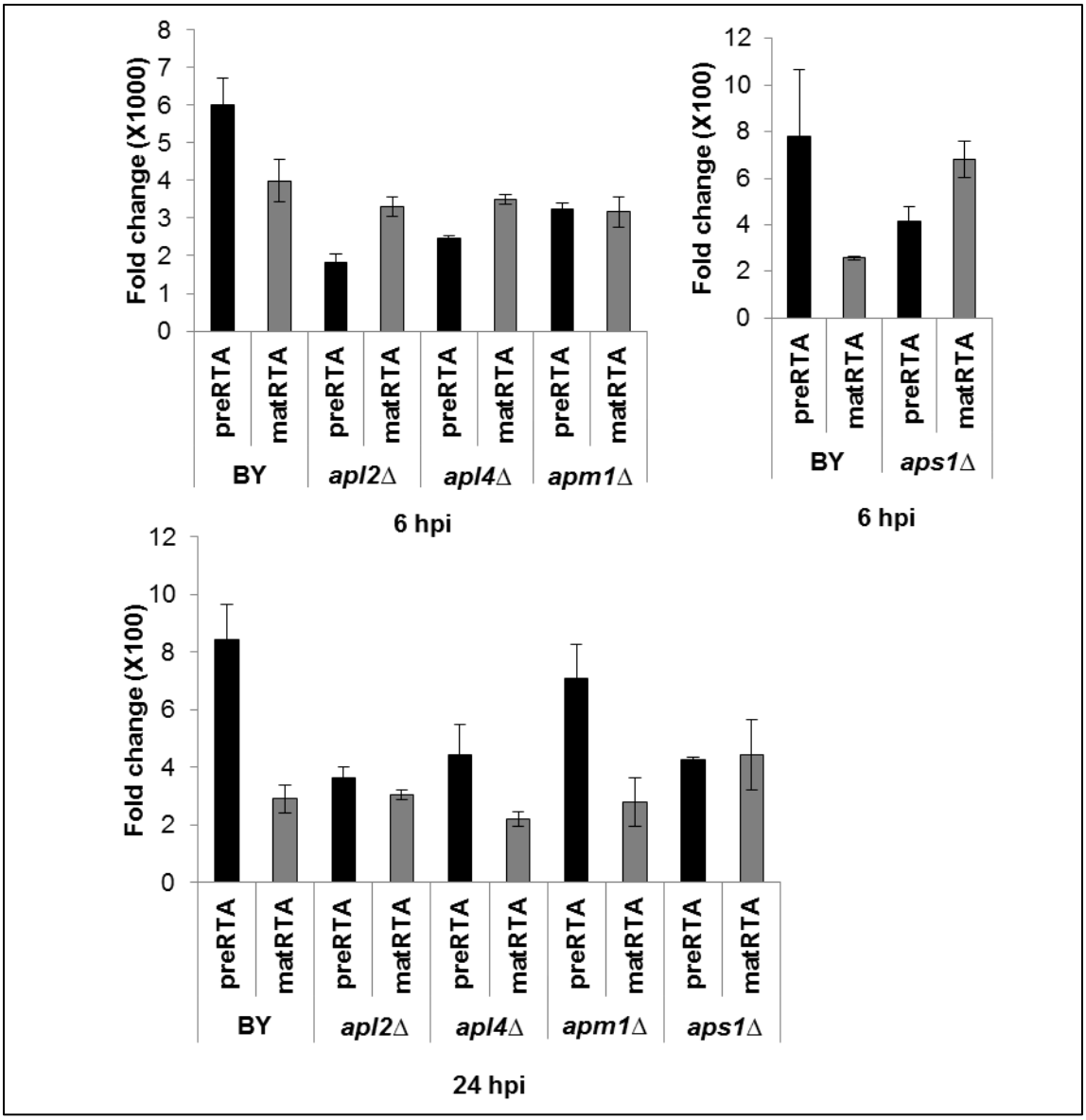

Figure 4.14 Ribosome depurination by preRTA-EGFP and matRTA-EGFP in BY4743, *apl2*Δ, *apl4*Δ, *apm1*Δ and *aps1*Δ strains *in vivo* by qRT-PCR. Yeast ribosomes were extracted at 6 and 24 hpi. Two pairs of primers were designed to amplify the target amplicon (depurinated SRL) and the reference amplicon (25S rRNA). The data was analyzed by comparative ΔC_T method ($\Delta\Delta C_T$). The y-axis indicates the fold change in depurination in yeast harboring the preRTA-EGFP and matRTA-EGFP over yeast harboring the empty vector.

DISCUSSION

Golgi is an important compartment regulating RTA intoxication

Our screen is focused on identifying the cellular components in yeast that are important for RTA trafficking after its ER import. My work characterized the involvement of new genes in the RTA trafficking pathway, and found genes that implied novel trafficking pathways for RTA. The genome wide screen presented us an exhaustive view of the genes regulating the RTA trafficking pathway. Previous genome-wide RNAi screen against ricin in mammalian cells suggested that retrotranslocation of ricin required prior functional ER-to-Golgi transport. In fact, a large number of ERAD substrates were retrieved from the Golgi before dislocation (136). From the RNAi screen, genes that function in the ER-to-Golgi vesicle mediated transport were identified. Three subunits of the TRAPP complex, including TRAPPC2, TRAPPC3 and TRAPPC8 showed strong rescue of ricin intoxication, which suggests that ricin trafficking requires the integrity of the Golgi apparatus (123). SEC22B, which encodes protein involved in the targeting and fusion of vesicle mediated transport between the ER and Golgi, was also identified as a protective hit for ricin. ERGIC2 (a mammalian homolog of yeast Erv41p), cycling between ER and Golgi, provided strong rescue for ricin and PE intoxication, which indicates that it is an important regulator for toxin trafficking between the Golgi and the ER. Consistent with these results, a genome-wide shRNA screen against ricin in mammalian cells also demonstrated the knockdown of several components of the vesicle-tethering TRAPP complex provided strong protective hits (110). Significantly, the results proposed that two

functionally distinctive TRAPP complexes exist in mammalian cells. One complex functions in COPII mediated ER-to-Golgi transport, knockdown of which provided the strong protection hits. The other TRAPP complex interacts with COPI, which is involved in the retrograde transport of ricin from endosome to Golgi and Golgi to ER, knockdown of which provided sensitizing hits. The sensitization to the cell by COPI depletion was demonstrated to be a result of enhanced ER transport of ricin, suggesting an alternative pathway may be activated upon deficiency in COPI mediated Golgi to ER retrieval (110). In yeast, it was also demonstrated that the trafficking to the Golgi is required for RTA dislocation (53). Mutant strains containing a temperature sensitive lesion in Sec12p or Sec23p, which affected COPII mediated vesicle transport in ER-to-Golgi, stabilized RTA in pulse-chase analysis at restrictive temperature. In line with this, Erp2p of the p24 mediator of the ER-to-Golgi trafficking conferred growth advantage when deleted (53). In our screen, we also identified genes functioning in the Golgi trafficking as protective hits. Coy1, which is the yeast homolog of mammalian CASP, acts as a Golgi tethering protein and interacts with COPII adaptor Sec23 in yeast (137). Glo3, a GTPase-activating protein (GAP) for ADP-ribosylation factor (ARF), has a key function in ARF-GAP which is involved in Golgi-to-ER retrieval. The identification of these two genes confirmed that the bidirectional transport between ER and Golgi compartment is important for the dislocation of RTA. These genes were identified for the first time to be involved in the ER-to-Golgi trafficking of RTA. In addition to the vesicle mediated Golgi transport, we identified gene encoding protein involved in the post-translational modification in the Golgi apparatus that

is responsible for the toxicity of RTA. Mnn9, a subunit of the Golgi-resident mannosyltransferase, elongates the polysaccharide mannan backbone. In addition to the importance of the ER resident *N*-glycosylation in the ER export of preRTA (103), the requirement for Mnn9 in the toxicity of preRTA indicates that the Golgi modified carbohydrate chain is also required as signaling element in the trafficking pathway of RTA. We also identified two other Golgi localized genes, Grx6 and Grx7, which are monothiol glutaredoxin with overlapping functions, and yet different localizations. Grx6 is localized in the ER and Golgi compartments, whereas Grx7 is localized in the Golgi. They have a role in the early secretory pathway (138). In addition to the trafficking, they also respond to the oxidative stress (139). The fact that deleting either one of them conferred resistance to the cells expressing preRTA suggested that their individual functions in the RTA toxicity are not redundant.

Hrd1 ubiquitin ligase complex is involved in the RTA dislocation

The dislocation of preRTA across the ER membrane is essential for the ribosome depurination. RTA was first reported to use the Sec61p translocon for retrotranslocation (57). However, later study found that Der1p, which is the subunit of Hrd1p ubiquitin ligase complex, but not Sec61p, was required for RTAΔ/RTL degradation (54). Recent study also showed that deletion of the Hrd1p ubiquitin ligase complex stabilized both RTA_{E177D} and RTA_{Δ} (53), suggesting a role of Hrd1p ubiquitin ligase complex in the dislocation of folding competent form RTA_{E177D} and defective form RTA_{Δ}. In mammalian cells, Derlins,

the mammalian homologs of yeast Der1p, were also required for ricin toxicity. The siRNAs against DERL1, 2 and 3 showed significant rescue of ricin intoxication. In line with this, UFD1L and NPLOC4 subunits of the Derlins binding ternary complex (140), were identified to be specific factors for ricin intoxication (123). However, in other studies there were no apparent roles for Derlin1 and Derlin2 in the dislocation of RTA (4, 102). In the present study, I demonstrated that Hrd1p, Der1p and Usa1p of the Hrd1p ubiquitin ligase complex are involved in the retrotranslocation of RTA. Hrd1p and Der1p have major roles in the dislocation of RTA. Their deletions caused significant reduction in the depurination levels and increase in the ER retention. The Usa1p takes a secondary role. Although the deletion of *USA1* caused increased association of preRTA with the ER membrane, preRTA was able to dislocate to the cytosolic side of the ER and depurinate ribosomes as in the wild type parental strain. However, *USA1* deletion inhibited the dislocation of preG83D which formed aggregates with a bigger dimension, confirming the role of Usa1p in facilitating the higher order oligomerization of the Hrd1p, which is the major component to form the retrotranslocon. The defects in the Hrd1p ubiquitin ligase complex would induce unfolded protein response (UPR) which upregulates genes involved in the vesicular transport and vacuolar protein targeting (117). Our results also demonstrated that the deletion strains of this complex had a faster vacuole delivery of preRTA and promoted the transport of propeptide attached RTA species to the vacuole. The faster vacuole turnover together with inhibited ER dislocation of RTA in these deletion strains contributed to the reduced toxicity.

Cytosolic chaperones have different roles in RTA intoxication

The ER luminal and cytosolic chaperones are also important parts in the ERAD pathway for the toxicity of RTA. In the ER lumen, the lectin chaperone Yos9p was shown to be important for the RTA delivery to the Hrd1p ubiquitin ligase complex in yeast (54). The ER mannosidase Mns1p, however, does not affect the retrotranslocation of RTA, unlike other ERAD substrates (123). In mammalian cells, ER lumen chaperones PDILT and ERO1L were identified in the RNAi screen and were required for the intoxication of both ricin and PE (123). After dislocation from the ER, preRTA refolds into a catalytically active confirmation. The cytosolic heat shock protein may assist the folding and help RTA regain optimal activity (141). In yeast, members of the Hsp40s in conjunction were shown to assist RTA in obtaining the optimal toxicity. The double knockout of Hsp40 *scj1*Δ*jem1*Δ conferred slightly increased survival when expressing RTA. However, cells lacking individual Hsp40, Hsp70 and Hsp90 family members or Hsp70 and Hsp90 cochaperones did not show growth advantage. This observation implied the possibility of the redundancy of the cytosolic chaperones (53). In mammalian cells, HSPA8 and HSCB encoding members of the heat shock protein 70 family were identified in the RNAi screen against ricin (123), suggesting a role of heat shock protein 70 family as a cytosolic refolding factor for ricin. In the present study, Sse1p, which is a component of the cytosolic Hsp90 chaperone complex in yeast, conferred hypersensitive to cells expressing both preRTA and matRTA when deleted. The results suggested that its role in ricin intoxication is not related to the trafficking

and the effects are cytosolic. The role of Sse1p is not associated with the assistance of the folding of RTA, because its absence increased RTA toxicity. However, the exact role of Sse1p in the cytotoxicity of RTA should be further determined.

AP2 Complex has a potential role in RTA trafficking

AP2S1 was identified to be involved in ricin and PE intoxication in mammalian cells (123). This gene encodes the small subunit of the AP-2 complex in mammalian cells (135). It was implicated that all four components of AP-2 complex in yeast were involved in the endocytosis of A/B toxin K28 (124). In our study, preRTA was expressed endogenously, which precluded the possible roles of these host factors in the transport routes upstream of the ER. The deletion of Apl3p or Apm4p subunits of AP-2 complex affected the toxicity of preRTA, and deletion of Apl3p inhibited the vacuole transport of RTA, suggesting a novel role of the AP-2 complex. The mechanism of vacuole transport pathway for RTA was not understood. The identification of Apl3p in the vacuole transport of preRTA suggested the involvement of AP2 complex in the ER-to-vacuole transport of RTA. However, with the knowledge of other misfolded proteins (142, 143), another possibility exists. PreRTA may be transported to the plasma membrane from the ER. The residence on the plasma membrane is transient and preRTA is subsequently endocytosed involving the function of the AP-2 complex and is delivered to the vacuole. In this pathway, AP-2 complex is involved in the endocytosis and delivery of preRTA to the vacuole after preRTA reaches the

plasma membrane. Further study will be needed to test this novel trafficking pathway for preRTA.

MATERIALS AND METHODS

Yeast strains and plasmids

A yeast gene knockout collection derived from heterozygous diploid strain BY4743 (*MATa/a his3D1/his3D1 leu2D0 /leu2D0 lys2D0/LYS2 MET15/met15D0 ura3D0 /ura3D0*) was purchased from Open Biosystems (Huntsville, AL) (144). The parental BY4743 was grown in rich YPD or synthetic drop-out medium lacking the appropriate amino acid. The deletion strains were grown in complete or synthetic drop-out medium supplemented with Geneticin (G418). Yeast strains used in this work are listed in Table 4.1.

The precursor and mature form of RTA were cloned into yeast vector containing the *LEU2* marker (NT198) downstream of the galactose-inducible *GAL1* promoter. Wild type preRTA contains a 35-residue signal sequence, followed by 267-residue RTA (NT849, preRTA); wild type mature RTA consists of 267-residue RTA (NT1456, matRTA). The preRTA and matRTA were fused with EGFP tag at the C-terminal end for observation under the fluorescence microscope (NT1205, preRTA-EGFP; NT1206, matRTA-EGFP). The plasmids were then transformed into Saccharomyces cerevisiae strain BY4743 or the deletion mutants with the same genomic background. The transformants in the parental BY4743 were selected on SD-Leu medium containing 2% glucose. The

transformants in the deletion strains were selected on SD-Leu medium supplemented with 2% glucose and G418.

Table 4.1 Strains used in this study

Strain	Strain background genotype	Source
BY4743	(*his3Δ1/his3Δ1 leu2Δ0/leu2Δ0 met15Δ0/+ lys2Δ0/+ ura3Δ0/ura3Δ0*)	Open Biosystems(145)
YKO_YOL013C	*hrd1Δ/hrd1Δ* in BY4743	Open Biosystems (145)
YKO_YBR201W	*der1Δ/der1Δ* in BY4743	Open Biosystems (145)
YKO_YML029W	*usa1Δ/usa1Δ* in BY4743	Open Biosystems (145)
YKO_YPL106C	*sse1Δ/sse1Δ* in BY4743	Open Biosystems(145)
YKO_YBL037W	*apl3Δ/apl3Δ* in BY4743	Open Biosystems (145)
YKO_YOL062C	*apm4Δ/apm4Δ* in BY4743	Open Biosystems (145)
YKO_YPL050C	*mnn9Δ/mnn9Δ* in BY4743	Open Biosystems (145)
YKO_YER122C	*glo3Δ/glo3Δ* in BY4743	Open Biosystems (145)
YKO_YKL179C	*coy1Δ/coy1Δ* in BY4743	Open Biosystems (145)
YKO_YDL010W	*grx6Δ/grx6Δ* in BY4743	Open Biosystems (145)
YKO_YBR014C	*grx7Δ/grx7Δ* in BY4743	Open Biosystems (145)
YKO_YJL012C	*vtc4Δ/vtc4Δ* in BY4743	Open Biosystems (145)
YKO_YDR485C	*vps72Δ/vps72Δ* in BY4743	Open Biosystems (145)
YKO_YGL104C	*vps73Δ/vps73Δ* in BY4743	Open Biosystems (145)
YKO_YJL172W	*cps1Δ/cps1Δ* in BY4743	Open Biosystems (145)

Analysis of protein expression

Yeast cells were grown in SD-Leu supplemented with 2% glucose overnight and then transferred to SD-Leu supplemented with 2% galactose at OD_{600} of 0.3 to induce RTA expression. Cells were collected at 6 hpi and membrane and cytosol fractions were isolated as previously described (91). Membrane fraction or cytosol fraction was treated with Endo H using the manufacturer's protocol (New England Biolabs, Ipswich, MA). The protein samples were separated on a 10% SDS-polyacrylamide gel and the blot was probed with monoclonal anti-RTA (1:5000), a gift of Dr. Nicholas J. Mantis. The blot was stripped with 8M guanidine hydrochloride and reprobed with antibody against the ER marker, dolichol phosphate mannose synthase (Dpm1p; Invitrogen, Eugene, Oregon) (1:1000) and developed using ChemiDoc MP imaging system (Bio-Rad, Philadelphia, PA).

Viability analysis

Yeast parental BY4743 and deletion strains carrying precursor and mature forms of RTA were induced as described above. A series of 10-fold dilutions of 15 µL from OD_{600} of 10^{-1} to 10^{-5} were plated on SD-Leu plates containing 2% glucose at 24 h post-induction. For spotting directly on galactose plate, BY 4743 and deletion strains expressing preRTA or preG83D were grown overnight in glucose as described above. The non-induced overnight culture were collected and plated on dropout plate with 2% galactose in a series of 10-fold dilutions of 10 µL from OD_{600} of 10^{-1} to 10^{-5}. The dilutions were replica plated on dropout plates containing 2% glucose at the same time. The galactose plates were

incubated at 30 °C for 4 days and the glucose plates were incubated at 30 °C for approximately 48 h.

Depurination analysis

For *in vivo* depurination, cells were harvested at time points indicated and total RNA was extracted using the RNeasy Mini Kit (Qiagen, Valencia, CA). The qRT-PCR analysis of depurination was carried out as previously described (78, 94).Total RNA was converted to cDNA using the High Capacity cDNA Reverse Transcription Kit (Applied Biosystems, Carlsbad, CA). The 25S rRNA was detected using (5'-AGA CCG TCG CTT GCT ACA AT-3'and 5'- ATG ACG AGG CAT TTG GCT AC- 3'). The depurinated rRNA was detected using the forward primer (5'- CTA TCG ATC CTT TAG TCC CTC-3') and the reverse primer (5'-CCG AAT GAA CTG TTC CAC A-3'). Real time PCR was performed using an ABI Prism 7000 Sequence Detection System (Applied Biosystems, Carlsbad, CA). The data was analyzed by the comparative ΔCT ($\Delta\Delta$CT) method for quantification (78).

Live cell imaging

Time course of RTA localization was carried out using yeast harboring the precursor and mature RTA with EGFP tag at 2, 4, 6, 8 and 24 hpi. The cells were directly added to 2% agar pads on slides. For vacuole stain, yeast cells were harvested at 2, 4, 6 and 24 hpi. FM4-64 (Invitrogen, Carlsbad, CA) dissolved in dimethyl sulfoxide (DMSO) was added at a final concentration of 80

μM and cells were incubated in the dark at 30°C for 60 min. Cells were pelleted, washed and resuspended in YP media containing 2% galatose, followed by chasing for 40 min at 30°C. The cell culture was applied to the agar pad and visualized using an Olympus BX41 fluorescence microscope equipped with a CCD camera (Hamamatsu, Bridgewater, NJ) and a 100X oil objective (1.45 N.A. Plan Apo, Olympus). Image acquisition and processing were performed using Metamorph Image Software (7.0; MDS Analytical Technologies).

CHAPTER 5: Conclusions

The fundamental intoxication mechanism of ricin is attributed to the ribosome depurination activity of RTA. The intracellular trafficking of RTA affects depurination indirectly by influencing its accessibility to the cytosolic ribosomes and has been shown with accumulated evidence as a major regulator in ricin mediated cell death. In this study, I take advantage of *S. cerevisiae* as a model system to investigate the intracellular trafficking pathway of RTA. Although the ultimate trafficking model of ricin should be established with mammalian cells, the basic intracellular trafficking machineries of yeast and mammalian cells are largely conserved and the genetic analyses of yeast cells are easily manipulated. The active subunit RTA was expressed endogenously under the control of the *GAL1* promoter in yeast, so that only the events after ER import were focused and the requirement of RTB for endocytosis was eliminated.

I first investigated how the important structural domains and sequence motifs within the RTA sequence contributed to the intracellular trafficking and toxicity of RTA. The precursor form of RTA (preRTA) has a 35-amino acid N-terminal extension, of which the first 26-amino acid signal peptide and the subsequent nine-amino acid propeptide are cleaved off sequentially in the endoplasmic reticulum (ER) and vacuole to produce the mature RTA (matRTA) in the producing castor bean plant (146). Our results suggest that wild type preRTA with the EGFP tag (preRTA-EGFP) follows two parallel pathways from the ER. In addition to the well characterized ER-to-cytosol dislocation through the ER associated degradation (ERAD) pathway, preRTA-EGFP is observed to be transported to the vacuole after initial localization to the ER. In contrast, mature

RTA with the EGFP tag (matRTA-EGFP) remains in the cytosol. I demonstrated that in yeast, the first 26-amino acid signal peptide is important for the ER targeting of RTA. The following nine-amino acid propeptide is responsible for *N*-glycosylation of RTA in the ER and efficient vacuole transport. The propeptide possibly contributes to the trafficking of preRTA by assisting in its proper folding as in the case of CPY* (147). The subcellular fractionation suggested that the propeptide attached wild type RTA forms are destined to the vacuole fraction exclusively, further confirms the role of propeptide as a sorting determinant to the vacuole. RTA has two consensus Asn-Xaa-Ser/Thr glycosylation sites. Although *N*-glycosylation has been demonstrated to be an essential signal for the ERAD pathway, the role of *N*-glycosylation in the trafficking of RTA has been overlooked. *N*-linked glycans function as tags for the nascent protein to be recognized by the ER luminal components (148). Its absence results in prolonged retention of several glycoproteins in the ER (97). I demonstrated that *N*-glycosylation is essential for the ER export of preRTA which further contributes to its toxicity. When the two *N*-glycosylation sites in RTA were mutated, the mature form was fully active and toxic, suggesting that the mutations of the glycosylation sites did not affect the catalytic activity itself. However, the nonglycosylated preRTA-EGFP had reduced toxicity, depurination and delayed vacuole transport. The results suggested that *N*-glycosylation affects the ER export of preRTA, confirming the role of *N*-linked glycan as a sorting determinant for RTA in the ER. Point Mutations in the C-terminal hydrophobic domain restricted RTA to the ER, thus eliminating the depurination and toxicity,

suggesting an important role of this domain in the retrotranslocation across the hydrophobic membrane bilayers (3, 55).

The ER quality control (ERQC) machineries sort nascent proteins into multiple pathways. It remains to be determined what signal elements within RTA are deciphered by the ERQC machineries, which further contribute to its trafficking and toxicity. Although previous study demonstrated that the unfolded RTA_{Δ} and folded RTA_{E177D} evidently required different sets of cytosolic ERAD components in yeast (53), it remains elusive whether the scrutiny of the ERQC recognizes sorting signals beyond the general unfolding of RTA for proper routing. By utilizing a range of nontoxic RTA mutants, I sought to investigate the different sorting pathways exploited by RTA and how it may affect the toxicity. The fact that these RTA mutants have varied depurination abilities, yet all nontoxic to yeast (80), suggests that their transport pathways may differ. With the EGFP tagged fusions, I observed two distinct trafficking patterns among these RTA mutants. One group had ER-to-cytosol and ER-to-vacuole transport, similar to the wild type, including preG212E-EGFP and preP95L/E145K-EGFP. The other group only had ER-to-cytosol transport and formed big punctate structures on the ER and cell periphery, including preG83D-EGFP and preS215F-EGFP. In the former group, preP95L/E145K-EGFP was not transported to the vacuole as efficiently as preG212E-EGFP and resulted in a higher ribosome depurination level *in vivo*, although G212E mutant was more active in the *in vitro* assay. The results suggest that vacuole transport is a degradation pathway for RTA. The faster vacuole turnover accounts for the lower *in vivo* depurination level of

preG212E-EGFP. When the ERAD pathway was blocked by deleting the components of the Hrd1p ubiquitin ligase complex, the vacuole transport of preRTA-EGFP was activated as shown with the microscopic images, further confirming that the vacuole transport is responsible for the degradation of RTA. The vacuole degradation pathway is important for the toxicity of RTA, since the proteolytic degradation in the vacuole provides a faster degradation route than the multistep ERAD. The fates of wild type RTA and nontoxic RTA mutants that dislocate to the cytosol are varied. Previous study demonstrated the unfolded RTA_{Δ}, but not the folded RTA_{E177D}, had growth defects when the cytosolic peptide:*N*-glycanase (PNGase; yeast Png1) was depleted. Because Png1 has stringent structural constraint for its substrates, I tested if the nontoxic RTA mutants could be discriminated by Png1 based on their altered sequence motifs. Wild type preRTA was deglycosylated by Png1 in the cytosol, but its degradation was not affected as indicated by the depurination and toxicity. The separation of the deglycosylation and the proteasomal degradation of wild type preRTA suggest that it is a substrate for the free pool of Png1 in the cytosol. Although preG212E-EGFP and preP95L/E145K-EGFP closely resembled wild type preRTA-EGFP in its intracellular transport, their deglycosylation was not affected by Png1, indicating different cytosolic requirements for the host cellular components. PreG83D mutant was deglycosylated by the Png1 at the ER membrane and its subsequent degradation was facilitated, suggesting that preG83D is a substrate for the Png1 which is in complex with the proteasome via the Rad23. This complex ensures efficient degradation by sequential processing

of the dislocated misfolded proteins (100). PreS215F-EGFP was not affected by Png1, suggesting that its translocation pathway is different compared with the preG83D-EGFP, although they all formed aggregates on the ER. Further experiment should confirm the model that different subsets of Png1 are involved in the deglycosylation of wild type RTA and preG83D. To test this, the Rad23 carrying mutations at the binding site with Png1 should be transformed in to *rad23*Δ strain. Under this condition, according to the model that I proposed, preG83D should be deglycosylated but not be degraded, and preRTA should be deglycosylated. Taken together, the results provide evidence that the sorting mechanisms of RTA are sophisticated and diverse. In the ER, RTA is subjected to the vacuole transport and/or the cytosol dislocation. Even if RTA variants are sorted similarly in the ER, subsequently, in the cytosol, the dislocated RTA is further differentiated by the cytosolic host factors. Since *N*-glycans plays a crucial role in the correct folding or degradation of proteins, the different sorting of wild type RTA and nontoxic RTA mutants could be a result of differences in the structure of their *N*-linked oligosaccharide chains. In the ERAD pathway, both ER luminal Yos9p and cytosolic Png1p have stringent structural requirements for the recognition of oligosaccharide chains on their substrates. Therefore, it allows sorting of proteins based on their subtle structural differences in the *N*-glycans. My results with western blot showed each nontoxic RTA mutant was processed differently from wild type RTA in the ER. There is a possibility that their different transport is due to the oligosaccharide structures. To test this possibility, future experiment should analyze the glycoforms with HPLC and mass spectrometry.

RTA was demonstrated to hijack the ERAD pathway for dislocation to the cytosol where it exerts its depurination activity (57). A number of known ERAD components have been tested on their engagement in the trafficking of RTA (53, 54, 58). However, the cellular components required by RTA may be diverse compared with other canonical ERAD substrates. At present, it is also evident that besides the ERAD pathway for ER-to-cytosol transport, the vacuole transport of RTA also exists. The host factors, especially those involved in the post-ER events of the RTA trafficking, are of significant importance to the understanding of the intoxication mechanisms of RTA and developing antidotes. To systematically understand the intracellular trafficking pathways of RTA, a genome wide screen of yeast nonessential gene deletion collection led to the identification of 137 genes, whose deletions conferred resistance to preRTA but not to matRTA. Based on the Gene Ontology (GO), I selected genes with cellular component GO in the cell compartments along the trafficking pathway or biological process GO in the anterograde trafficking or retrograde trafficking. The genes functioning in the Hrd1p ubiquitin ligase complex were selected, which dislocates misfolded proteins in the ERAD pathway (125). I tested the effects of the individual components of Hrd1p ubiquitin ligase complex on the trafficking, depurination and toxicity of wild type preRTA and the folding defective preG83D mutant. Hrd1p and Der1p of the complex are the major components that are indispensable for the dislocation of preRTA and preG83D. The Hrd1p carries six transmembrane domains which are beneficial for it to act as a retrotranslocon (149). The Der1p functions upstream of the Hrd1p and is possibly responsible for

the substrate delivery to the Hrd1p (126). The deletion of *HRD1* or *DER1* blocked the dislocation of both preRTA and preG83D. However, the deletion of *USA1* only prevented the dislocation of preG83D, but not preRTA. PreRTA was able to dislocate to the cytosolic face of the ER and depurinate. Usa1p is a scaffold protein which facilitates the higher order oligomerization of the Hrd1p. The differential requirements of Usa1p for dislocation of preG83D and preRTA could be plausibly explained by their differences in structure. PreRTA is able to dislocate via the spontaneous oligomerization of the Hrd1p, however, preG83D which forms aggregates needs the retrotranslocon with a bigger dimension, whose formation requires the assistance of the Usa1p (126). The deletion of the subunits in the Hrd1p ubiquitin ligase complex caused the defects in the ERAD pathway, which facilitated the vacuole transport of preRTA-EGFP. Consistent with this, the propeptide attached preRTA species, which was destined to the vacuole, disappeared from the ER membrane fraction faster, indicating the early onset of the vacuole transport, whereas did not affect preG83D which was unable to utilize the vacuole transport pathway.

The subunits of AP-2 complex, Apl3p and Apm4p, were both protective hits from the screen. Although AP-2 complex has well characterized function in the endocytosis of the cargo proteins and has been shown as a host factor that is involved in the intoxication of a similar A/B toxin K28, Apl3p and Apm4p were unexpected hits from our screen. Because in our experimental design, preRTA was synthesized endogenously and was co-transnationally imported to the ER in yeast, this precludes the possibility of the upstream endocytic uptake in the

retrograde pathway which is a well characterized function of the AP-2 complex. The deletion of Apl3p prevented the vacuole transport of preRTA completely, but did not affect ribosome depurination level, indicating that Apl3p has a role in vacuole transport. However, examination of preRTA-EGFP in the AP-1 complex or AP-2 complex deletion strains did not lead to the discovery of any other cellular components that could inhibit the vacuole transport when depleted. The results suggest a novel role for the AP-2 complex in the ER-to-vacuole transport of preRTA. However, with the knowledge of other misfolded proteins (142, 143), another possibility exists. preRTA may be transported to the plasma membrane from the ER. The residence on the plasma membrane is transient and preRTA is subsequently endocytosed involving the function of the AP-2 complex and is delivered to the vacuole. In this pathway, AP-2 complex is involved in the endocytosis and delivery of preRTA to the vacuole after preRTA reaches the plasma membrane. If this pathway is valid, in the absence of Apl3p, preRTA will be secreted out of the yeast cells. Therefore, future study should compare the secretion of preRTA in wild type BY4743 and *apl3*Δ strain to confirm this possibility.

In summary, this study provides significant mechanistic insights into the intracellular trafficking of RTA in yeast. It presents the first evidence that preRTA is transported to the vacuole in yeast, which is of significant importance to the toxicity of RTA. It also demonstrates the significance of *N*-glycosylation of RTA in its ER export and toxicity. The different intracellular translocations exploited by RTA mutants contribute to the understanding of the intoxication mechanisms of

RTA. The intracellular translocation of preRTA is affected by Hrd1p complex and AP-2 complex. The functions of these host factors engaged in the trafficking routes of RTA may be broadly applied to the trafficking of other cargo proteins.

REFERENCE

1. Lappi DA, Kapmeyer W, Beglau JM, Kaplan NO. The disulfide bond connecting the chains of ricin. Proc Natl Acad Sci U S A 1978;75(3):1096-1100.
2. Yan Q, Li XP, Tumer NE. N-glycosylation does not affect the catalytic activity of ricin A chain but stimulates cytotoxicity by promoting its transport out of the endoplasmic reticulum. Traffic.
3. Simpson JC, Lord JM, Roberts LM. Point mutations in the hydrophobic C-terminal region of ricin A chain indicate that Pro250 plays a key role in membrane translocation. Eur J Biochem 1995;232(2):458-463.
4. Slominska-Wojewodzka M, Gregers TF, Walchli S, Sandvig K. EDEM is involved in retrotranslocation of ricin from the endoplasmic reticulum to the cytosol. Mol Biol Cell 2006;17(4):1664-1675.
5. Montfort W, Villafranca JE, Monzingo AF, Ernst SR, Katzin B, Rutenber E, Xuong NH, Hamlin R, Robertus JD. The three-dimensional structure of ricin at 2.8 A. J Biol Chem 1987;262(11):5398-5403.
6. Frankel A, Welsh P, Richardson J, Robertus JD. Role of arginine 180 and glutamic acid 177 of ricin toxin A chain in enzymatic inactivation of ribosomes. Mol Cell Biol 1990;10(12):6257-6263.
7. Munishkin A, Wool IG. Systematic deletion analysis of ricin A-chain function. Single amino acid deletions. J Biol Chem 1995;270(51):30581-30587.
8. Schlossman D, Withers D, Welsh P, Alexander A, Robertus J, Frankel A. Role of glutamic acid 177 of the ricin toxin A chain in enzymatic inactivation of ribosomes. Mol Cell Biol 1989;9(11):5012-5021.
9. Morris KN, Wool IG. Analysis of the contribution of an amphiphilic alpha-helix to the structure and to the function of ricin A chain. Proc Natl Acad Sci U S A 1994;91(16):7530-7533.
10. Olson MA. Ricin A-chain structural determinant for binding substrate analogues: a molecular dynamics simulation analysis. Proteins 1997;27(1):80-95.
11. Monzingo AF, Robertus JD. X-ray analysis of substrate analogs in the ricin A-chain active site. J Mol Biol 1992;227(4):1136-1145.
12. Wales R, Richardson PT, Roberts LM, Lord JM. Recombinant ricin B chain fragments containing a single galactose binding site retain lectin activity. Arch Biochem Biophys 1992;294(1):291-296.
13. Fu T, Burbage C, Tagge EP, Brothers T, Willingham MC, Frankel AE. Ricin toxin contains three lectin sites which contribute to its in vivo toxicity. Int J Immunopharmacol 1996;18(12):685-692.
14. Wales R, Richardson PT, Roberts LM, Woodland HR, Lord JM. Mutational analysis of the galactose binding ability of recombinant ricin B chain. J Biol Chem 1991;266(29):19172-19179.
15. Earl Rutenber BJK, Stephen Ernst, Edward J. Collins, Debra Mlsna, Michael P. Ready, and Jon D. Robertus. Crystallographic refinement of ricin to 2.5 A. Proteins 1991;10(3):10.
16. Endo Y, Mitsui K, Motizuki M, Tsurugi K. The mechanism of action of ricin and related toxic lectins on eukaryotic ribosomes. The site and the characteristics of the modification in 28 S ribosomal RNA caused by the toxins. J Biol Chem 1987;262(12):5908-5912.

17. Endo Y, Tsurugi K. RNA N-glycosidase activity of ricin A-chain. Mechanism of action of the toxic lectin ricin on eukaryotic ribosomes. J Biol Chem 1987;262(17):8128-8130.
18. Stirpe F, Bailey S, Miller SP, Bodley JW. Modification of ribosomal RNA by ribosome-inactivating proteins from plants. Nucleic Acids Res 1988;16(4):1349-1357.
19. Endo Y, Tsurugi K. The RNA N-glycosidase activity of ricin A-chain. The characteristics of the enzymatic activity of ricin A-chain with ribosomes and with rRNA. J Biol Chem 1988;263(18):8735-8739.
20. Korennykh AV, Correll CC, Piccirilli JA. Evidence for the importance of electrostatics in the function of two distinct families of ribosome inactivating toxins. RNA 2007;13(9):1391-1396.
21. Li XP, Chiou JC, Remacha M, Ballesta JP, Tumer NE. A two-step binding model proposed for the electrostatic interactions of ricin a chain with ribosomes. Biochemistry 2009;48(18):3853-3863.
22. Chiou JC, Li XP, Remacha M, Ballesta JP, Tumer NE. The ribosomal stalk is required for ribosome binding, depurination of the rRNA and cytotoxicity of ricin A chain in Saccharomyces cerevisiae. Mol Microbiol 2008;70(6):1441-1452.
23. Brigotti M, Rambelli F, Zamboni M, Montanaro L, Sperti S. Effect of alpha-sarcin and ribosome-inactivating proteins on the interaction of elongation factors with ribosomes. Biochem J 1989;257(3):723-727.
24. Sandvig K, van Deurs B. Endocytosis, intracellular transport, and cytotoxic action of Shiga toxin and ricin. Physiol Rev 1996;76(4):949-966.
25. Sandvig K, Olsnes S, Petersen OW, van Deurs B. Acidification of the cytosol inhibits endocytosis from coated pits. J Cell Biol 1987;105(2):679-689.
26. Llorente A, Rapak A, Schmid SL, van Deurs B, Sandvig K. Expression of mutant dynamin inhibits toxicity and transport of endocytosed ricin to the Golgi apparatus. J Cell Biol 1998;140(3):553-563.
27. Moya M, Dautry-Varsat A, Goud B, Louvard D, Boquet P. Inhibition of coated pit formation in Hep2 cells blocks the cytotoxicity of diphtheria toxin but not that of ricin toxin. J Cell Biol 1985;101(2):548-559.
28. van Deurs B, Sandvig K, Petersen OW, Olsnes S, Simons K, Griffiths G. Estimation of the amount of internalized ricin that reaches the trans-Golgi network. J Cell Biol 1988;106(2):253-267.
29. Iversen TG, Skretting G, Llorente A, Nicoziani P, van Deurs B, Sandvig K. Endosome to Golgi transport of ricin is independent of clathrin and of the Rab9- and Rab11-GTPases. Mol Biol Cell 2001;12(7):2099-2107.
30. Utskarpen A, Slagsvold HH, Iversen TG, Walchli S, Sandvig K. Transport of ricin from endosomes to the Golgi apparatus is regulated by Rab6A and Rab6A'. Traffic 2006;7(6):663-672.
31. Lauvrak SU, Llorente A, Iversen TG, Sandvig K. Selective regulation of the Rab9-independent transport of ricin to the Golgi apparatus by calcium. J Cell Sci 2002;115(Pt 17):3449-3456.
32. Skanland SS, Walchli S, Utskarpen A, Wandinger-Ness A, Sandvig K. Phosphoinositide-regulated retrograde transport of ricin: crosstalk between hVps34 and sorting nexins. Traffic 2007;8(3):297-309.

33. Dyve AB, Bergan J, Utskarpen A, Sandvig K. Sorting nexin 8 regulates endosome-to-Golgi transport. Biochem Biophys Res Commun 2009;390(1):109-114.
34. Grimmer S, Iversen TG, van Deurs B, Sandvig K. Endosome to Golgi transport of ricin is regulated by cholesterol. Mol Biol Cell 2000;11(12):4205-4216.
35. Spilsberg B, Van Meer G, Sandvig K. Role of lipids in the retrograde pathway of ricin intoxication. Traffic 2003;4(8):544-552.
36. Stechmann B, Bai SK, Gobbo E, Lopez R, Merer G, Pinchard S, Panigai L, Tenza D, Raposo G, Beaumelle B, Sauvaire D, Gillet D, Johannes L, Barbier J. Inhibition of retrograde transport protects mice from lethal ricin challenge. Cell;141(2):231-242.
37. Wales R, Roberts LM, Lord JM. Addition of an endoplasmic reticulum retrieval sequence to ricin A chain significantly increases its cytotoxicity to mammalian cells. J Biol Chem 1993;268(32):23986-23990.
38. Lamb FI, Roberts LM, Lord JM. Nucleotide sequence of cloned cDNA coding for preproricin. Eur J Biochem 1985;148(2):265-270.
39. Chen A, AbuJarour RJ, Draper RK. Evidence that the transport of ricin to the cytoplasm is independent of both Rab6A and COPI. J Cell Sci 2003;116(Pt 17):3503-3510.
40. Newton DL, Wales R, Richardson PT, Walbridge S, Saxena SK, Ackerman EJ, Roberts LM, Lord JM, Youle RJ. Cell surface and intracellular functions for ricin galactose binding. J Biol Chem 1992;267(17):11917-11922.
41. Day PJ, Owens SR, Wesche J, Olsnes S, Roberts LM, Lord JM. An interaction between ricin and calreticulin that may have implications for toxin trafficking. J Biol Chem 2001;276(10):7202-7208.
42. Klokk TI, Lingelem AB, Myrann AG, Sandvig K. Role of phospholipase a(2) in retrograde transport of ricin. Toxins (Basel);3(9):1203-1219.
43. Llorente A, Lauvrak SU, van Deurs B, Sandvig K. Induction of direct endosome to endoplasmic reticulum transport in Chinese hamster ovary (CHO) cells (LdlF) with a temperature-sensitive defect in epsilon-coatomer protein (epsilon-COP). J Biol Chem 2003;278(37):35850-35855.
44. Wright HT, Robertus JD. The intersubunit disulfide bridge of ricin is essential for cytotoxicity. Arch Biochem Biophys 1987;256(1):280-284.
45. Frigerio L, Vitale A, Lord JM, Ceriotti A, Roberts LM. Free ricin A chain, proricin, and native toxin have different cellular fates when expressed in tobacco protoplasts. J Biol Chem 1998;273(23):14194-14199.
46. Di Cola A, Frigerio L, Lord JM, Ceriotti A, Roberts LM. Ricin A chain without its partner B chain is degraded after retrotranslocation from the endoplasmic reticulum to the cytosol in plant cells. Proc Natl Acad Sci U S A 2001;98(25):14726-14731.
47. Spooner RA, Watson PD, Marsden CJ, Smith DC, Moore KA, Cook JP, Lord JM, Roberts LM. Protein disulphide-isomerase reduces ricin to its A and B chains in the endoplasmic reticulum. Biochem J 2004;383(Pt 2):285-293.
48. Bellisola G, Fracasso G, Ippoliti R, Menestrina G, Rosen A, Solda S, Udali S, Tomazzolli R, Tridente G, Colombatti M. Reductive activation of ricin and ricin

A-chain immunotoxins by protein disulfide isomerase and thioredoxin reductase. Biochem Pharmacol 2004;67(9):1721-1731.
49. Pasetto M, Barison E, Castagna M, Della Cristina P, Anselmi C, Colombatti M. Reductive activation of type 2 ribosome-inactivating proteins is promoted by transmembrane thioredoxin-related protein. J Biol Chem;287(10):7367-7373.
50. Argent RH, Roberts LM, Wales R, Robertus JD, Lord JM. Introduction of a disulfide bond into ricin A chain decreases the cytotoxicity of the ricin holotoxin. J Biol Chem 1994;269(43):26705-26710.
51. Mayerhofer PU, Cook JP, Wahlman J, Pinheiro TT, Moore KA, Lord JM, Johnson AE, Roberts LM. Ricin A chain insertion into endoplasmic reticulum membranes is triggered by a temperature increase to 37 {degrees}C. J Biol Chem 2009;284(15):10232-10242.
52. Spooner RA, Lord JM. How ricin and Shiga toxin reach the cytosol of target cells: retrotranslocation from the endoplasmic reticulum. Curr Top Microbiol Immunol;357:19-40.
53. Li S, Spooner RA, Allen SC, Guise CP, Ladds G, Schnoder T, Schmitt MJ, Lord JM, Roberts LM. Folding-competent and folding-defective forms of ricin A chain have different fates after retrotranslocation from the endoplasmic reticulum. Mol Biol Cell;21(15):2543-2554.
54. Hosomi A, Tanabe K, Hirayama H, Kim I, Rao H, Suzuki T. Identification of an Htm1 (EDEM)-dependent, Mns1-independent Endoplasmic Reticulum-associated Degradation (ERAD) pathway in Saccharomyces cerevisiae: application of a novel assay for glycoprotein ERAD. J Biol Chem;285(32):24324-24334.
55. Sokolowska I, Walchli S, Wegrzyn G, Sandvig K, Slominska-Wojewodzka M. A single point mutation in ricin A-chain increases toxin degradation and inhibits EDEM1-dependent ER retrotranslocation. Biochem J;436(2):371-385.
56. Wesche J, Rapak A, Olsnes S. Dependence of ricin toxicity on translocation of the toxin A-chain from the endoplasmic reticulum to the cytosol. J Biol Chem 1999;274(48):34443-34449.
57. Simpson JC, Roberts LM, Romisch K, Davey J, Wolf DH, Lord JM. Ricin A chain utilises the endoplasmic reticulum-associated protein degradation pathway to enter the cytosol of yeast. FEBS Lett 1999;459(1):80-84.
58. Kim I, Ahn J, Liu C, Tanabe K, Apodaca J, Suzuki T, Rao H. The Png1-Rad23 complex regulates glycoprotein turnover. J Cell Biol 2006;172(2):211-219.
59. Deeks ED, Cook JP, Day PJ, Smith DC, Roberts LM, Lord JM. The low lysine content of ricin A chain reduces the risk of proteolytic degradation after translocation from the endoplasmic reticulum to the cytosol. Biochemistry 2002;41(10):3405-3413.
60. Sandvig K, Grimmer S, Lauvrak SU, Torgersen ML, Skretting G, van Deurs B, Iversen TG. Pathways followed by ricin and Shiga toxin into cells. Histochem Cell Biol 2002;117(2):131-141.
61. Halling KC, Halling AC, Murray EE, Ladin BF, Houston LL, Weaver RF. Genomic cloning and characterization of a ricin gene from Ricinus communis. Nucleic Acids Res 1985;13(22):8019-8033.

62. Lord JM. Precursors of ricin and Ricinus communis agglutinin. Glycosylation and processing during synthesis and intracellular transport. Eur J Biochem 1985;146(2):411-416.
63. van Deurs B, Tonnessen TI, Petersen OW, Sandvig K, Olsnes S. Routing of internalized ricin and ricin conjugates to the Golgi complex. J Cell Biol 1986;102(1):37-47.
64. Gillece P, Pilon M, Romisch K. The protein translocation channel mediates glycopeptide export across the endoplasmic reticulum membrane. Proc Natl Acad Sci U S A 2000;97(9):4609-4614.
65. Spooner RA, Lord JM. How ricin and Shiga toxin reach the cytosol of target cells: retrotranslocation from the endoplasmic reticulum. Current topics in microbiology and immunology 2012;357:19-40.
66. Rapak A, Falnes PO, Olsnes S. Retrograde transport of mutant ricin to the endoplasmic reticulum with subsequent translocation to cytosol. Proc Natl Acad Sci U S A 1997;94(8):3783-3788.
67. Li S, Spooner RA, Allen SC, Guise CP, Ladds G, Schnoder T, Schmitt MJ, Lord JM, Roberts LM. Folding-competent and folding-defective forms of ricin A chain have different fates after retrotranslocation from the endoplasmic reticulum. Molecular biology of the cell 2010;21(15):2543-2554.
68. Redmann V, Oresic K, Tortorella LL, Cook JP, Lord M, Tortorella D. Dislocation of ricin toxin A chains in human cells utilizes selective cellular factors. The Journal of biological chemistry 2011;286(24):21231-21238.
69. Hosomi A, Tanabe K, Hirayama H, Kim I, Rao H, Suzuki T. Identification of an Htm1 (EDEM)-dependent, Mns1-independent Endoplasmic Reticulum-associated Degradation (ERAD) pathway in Saccharomyces cerevisiae: application of a novel assay for glycoprotein ERAD. J Biol Chem 2010;285(32):24324-24334.
70. Rutenber E, Katzin BJ, Ernst S, Collins EJ, Mlsna D, Ready MP, Robertus JD. Crystallographic refinement of ricin to 2.5 A. Proteins 1991;10(3):240-250.
71. Soler-Rodriguez AM, Uhr JW, Richardson J, Vitetta ES. The toxicity of chemically deglycosylated ricin A-chain in mice. Int J Immunopharmacol 1992;14(2):281-291.
72. Sehgal P, Kumar O, Kameswararao M, Ravindran J, Khan M, Sharma S, Vijayaraghavan R, Prasad GB. Differential toxicity profile of ricin isoforms correlates with their glycosylation levels. Toxicology 2011;282(1-2):56-67.
73. Parikh BA, Coetzer C, Tumer NE. Pokeweed antiviral protein regulates the stability of its own mRNA by a mechanism that requires depurination but can be separated from depurination of the alpha-sarcin/ricin loop of rRNA. J Biol Chem 2002;277(44):41428-41437.
74. Faulhammer F, Konrad G, Brankatschk B, Tahirovic S, Knodler A, Mayinger P. Cell growth-dependent coordination of lipid signaling and glycosylation is mediated by interactions between Sac1p and Dpm1p. The Journal of cell biology 2005;168(2):185-191.
75. Vida TA, Emr SD. A new vital stain for visualizing vacuolar membrane dynamics and endocytosis in yeast. J Cell Biol 1995;128(5):779-792.

76. Maley F, Trimble RB, Tarentino AL, Plummer TH, Jr. Characterization of glycoproteins and their associated oligosaccharides through the use of endoglycosidases. Anal Biochem 1989;180(2):195-204.
77. Kane PM, Kuehn MC, Howald-Stevenson I, Stevens TH. Assembly and targeting of peripheral and integral membrane subunits of the yeast vacuolar H(+)-ATPase. J Biol Chem 1992;267(1):447-454.
78. Pierce M, Kahn JN, Chiou J, Tumer NE. Development of a quantitative RT-PCR assay to examine the kinetics of ribosome depurination by ribosome inactivating proteins using Saccharomyces cerevisiae as a model. RNA 2011;17(1):201-210.
79. Jolliffe NA, Di Cola A, Marsden CJ, Lord JM, Ceriotti A, Frigerio L, Roberts LM. The N-terminal ricin propeptide influences the fate of ricin A-chain in tobacco protoplasts. J Biol Chem 2006;281(33):23377-23385.
80. Li XP, Baricevic M, Saidasan H, Tumer NE. Ribosome depurination is not sufficient for ricin-mediated cell death in Saccharomyces cerevisiae. Infect Immun 2007;75(1):417-428.
81. Parikh BA, Tortora A, Li XP, Tumer NE. Ricin inhibits activation of the unfolded protein response by preventing splicing of the HAC1 mRNA. J Biol Chem 2008;283(10):6145-6153.
82. Mulholland J, Botstein D. Immunoelectron microscopy of aldehyde-fixed yeast cells. Methods Enzymol 2002;351:50-81.
83. Lehrman MA. Oligosaccharide-based information in endoplasmic reticulum quality control and other biological systems. J Biol Chem 2001;276(12):8623-8626.
84. Helenius A. How N-linked oligosaccharides affect glycoprotein folding in the endoplasmic reticulum. Mol Biol Cell 1994;5(3):253-265.
85. Parodi AJ. Protein glucosylation and its role in protein folding. Annu Rev Biochem 2000;69:69-93.
86. Spiro RG. Glucose residues as key determinants in the biosynthesis and quality control of glycoproteins with N-linked oligosaccharides. J Biol Chem 2000;275(46):35657-35660.
87. Banerjee S, Vishwanath P, Cui J, Kelleher DJ, Gilmore R, Robbins PW, Samuelson J. The evolution of N-glycan-dependent endoplasmic reticulum quality control factors for glycoprotein folding and degradation. Proc Natl Acad Sci U S A 2007;104(28):11676-11681.
88. Sokolowska I, Walchli S, Wegrzyn G, Sandvig K, Slominska-Wojewodzka M. A single point mutation in ricin A-chain increases toxin degradation and inhibits EDEM1-dependent ER retrotranslocation. Biochem J 2011;436(2):371-385.
89. Winther JR, Stevens TH, Kielland-Brandt MC. Yeast carboxypeptidase Y requires glycosylation for efficient intracellular transport, but not for vacuolar sorting, in vivo stability, or activity. Eur J Biochem 1991;197(3):681-689.
90. Wilkins TA, Bednarek SY, Raikhel NV. Role of propeptide glycan in post-translational processing and transport of barley lectin to vacuoles in transgenic tobacco. Plant Cell 1990;2(4):301-313.

91. Parikh BA, Baykal U, Di R, Tumer NE. Evidence for retro-translocation of pokeweed antiviral protein from endoplasmic reticulum into cytosol and separation of its activity on ribosomes from its activity on capped RNA. Biochemistry 2005;44(7):2478-2490.
92. Baykal U, Tumer NE. The C-terminus of pokeweed antiviral protein has distinct roles in transport to the cytosol, ribosome depurination and cytotoxicity. Plant J 2007;49(6):995-1007.
93. Cabrera M, Ungermann C. Purification and in vitro analysis of yeast vacuoles. Methods Enzymol 2008;451:177-196.
94. Chiou JC, Li XP, Remacha M, Ballesta JP, Tumer NE. Shiga toxin 1 is more dependent on the P proteins of the ribosomal stalk for depurination activity than Shiga toxin 2. The international journal of biochemistry & cell biology 2011;43(12):1792-1801.
95. May MJ, Hartley MR, Roberts LM, Krieg PA, Osborn RW, Lord JM. Ribosome inactivation by ricin A chain: a sensitive method to assess the activity of wild-type and mutant polypeptides. EMBO J 1989;8(1):301-308.
96. Suzuki T, Park H, Lennarz WJ. Cytoplasmic peptide:N-glycanase (PNGase) in eukaryotic cells: occurrence, primary structure, and potential functions. FASEB J 2002;16(7):635-641.
97. Spiro RG. Role of N-linked polymannose oligosaccharides in targeting glycoproteins for endoplasmic reticulum-associated degradation. Cell Mol Life Sci 2004;61(9):1025-1041.
98. Hirsch C, Misaghi S, Blom D, Pacold ME, Ploegh HL. Yeast N-glycanase distinguishes between native and non-native glycoproteins. EMBO Rep 2004;5(2):201-206.
99. Joshi S, Katiyar S, Lennarz WJ. Misfolding of glycoproteins is a prerequisite for peptide: N-glycanase mediated deglycosylation. FEBS Lett 2005;579(3):823-826.
100. Lee JH, Choi JM, Lee C, Yi KJ, Cho Y. Structure of a peptide:N-glycanase-Rad23 complex: insight into the deglycosylation for denatured glycoproteins. Proc Natl Acad Sci U S A 2005;102(26):9144-9149.
101. Tanabe K, Lennarz WJ, Suzuki T. A cytoplasmic peptide: N-glycanase. Methods Enzymol 2006;415:46-55.
102. Redmann V, Oresic K, Tortorella LL, Cook JP, Lord M, Tortorella D. Dislocation of ricin toxin A chains in human cells utilizes selective cellular factors. J Biol Chem;286(24):21231-21238.
103. Yan Q, Li XP, Tumer NE. N-glycosylation does not affect the catalytic activity of ricin a chain but stimulates cytotoxicity by promoting its transport out of the endoplasmic reticulum. Traffic;13(11):1508-1521.
104. Kincaid MM, Cooper AA. Misfolded proteins traffic from the endoplasmic reticulum (ER) due to ER export signals. Mol Biol Cell 2007;18(2):455-463.
105. Kawaguchi S, Hsu CL, Ng DT. Interplay of substrate retention and export signals in endoplasmic reticulum quality control. PLoS One;5(11):e15532.
106. Vashist S, Ng DT. Misfolded proteins are sorted by a sequential checkpoint mechanism of ER quality control. J Cell Biol 2004;165(1):41-52.

107. Russell SJ, Steger KA, Johnston SA. Subcellular localization, stoichiometry, and protein levels of 26 S proteasome subunits in yeast. J Biol Chem 1999;274(31):21943-21952.
108. Pierce M, Kahn JN, Chiou J, Tumer NE. Development of a quantitative RT-PCR assay to examine the kinetics of ribosome depurination by ribosome inactivating proteins using Saccharomyces cerevisiae as a model. Rna;17(1):201-210.
109. Suzuki T, Park H, Hollingsworth NM, Sternglanz R, Lennarz WJ. PNG1, a yeast gene encoding a highly conserved peptide:N-glycanase. J Cell Biol 2000;149(5):1039-1052.
110. Bassik MC, Kampmann M, Lebbink RJ, Wang S, Hein MY, Poser I, Weibezahn J, Horlbeck MA, Chen S, Mann M, Hyman AA, Leproust EM, McManus MT, Weissman JS. A systematic mammalian genetic interaction map reveals pathways underlying ricin susceptibility. Cell;152(4):909-922.
111. Barlowe C. Signals for COPII-dependent export from the ER: what's the ticket out? Trends Cell Biol 2003;13(6):295-300.
112. Winther JR, Sorensen P. Propeptide of carboxypeptidase Y provides a chaperone-like function as well as inhibition of the enzymatic activity. Proc Natl Acad Sci U S A 1991;88(20):9330-9334.
113. Winther JR, Sorensen P, Kielland-Brandt MC. Refolding of a carboxypeptidase Y folding intermediate in vitro by low-affinity binding of the proregion. J Biol Chem 1994;269(35):22007-22013.
114. Hirsch C, Blom D, Ploegh HL. A role for N-glycanase in the cytosolic turnover of glycoproteins. EMBO J 2003;22(5):1036-1046.
115. Zhao G, Li G, Zhou X, Matsuo I, Ito Y, Suzuki T, Lennarz WJ, Schindelin H. Structural and mutational studies on the importance of oligosaccharide binding for the activity of yeast PNGase. Glycobiology 2009;19(2):118-125.
116. Katiyar S, Li G, Lennarz WJ. A complex between peptide:N-glycanase and two proteasome-linked proteins suggests a mechanism for the degradation of misfolded glycoproteins. Proc Natl Acad Sci U S A 2004;101(38):13774-13779.
117. Travers KJ, Patil CK, Wodicka L, Lockhart DJ, Weissman JS, Walter P. Functional and genomic analyses reveal an essential coordination between the unfolded protein response and ER-associated degradation. Cell 2000;101(3):249-258.
118. Gelperin DM, White MA, Wilkinson ML, Kon Y, Kung LA, Wise KJ, Lopez-Hoyo N, Jiang L, Piccirillo S, Yu H, Gerstein M, Dumont ME, Phizicky EM, Snyder M, Grayhack EJ. Biochemical and genetic analysis of the yeast proteome with a movable ORF collection. Genes Dev 2005;19(23):2816-2826.
119. Alberti S, Gitler AD, Lindquist S. A suite of Gateway cloning vectors for high-throughput genetic analysis in Saccharomyces cerevisiae. Yeast 2007;24(10):913-919.
120. Mumberg D, Muller R, Funk M. Yeast vectors for the controlled expression of heterologous proteins in different genetic backgrounds. Gene 1995;156(1):119-122.

121. Zhang T, Lei J, Yang H, Xu K, Wang R, Zhang Z. An improved method for whole protein extraction from yeast Saccharomyces cerevisiae. Yeast;28(11):795-798.
122. Jarosch E, Taxis C, Volkwein C, Bordallo J, Finley D, Wolf DH, Sommer T. Protein dislocation from the ER requires polyubiquitination and the AAA-ATPase Cdc48. Nat Cell Biol 2002;4(2):134-139.
123. Moreau D, Kumar P, Wang SC, Chaumet A, Chew SY, Chevalley H, Bard F. Genome-wide RNAi screens identify genes required for Ricin and PE intoxications. Dev Cell;21(2):231-244.
124. Carroll SY, Stirling PC, Stimpson HE, Giesselmann E, Schmitt MJ, Drubin DG. A yeast killer toxin screen provides insights into a/b toxin entry, trafficking, and killing mechanisms. Dev Cell 2009;17(4):552-560.
125. Bordallo J, Plemper RK, Finger A, Wolf DH. Der3p/Hrd1p is required for endoplasmic reticulum-associated degradation of misfolded lumenal and integral membrane proteins. Mol Biol Cell 1998;9(1):209-222.
126. Carvalho P, Stanley AM, Rapoport TA. Retrotranslocation of a misfolded luminal ER protein by the ubiquitin-ligase Hrd1p. Cell;143(4):579-591.
127. Gauss R, Sommer T, Jarosch E. The Hrd1p ligase complex forms a linchpin between ER-lumenal substrate selection and Cdc48p recruitment. EMBO J 2006;25(9):1827-1835.
128. Horn SC, Hanna J, Hirsch C, Volkwein C, Schutz A, Heinemann U, Sommer T, Jarosch E. Usa1 functions as a scaffold of the HRD-ubiquitin ligase. Mol Cell 2009;36(5):782-793.
129. Toshiaki Izawa HN, Toshiya Endo, and Shuh-ichi Nishikawa. Yos9p and Hrd1p mediate ER retention of misfolded proteins for ER-associated degradation. Mol Biol Cell 2012;23(7):1283-1293.
130. Carroll SM, Hampton RY. Usa1p is required for optimal function and regulation of the Hrd1p endoplasmic reticulum-associated degradation ubiquitin ligase. J Biol Chem;285(8):5146-5156.
131. Haynes CM, Caldwell S, Cooper AA. An HRD/DER-independent ER quality control mechanism involves Rsp5p-dependent ubiquitination and ER-Golgi transport. J Cell Biol 2002;158(1):91-101.
132. Katiyar S, Joshi S, Lennarz WJ. The retrotranslocation protein Derlin-1 binds peptide:N-glycanase to the endoplasmic reticulum. Mol Biol Cell 2005;16(10):4584-4594.
133. Owen DJ, Collins BM, Evans PR. Adaptors for clathrin coats: structure and function. Annu Rev Cell Dev Biol 2004;20:153-191.
134. Traub LM. Common principles in clathrin-mediated sorting at the Golgi and the plasma membrane. Biochim Biophys Acta 2005;1744(3):415-437.
135. Collins BM, McCoy AJ, Kent HM, Evans PR, Owen DJ. Molecular architecture and functional model of the endocytic AP2 complex. Cell 2002;109(4):523-535.
136. Hirayama H, Seino J, Kitajima T, Jigami Y, Suzuki T. Free oligosaccharides to monitor glycoprotein endoplasmic reticulum-associated degradation in Saccharomyces cerevisiae. J Biol Chem;285(16):12390-12404.

137. Gillingham AK, Pfeifer AC, Munro S. CASP, the alternatively spliced product of the gene encoding the CCAAT-displacement protein transcription factor, is a Golgi membrane protein related to giantin. Mol Biol Cell 2002;13(11):3761-3774.
138. Izquierdo A, Casas C, Muhlenhoff U, Lillig CH, Herrero E. Saccharomyces cerevisiae Grx6 and Grx7 are monothiol glutaredoxins associated with the early secretory pathway. Eukaryot Cell 2008;7(8):1415-1426.
139. Mesecke N, Spang A, Deponte M, Herrmann JM. A novel group of glutaredoxins in the cis-Golgi critical for oxidative stress resistance. Mol Biol Cell 2008;19(6):2673-2680.
140. Oda Y, Okada T, Yoshida H, Kaufman RJ, Nagata K, Mori K. Derlin-2 and Derlin-3 are regulated by the mammalian unfolded protein response and are required for ER-associated degradation. J Cell Biol 2006;172(3):383-393.
141. Spooner RA, Hart PJ, Cook JP, Pietroni P, Rogon C, Hohfeld J, Roberts LM, Lord JM. Cytosolic chaperones influence the fate of a toxin dislocated from the endoplasmic reticulum. Proc Natl Acad Sci U S A 2008;105(45):17408-17413.
142. Fayadat L, Kopito RR. Recognition of a single transmembrane degron by sequential quality control checkpoints. Mol Biol Cell 2003;14(3):1268-1278.
143. Ferreira T, Mason AB, Pypaert M, Allen KE, Slayman CW. Quality control in the yeast secretory pathway: a misfolded PMA1 H+-ATPase reveals two checkpoints. J Biol Chem 2002;277(23):21027-21040.
144. Winzeler EA, Shoemaker DD, Astromoff A, Liang H, Anderson K, Andre B, Bangham R, Benito R, Boeke JD, Bussey H, Chu AM, Connelly C, Davis K, Dietrich F, Dow SW*, et al.* Functional characterization of the S. cerevisiae genome by gene deletion and parallel analysis. Science 1999;285(5429):901-906.
145. Brachmann CB DA, Cost GJ, Caputo E, Li J, Hieter P, Boeke JD. Designer deletion strains derived from Saccharomyces cerevisiae S288C: a useful set of strains and plasmids for PCR-mediated gene disruption and other applications. Yeast 1998;14(2):115-132.
146. Lord JM, Roberts LM, Robertus JD. Ricin: structure, mode of action, and some current applications. FASEB J 1994;8(2):201-208.
147. Holst B, Bruun AW, Kielland-Brandt MC, Winther JR. Competition between folding and glycosylation in the endoplasmic reticulum. EMBO J 1996;15(14):3538-3546.
148. Yoshida Y. A novel role for N-glycans in the ERAD system. J Biochem 2003;134(2):183-190.
149. Hampton RY, Sommer T. Finding the will and the way of ERAD substrate retrotranslocation. Curr Opin Cell Biol;24(4):460-466.

CURRICULUM VITA

EDUCATION

2006-2013 Ph.D. Plant Biology
Rutgers University, New Jersey, U.S.
2002-2006 B.E. Biotechnology
China Agricultural University, Beijing, China

RESEARCH EXPERIENCE

2007-2013 Graduate Assistant, Department of Plant Biology, Rutgers University, New Brunswick, NJ.
2006-2007 Graduate Fellow, Department of Plant Biology, Rutgers University, New Brunswick, NJ.

PUBLICATIONS

1. **Qing Yan**, Xiaoping Li and Nilgun E. Tumer (2013) **peptide:*N*-glycanase affects depurination activity and cytotoxicity of ricin A chain.** In preparation.
2. Kerrie L. May, **Qing Yan** and Nilgun E. Tumer (2013) **Targeting ricin to the ribosome.** Toxicon. 69(2013):143-51.
3. **Qing Yan,** Xiaoping Li and Nilgun E. Tumer (2012) **N-glycosylation does not affect the catalytic activity of ricin A chain but stimulates cytotoxicity by promoting its transport out of the endoplasmic reticulum.** Traffic. 13(11):1508-21.
4. Thomas Widiez, Thomas G. Hartman, Nativ Dudai, **Qing Yan,** Michael Lawton, Daphna Havkin-Frenkel and Faith C. Belanger (2011) **Functional characterization of two new members of the caffeoyl CoA O-methyltransferase-like gene family from Vanilla planifolia reveals a new class of plastid-localized O-methyltransferases.** Plant Molecular Biology. 76(6):475-88.